JAERI-M
8215

DIVERTOR EXPERIMENT FOR IMPURITY CONTROL IN DIVA

April 1979

Masayuki NAGAMI

日本原子力研究所
Japan Atomic Energy Research Institute

この報告書は，日本原子力研究所がJAERI-Mレポートとして，不定期に刊行している研究報告書です．入手，複製などのお問合わせは，日本原子力研究所技術情報部（茨城県那珂郡東海村）あて，お申しこしください．

JAERI-M reports, issued irregularly, describe the results of research works carried out in JAERI. Inquiries about the availability of reports and their reproduction should be addressed to Division of Technical Information, Japan Atomic Energy Research Institute, Tokai-mura, Naka-gun, Ibaraki-ken, Japan.

JAERI-M 8215

DIVERTOR EXPERIMENT FOR IMPURITY CONTROL IN DIVA

Masayuki NAGAMI

Division of Thermonuclear Fusion Research
Tokai Research Establishment, JAERI

(Received March 28, 1979)

Divertor actions of controlling the impurities and the transport of impurity ions in the plasma have been investigated in the DIVA device. Following are the results:

(1) The radial transport of impurity ions is not described only by neoclassical theory, but it is strongly influenced by anomalous process. Radial diffusion of impurity ions across the whole minor radius is well described by a neoclassical diffusion superposed by the anomalous diffusion for protons. Due to this anomalous process, which spreads the radial density profile of impurity ions, 80 to 90 % of the impurity flux in the plasma outer edge is shielded even in a non-diverted discharge.

(2) The divertor reduces the impurity flux entering the main plasma by a factor of 2 to 4. The impurity ions shielded by the scrape-off plasma are rapidly guided into the burial chamber with a poloidal excursion time roughly equal to that of the scrape-off plasma.

(3) The divertor reduces the impurity ion flux onto the main vacuum chamber by guiding the impurity ions diffusing from the main plasma into the burial chamber, thereby reducing the plasma-wall interaction caused by diffusing impurity ions at the main vacuum chamber. The impurity ions produced in the burial chamber may flow back to the main plasma through the scrape-off layer. However, roughly only 0.3 % of the impurity flux into the scrape-off plasma in the burial chamber penetrates into the main plasma due to the impurity backflow.

(4) A slight cooling of the scrape-off plasma with light-impurity injection effectively reduces the metal impurity production at the first wall by reducing the potential difference between the plasma and the wall, thereby reducing the accumulation of the metal impurity in the discharge. Radiation cooling by low-Z impurities in the plasma outer edge, which may become an important feature in future large tokamaks both with and without divertor, is numerically evaluated for carbon, oxygen and neon.

Key Words: DIVA Tokamak, Divertor, Impurity Transport, Impurity Shielding, Impurity Sweeping-Out, Impurity Back Flow, Edge Cooling

JAERI－M 8215

DIVAにおけるダイバーターによる不純物制御実験

日本原子力研究所東海研究所核融合研究部
永　見　正　幸

（1979年3月28日受理）

DIVA装置において，ダイバーターの不純物制御作用，及び，不純物イオンのプラズマ中での拡散過程を明らかにした。結果は以下の通りである。

1）プラズマ中の不純物イオンは，新古典理論に基づくプラズマ中心へ向かう拡散に加え，プロトンの拡散と同程度の大きさの異常拡散を行なう。この異常拡散によって生じる外向きの拡散束のために，ダイバーターを用いない場合でもプラズマ中心領域に達する不純物イオン束は，壁からの流入束の20％程度に減少する。

2）ダイバーターは，壁で発生しプラズマ中に侵入する不純物粒子をスクレイプ・オフ層で遮蔽することにより，プラズマ中心領域へ向かう不純物イオン束を1／2～1／4に減少させる。遮蔽された不純物イオンは，スクレイプ・オフ層プラズマの磁力線に沿う流速にほぼ等しい速度でダイバーター室に流入する。

3）ダイバーターは，プラズマ中心部より壁へ向かい拡散する不純物イオンをスクレイプ・オフ層を通してダイバーター室に導き，壁に達する不純物粒子束を減少させることにより，不純物イオンのスパッタリングによる壁での不純物発生を減少させる。ダイバーター室内で発生する不純物粒子がスクレイプ・オフ層を逆流し主プラズマに混入する割合は小さく，0.3％程度である。

4）ガス不純物の注入を行ない，スクレイプ・オフ・プラズマを冷却することにより，プラズマ中の金属不純物の混入量は更に低減できる。これは，イオン・スパッタリングによる壁表面での金属不純物の発生を，壁に接触するプラズマを冷却することにより低下させるためである。将来の大型装置で必要である，周辺プラズマの冷却の手段として有力な，ガス不純物による冷却について，炭素，酸素，ネオンの冷却能力を評価した。

CONTENTS

目　　次

1. INTRODUCTION

1.1 Need for Impurity Control in Tokamak Fusion Development

Impurity has a significant effect on the operation of present generation tokamaks, and will be a key factor in determining the feasibility of tokamak reactors. Especially the impurity radiation losses affect the energy balance of the reacting plasma. The maximum tolerable concentrations in order to attain given Q-values in the range Q = 1 to ∞ are calculated in Ref.[1] for six impurity species, where

Q = Fusion Power/Auxiliary Heating Power

Figure 1 shows the maximum allowed impurity concentration for ignition (Q = ∞) as a function of plasma temperature, assuming zero nonradiative losses. To obtain an ignition below 10 keV of the plasma temperature, for example, the concentrations of low-Z and high-Z impurities must be suppressed below 3-5 % and 0.1-0.01 % of the fuel ions respectively. For low-Z impurities, this seems attainable in future tokamaks, because low-Z impurity can be relatively easily controlled in recent experiments by employing gettered wall surface with titanium [2], low power discharge cleaning [3], or inert wall surface [4]. On the other hand since even in the present tokamaks, 0.1 % contamination by high-Z impurity is prevailed, and the plasma-wall interaction becomes much more serious in future large tokamaks, finding the methods controlling the high-Z impurity (first wall or limiter material) is one of the most important problems in developing a tokamak reactor.

In order to control the accumulation of impurity ions in the tokamak discharge, at least one of the following three processes must be controlled; 1) impurity production at the limiter and the first wall, 2) penetration of impurity influx in the plasma outer edge, and 3) transport of impurity ions across the plasma minor radius. Therefore the following three problems must be investigated; 1) origin of impurity production at material surfaces, 2) transport properties of impurity ions in the plasma, and 3) methods to control the above two processes. The first problem is recently investigated in DIVA device [5]. This work concerns the rest two problems, i.e. the transport properties of

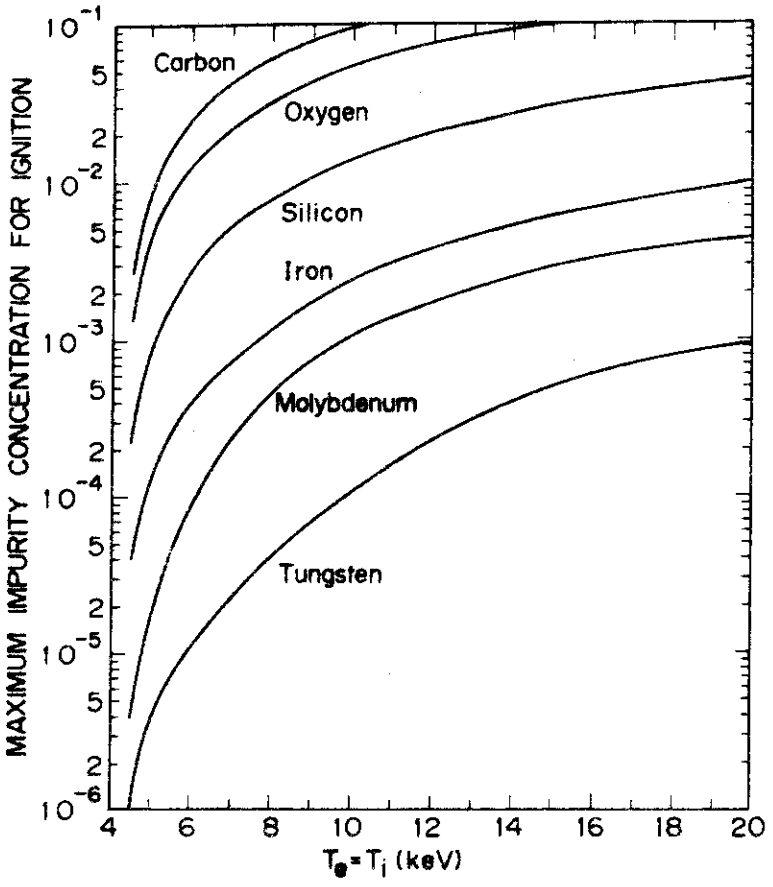

Fig.1 Maximum allowed impurity concentration for ignition as a function of plasma temperature, assuming zero nonradiative losses.(by Jensen, Post and Jassby, ref.[1])

impurity ions in the plasma, and the methods to control the impurity production and the penetration of impurity ions towards the plasma center.

1.2 Impurities in Tokamak Discharges

In regard to the penetration of impurity ions into the plasma center, considerable efforts have been made to measure the radial transport of impurity ions for intrinsic content [6] or injected impurity ions [7]. In these experiments, the inward flux measured at the peak position of the radial profile of respective ionization states are consistent with the prediction from the neoclassical theory: In TFR, OV ions present in a peripheral plasma shell, have inward diffusion velocity

of 2×10^3 cm/sec, and in ATC, injected aluminum ions show inward diffusion with a transport coefficient close to neoclassical theory. In these experiments, however, understanding about the global behaviour of impurity ions across the plasma whole cross section is beyond the scope of these experiments. In this work, the transport of impurity ions across the whole plasma minor radius is investigated, and the confinement property of impurity ions in the tokamak discharge is clarified.

In regard to the accumulation level of metal impurity in discharges, the relation between the content of high-Z impurity and that of low-Z impurity in discharge was first found in ST tokamak [8], i.e. presence of low-Z impurity in the discharge reduces the contamination level of the high-Z impurity. Similar phenomenon was found in PULSATOR [9] with strong additional fuelling during the discharge. In TFR, these phenomena were investigated with oxygen gas injection during the current plateau of the discharge [10]. However, the mechanisms reducing the high-Z impurity level in the discharge with the additional low-Z impurity injection or cold gas fueling are not clearly known: whether due to a change in radial transport of impurity ions or in the impurity influx (production) in the plasma outer edge. Recently it is shown that ion-sputtering at the limiter or the wall is the dominant process of releasing metal impurity in DIVA device [5]. Therefore the above noted phenomenon may be explained as follows: The additional low-Z impurity and cold gas cool the edge plasma, thereby reduce the energy of ions hitting material surfaces and the amount of the release of metal impurity [11]. This work experimentally demonstrates the effectiveness of plasma edge cooling by light-impurity injection, and numerically evaluates the radiative cooling capabilities of three ligh-impurities (carbon, oxygen and neon).

1.3 Divertor Actions on Impurity

Divertor is one of the most promising methods controlling impurities. The important divertor actions on impurities are as follows:

(1) Impurity shielding; Impurity atoms that originate from the vacuum chamber wall are ionized in the divertor scrape-off, and the resultant impurity ions are swept into the burial chamber by the escaping plasma.

With this action, divertor reduces the impurity flux penetrating into the main plasma.

(2) Plasma sweeping-out; Divertor guides the charged particles diffusing from the main plasma into the remote burial chamber. By this action, plasma-wall interactions and impurity production caused by diffusing ions are removed from the main chamber to the burial chamber.

In DIVA and DITE, both the low and high-Z impurity radiation in the plasma can be successfuly reduced by employing an axisymmetric divertor [12, 13] and the bundle divertor [14] respectively. As another type of divertor, a built-in divertor in Heliotron is presented in Ref.[15], and its fundamental properties are experimentally studied in Heliotron-D device [16].

As for the above noted divertor actions, the shielding action against injected impurity was studied in DITE [17] with the bundle divertor. They find an increment of plasma resistance by a factor of 4.5 with a non-diverted discharge, although the resistance is not changed in a diverted discharge for puffing the same amount of oxygen. Impurity flow into the remote burial chamber and the comparison of the accumulation of injected impurity in the main plasma with the spectroscopic measurements are, however, beyond the scope of this experiment.

In the situation where the plasma sweeping-out is attained by employing the divertor, the material surface which contacts a high temperature scrape-off plasma is replaced by a neutralizer plate in the burial chamber. In this case the impurity efflux from the neutralizer plate becomes the problem. Therefore it is important to investigate the effect of the impurity backflow from the neutralizer plate into the main plasma.

In this work above noted fundamental divertor actions are investigated in detail. Accumulations of impurity ions in the plasma center are compared in discharges with and without divertor for a same amount of impurity influx in the plasma outer edge. The flow of shielded impurity ions along the scrape-off field lines towards the burial chamber, the guidance of impurity ions diffusing from the main plasma into the remote burial chamber, and the impurity backflow are observed in the diverted discharge.

The following chapters are structured as follows. Chapter 2 presents the experimental arrangements and the outline of divertor effects on impurities. Chapter 3 presents the radial penetration of pulsively injected light-impurity ions. Time development of the radial penetration of pulsively injected carbon ions is investigated using an impurity transport code. Chapter 4 presents the divertor actions which shield the impurity influx, sweep out the impurity ions diffusing from the main plasma column into the remote burial chamber. Chapter 5 presents the divertor actions reducing the plasma-wall interaction caused by diffusing impurity ions, impurity backflow from the burial chamber into the main plasma, suppression of metal impurity production by cooling the scrape-off plasma with light-impurity injection, and the confinement property of metal impurity ions in the plasma. Summary is presented in Chapter 6. In Appendix, radiative cooling capabilities of three gaseous impurities in a tokamak outer edge are presented.

REFERENCES

[1] JENSEN, R.V., POST, D.E., JASSBY, A.L., Critical Impurity Concentrations for Power Multiplication in Beam-Heated Toroidal Fusion Reactors, PPPL-1350 (1977).

[2] STOTT, P.E., DAUGHNEY, C.C., ELLIS, R.A., Nucl. Fusion 15 (1975) 431.

[3] OREN, L., TAYLOR, R.J., Nucl. Fusion 17 (1977) 1143.

[4] NAGAMI, M., SHIMOMURA, Y., MAEDA, H., OHTSUKA, H., SHIHO, M., et al., Nucl. Fusion 18 (1978) 529.

[5] OHASA, K., MAEDA, H., YAMAMOTO, S., NAGAMI, M., OHTSUKA, H., et al., Nucl. Fusion 18 (1978) 872.

[6] EQUIPE TFR, Phys. Rev. Lett. 36 (1976) 1306.

[7] COHEN, S.A., CECCHI, J.L., MARMER, E.S., Phys. Rev. Lett. 35 (1975) 1507.

[8] MESERVEY, E., BRETZ, N., DIMOCK, D., HINNOV, E., Nucl. Fusion 15 (1975) 313.

[9] MEISEL, D., KLÜBER, O., CANNICI, B., et al., in Plasma Physics and Controlled Nuclear Fusion Research (Proc. 6th Int. Conf. Berchtesgaden, 1976), 1, IAEA, Vienna (1977) 259.

[10] EQUIPE TFR, Nucl. Fusion 17 (1977) 1297.

[11] SHIMOMURA, Y., Nucl. Fusion 17 (1977) 626.

[12] MAEDA, H., OHTSUKA, H., SHIMOMURA, Y., YAMAMOTO, S., NAGAMI, M., et al., in Plasma Wall Interaction (Proc. Symp. 1976) Pergamon Press (1977) 537.

[13] YAMAMOTO, S., MAEDA, H., SHIMOMURA, Y., ODAJIMA, K., NAGAMI, M., et al., in Controlled Fusion and Plasma Physics (Proc. 8th Europ. Conf. 1976) 1 (1977) 33.

[14] FIELDING, S.J., HOBBY, M., HUGILL, J., MCCRACKEN, G.M., PAUL, J.W.M., et al., ibid. 1 (1977) 36.

[15] IIYOSHI, A., UO, K., in Plasma Physics and Controlled Nuclear Fusion Research (Proc. 5th Int. Conf. Tokyo, 1974) 3, IAEA, Vienna (1975) 619.

[16] MOTOJIMA, O., IIYOSHI, A., UO, K., Nucl. Fusion 15 (1975) 985.

[17] STOTT, P.E., BURT, J., ERENTS, S.K., FIELDING, S.J., GOODALL, D.H.J., et al., in Plasma Wall Interaction (Proc. Symp. 1976) Pergamon Press (1977) 39.

2. EXPERIMENTAL ARRANGEMENTS

2.1 Description of the Device

DIVA is a tokamak with an axisymmetric divertor. Basic machine parameters are: the toroidal magnetic field 20 kG, plasma major radius 60 cm and plasma minor radius 10 cm. Figure 1 is a photograph of the DIVA. The cross sectional view and the plan view showing the arrangement of the diagnostic system are shown in Fig.2 and Fig.3 respectively. Since most of the components shown are self-evident, a brief description is given in the following only for those un-common in standard tokamaks. More detailed description of the device is presented in Ref.[1]

(1) Shell; The plasma is enclosed in a copper shell devided into four sector pieces. Its surface is ion-plated with gold in 20 μm in thickness to reduce adsorption of gases.

(2) Divertor hoop; A four-turn coil enclosed in a vacuum-tight stainless steel tube. A pair of divertor plates made of titanium intersect the separatrix magnetic surface.

(3) Protection plates; Three gold pieces shown in Fig.2 are manually movable as the protection for the damage of the shell surface.

(4) Gas feeders; The gas can be introduced into the device through four fast acting gas valves at a same time, and additional gas injection can be made with another gas valve in either fast or slow operation mode.

(5) Vacuum system; The vessel is made of stainless steel with an insulating break, pumped by a turbo-molecular pump with an effective speed of 400 l/sec to a base pressure of $1.5\text{-}0.5 \times 10^{-7}$ Torr.

2.2 Diagnostics

2.2.1 Spectroscopies

The spectroscopies used for studying the behavior of impurities are the following:

(1) A 3 m grazing-incidence monochromator (10-1300 Å) equipped with a 600 grooves/mm and 1200 grooves/mm gratings, which are exchangable each other and coated with platinum. The monochromator is calibrated absolutely by means of the atomic branching-ratio method using

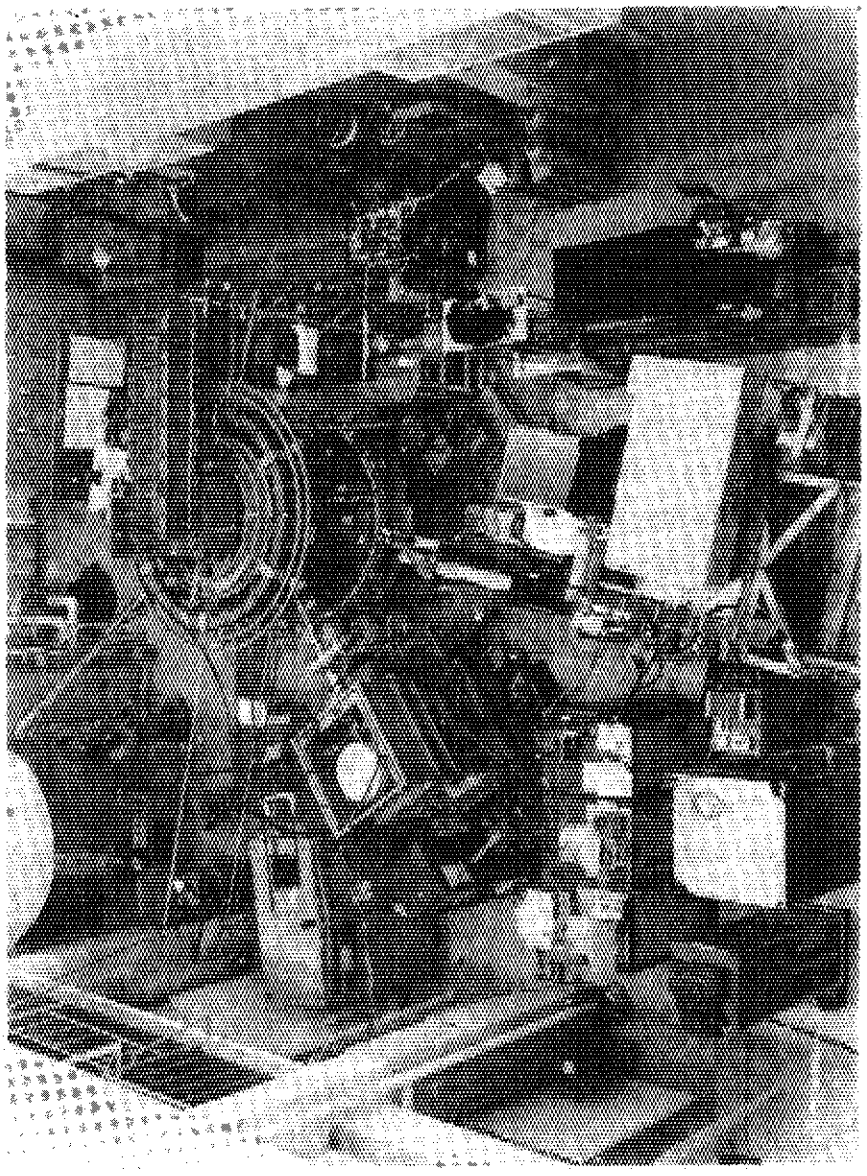

Fig.1 The DIVA tokamak

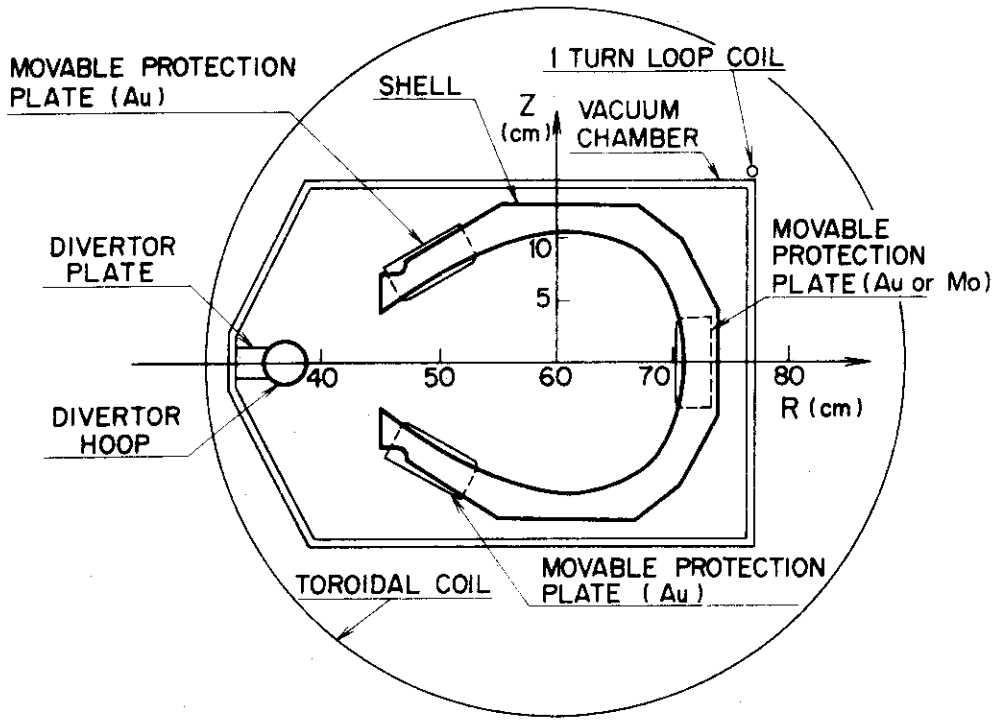

Fig.2 Cross-sectional view of DIVA

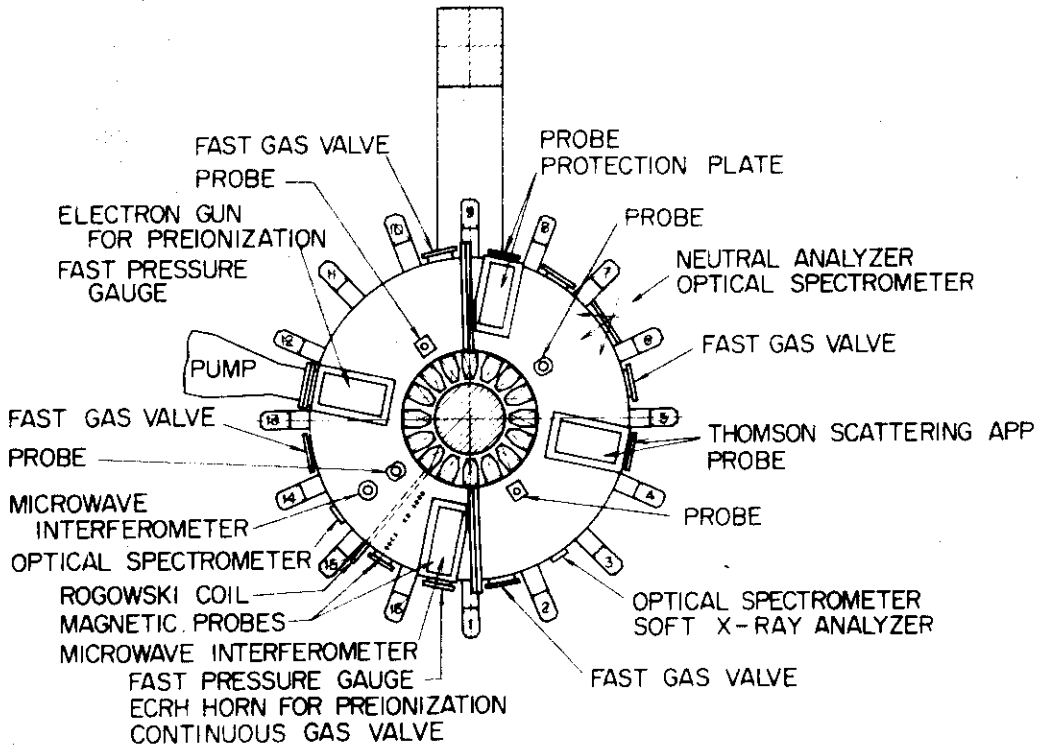

Fig.3 Arrangement of the diagnostic system

suitable line-pairs [2].

(2) 25 cm and 1 m visible and uv monochromators calibrated by means of a standard tungsten ribbon lamp and a NBS-uv hydrogen discharge standard lamp.

(3) A 1 m Czerny-Terner type vacuum monochromator [3].

The arrangements of these monochromators in respective impurity experiments will be presented in the following respective chapters.

2.2.2 Other diagnostics

In addition to conventional measurements of a main plasma such as Thomson scattering, charge exchange neutral-particle energy analysis, soft x-ray energy analysis, and microwave interferometry, the following measurements are employed:

(1) Spacial distribution of radiation loss including charge-exchange loss is measured by a colimated pyroelectric detector. The detector is calibrated by using the radiation from highly resistive discharge [4].

(2) Each particle loss flux onto four sectors of the shell, three protection plates and vacuum chamber are measured as ion saturation current onto each surface.

(3) Langmuir probes, one-directional Langmuir probes, and Faraday cup are used for measurements of electron temperature, ion temperature, and particle flow in a scrape-off layer [5]. Ion temperature of a scrape-off layer plasma is also investigated by measuring Doppler broadenning of impurity lines in the burial chamber.

2.3 Outline of Divertor Effects on Impurities

In this section we briefly describe the effectiveness of the divertor which has been found in DIVA [6,7].

Figure 4 shows oscillograms of typical discharges with and without the divertor in which toroidal magnetic field B_T = 2 T, and plasma current I_p = 40 kA. The plasma density n_e is controlled at the appreciably same value with five fast acting gas valves. In diverted discharge, where the ratio of divertor hoop current I_D to the plasma

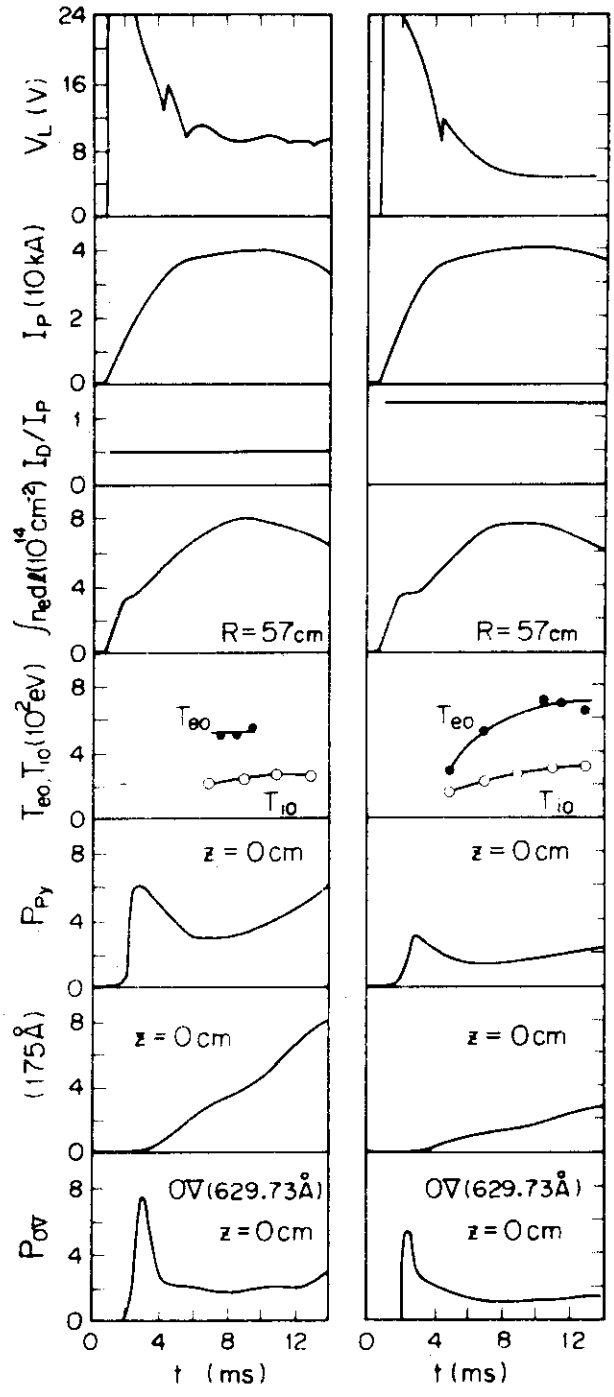

Fig.4 Time behaviours of plasma parameters with the divertor (right side) and without the divertor (left side). V_L: loop voltage, I_p: Plasma current, I_D/I_p: ratio of divertor coil current to plasma current, $\int n_e d\ell$: line density, T_{eo}: center electron temperature, T_{io}: center ion temperature, P_{py}: loss power due to charge-exchange and radiation, intensity of pseudo continuum at 175 Å and P_{ov}: intensity of OV-line (629.73 Å). Toroidal magnetic field is 2T.

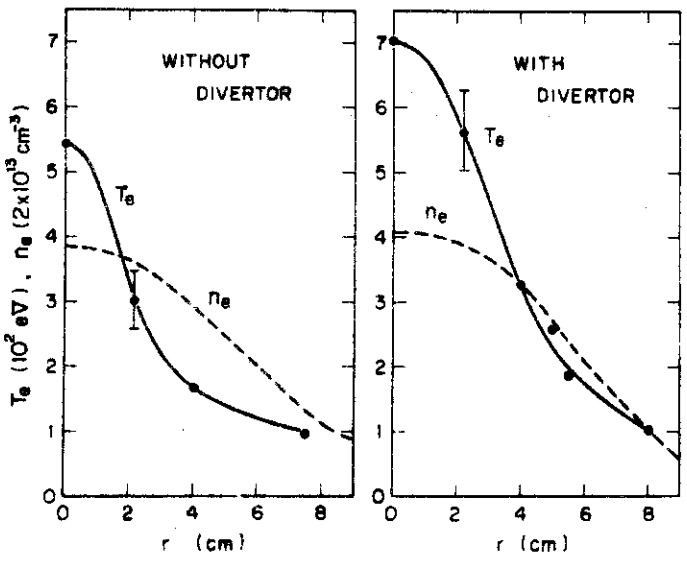

Fig.5 Radial profiles of electron temperature (——) and density (---) with and without the divertor at 9 ms. The discharge conditions are the same as shown in Fig. 4.

current I_p, I_D/I_p = 1.2, the separatrix magnetic surface is located at about 1.5 cm from the shell surface, and 33 % of the particle flux and 75 % of the heat flux diffusing from the main plasma are guided into the burial chamber. In non-diverted discharge, where I_D/I_p = 0.46, no particle and heat fluxes into the burial chamber is observed. The profiles of electron temperature and density are shown in Fig.5. In these discharges, the radiation loss measured by the pyro-electric detector P_{py}, intensity of OV-line (629.7 Å) and intensity of crowded many lines emitted from gold at 175 Å are reduced by a factor of 2-3 by the divertor as are shown in the figure.

Avel-inverted radial profiles of the intensities of pseudo-continuum emission at 100 Å, OVII 21.6 Å, OV 629.7 Å, and P_{py} are shown in Fig.6. It shows that divertor reduces the radiation emitted from metal impurity and oxygen impurity present in the central region of the plasma, and also reduces the oxygen influx in the peripheral region of the plasma.

The radiation loss power investigated over a range of I_p = 8-53 kA, and B_T = 0.8-2.0 T is summarized in Fig.7. In conventional tokamak discharges, the radiation loss power is proportional to the plasma current as are shown by closed circles. By operating the divertor, the radiation loss power is reduced by a factor of 2-4 and is a slowly

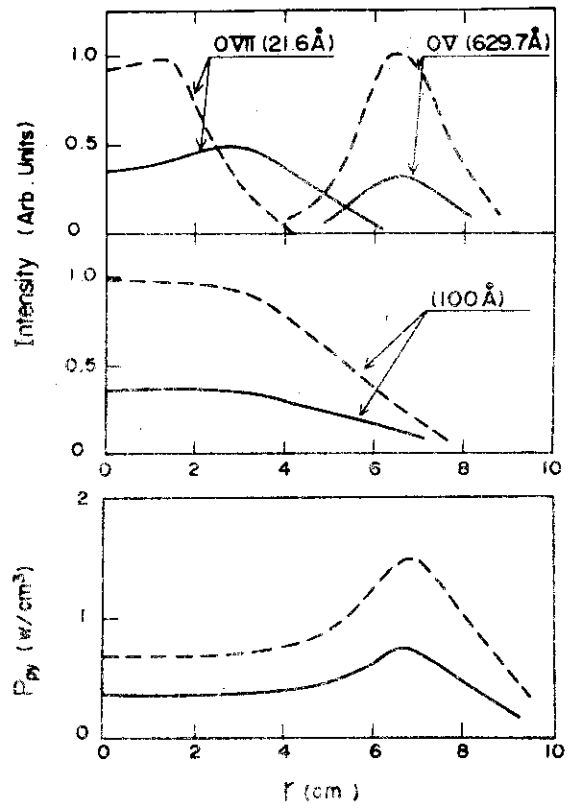

Fig.6 Radial profiles of intensities of OVII (21.6 Å), OV (629.7 Å) and pseudo-continuum at 100 Å and power loss P_{py} due to charge-exchange and radiation with the divertor (——) and without the divertor (---) at 9 ms. The discharge conditions are the same as shown in Fig. 4.

increasing function of the plasma current as are shown by open circles.

In regard to the energy confinement property, divertor increases it by a factor of 2.5. The energy confinement appears to have the functional dependence of the ALCATOR scaling low [8], and is expressed as $\tau_E = 1.5 \sqrt{q_a}\ \bar{n}_{14}$ ms without the divertor, and $\tau_E = 4.0 \sqrt{q_a}\ \bar{n}_{14}$ ms with the divertor, where q_a is the safety factor at the plasma surface and $\bar{n}_{14} = 10^{-14}\ \bar{n}_e$. This improvement can be considered as a result of lowering the radiation loss with the divertor. Because, although the radiation loss power is not a large portion of the total energy loss (30-40 % of the ohmic power without the divertor, and 15-30 % with the divertor), electron temperature profiles, however, are strongly affected by the radiation power, as is shown in the Fig.5. Therefore it can be said that divertor increases the radius of the hot column by reducing the radiation loss, thereby increases the energy confinement time.

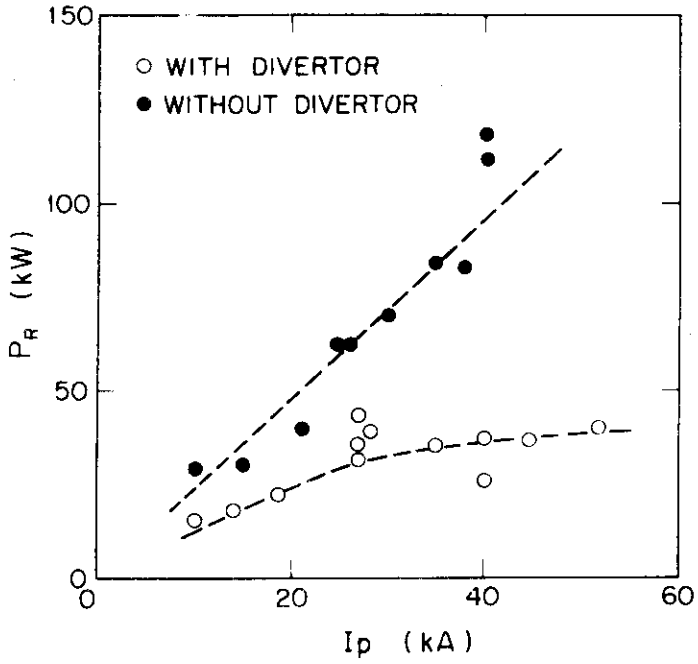

Fig.7 Radiation loss power vs. plasma current I_p. In conventional tokamak discharges, the radiation loss power is proportional to the plasma current. By operating the divertor, it is reduced by a factor of 2 to 4, and is a slowly increasing function of the plasma current.

REFERENCES

[1] SHIMOMURA, Y., MAEDA, H., KITSUNEZAKI, A., NAGASHIMA, T., OHTSUKA, H., et al., An Outline of the JFT-2a device, JAERI-M 6135 (1975).

[2] KASAI, S., FUNAHASHI, A., KONOSHIMA, S., NAGAMI, M., SUGIE, T., MORI, K., Japan. J. Appl. Phys. 17 (1978) 1625.

[3] SUGIE, T., TAKEUCHI, H., KASAI, S., FUNAHASHI, A., TAKAHASHI, K., KIMURA, H., J. Phys. Soc. Japan 44 (1978) 1960.

[4] SHIHO, M., ODAJIMA, K., SUGIE, T., MAEDA, H., KASAI, S., et al., Spectroscopic and Bolometric Measurements of Radiation Loss in DIVA, JAERI-M 7397 (1977).

[5] KIMURA, H., NAGAMI, M., YAMAMOTO, S., UEDA, N., OHTSUKA, H., et al., Diagnostics of a Scrape-Off Layer Plasma, JAERI-M 6971 (1977).

[6] YAMAMOTO, S., MAEDA, H., SHIMOMURA, Y., ODAJIMA, K., NAGAMI, M., et al., in Controlled Fusion and Plasma Physics (Proc. 8th Europ. Conf. 1976) 1 (1977) 33.

[7] DIVA GROUP, Divertor Experiment in DIVA, to be published in Nucl. Fusion.

[8] APGAR, E., COPPI, B., CONDLHALKER, A., HELAVA, H., KOMM, D., et al., in Proceedings of the Sixth International Conference on Plasma Physics and Controlled Nuclear Fusion Research, Berchtesgaden, 1976 (IAEA, Vienna, 1977), Vol.1, 247.

3. LIGHT-IMPURITY TRANSPORT

3.1 Introduction

The transport of light-impurity ions, present in a peripheral region of the tokamak plasma, is of especial importance, because 1) light-impurities may protect the materials nearest to the plasma from dangerous plasma-wall interactions by the intensive radiative cooling in the outer edge region, and 2) from that we can easily obtain the penetration process of impurity ions from the outer edge region to the plasma center, although for the metallic impurities it is difficult to obtain that due to the poor spectroscopic data.

DIVA plasma is dominated by collisional effect and is possible to simulate the important transport conditions for impurity ions that will be found at the outer edge of the thermonuclear plasmas. In this chapter we have investigated the process by which impurity ions are transported into the central region of the plasma across the whole minor radius. By employing pulsed gas impurity injection, and in conjunction with visible and vacuum ultraviolet spectroscopies, we have been able to measure the radial transport of carbon ions in DIVA plasma. The experimental results are compared with results of a transport code which includes Pfirsh-Schlüter diffusion with a superimposed anomalous diffusion, as well as ionization, recombination and recycling processes.

In Section 3.2 the experimental arrangement and results are presented. In Section 3.3 and 3.4, the computer model is presented, and comparison between experimental results and computational results are discussed. The conclusion is presented in Section 3.5.

3.2 Experimental Results

3.2.1 Experimental Arrangements

In the present experiment, the experimental conditions of the base plasma into which methane gas is injected are as follows: toroidal field is 10 kG, peak plasma current is 14 kA and the ratio of the divertor hoop current I_D to the plasma current I_p is 1.2.

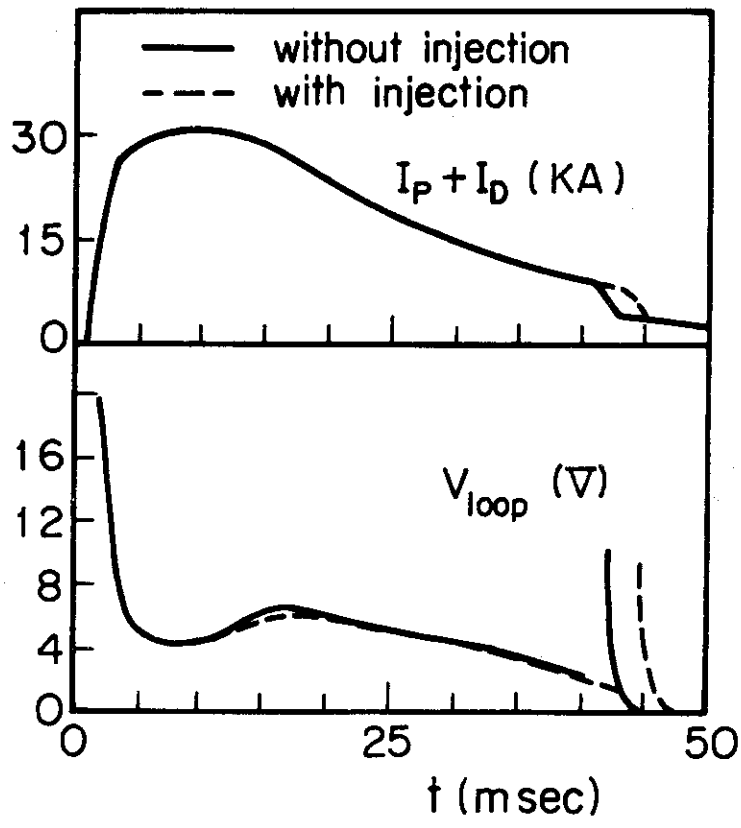

Fig.1 Time behaviour of plasma current I_P plus divertor hoop current I_D and of loop voltage.

Figure 1 shows the time dependence of plasma and divertor hoop currents and of the loop voltage. A five-channel 4-mm microwave interferometer is used to measure the line-integrated electron density profile. In the stationary state (7-12 ms) with which we are concerned in the present experiment, the averaged electron density is 0.9×10^{13} cm^{-3}, and its radial profile is approximately parabolic. A Thomson-scattering measurement of the electron temperature shows that the electron temperature at the centre is about 200 eV and the profile is approximately the square of a parabola.

Electron temperature and density 1.5 cm from the shell surface were measured, by Langmuir probes, to be 30 eV and 1×10^{12} cm^{-3}, respectively. The ion temperature in the central region of the plasma measured by a neutral particle analyser is 70 eV. The global confinement time of the protons estimated from H_α measurement [1] is 1.4 ms, which also coincides within a factor of two with the value estimated from the total ion saturation current to the shell surface.

In the present discharge of I_D/I_P = 1.2, the separatrix magnetic surface is located at about 1 cm from the shell surface, and the particle flux guided to the burial chamber is about 10 % of the total particle flux which diffuses from the main plasma. A large portion of the total proton loss flux consists in direct recycling at the gold-plated shell surface [2]. With these facts, in the present paper, we assume that the presence of the scrape-off layer which guides charged particles to the burial chamber can be neglected. Using the electron temperature profile and the loop voltage and assuming a constant value of Z_{eff} in space, we calculate Z_{eff} to be 2-3, where Z_{eff} is the effective ion charge in the Spitzer conductivity. In standard discharge conditions in DIVA, the oxygen and carbon content is 1 % or less of the electron density as ascertained by spectroscopic measurements. This is due to the fact that the inert gold surface eliminates the light-impurity contamination of the plasma. Although, in the methane injection experiment, the intrinsic carbon contamination grows to 3 % of the electron density in the central region, a sizeable fraction of Z_{eff} is accounted for by metallic impurities since resistivity and radiation losses, which are measured by a pyro-electric detector, are not changed when the amount of light impurity is reduced to half of its value by flashing titanium on about half of the divertor chamber [2].

The methane injection experiment is performed in the following manner. Through the gas inlet which is located at the outer position in the major radius of the copper shell, pulsed methane gas (pulse duration 1.5 ms) is injected at 7 ms, just at the beginning of the plateau in the loop voltage. Discharges with and without injection are made alternately and in about 60 shots, the reproducibility of the emissivity of each spectral line is fairly good.

The injected methane gas penetrates into the plasma before it is ionized. The ionization process continues as the ions rapidly circulate along the field lines and, less rapidly, move across them. At a position 45° apart in toroidal direction from the gas inlet, the time evolutions of the line integrals of the emissivity for different carbon ionization states are measured along the chords of the minor cross-section by using an absolutely calibrated visible monochromator. Observations are made of the CV 2271 Å, CIII 2297 Å and H_α lines with a spatial resolution of

1 cm. Assuming that the non-circular effect is negligible, these signals are Abel-inverted, and the impurity ion density and proton particle birth strength are unfolded from the photon signals.

3.2.2 Discharge without Methane Injection

The time evolution of the line integral across the minor diameter of photon signals of the CV 2271 Å and CIII 2297 Å lines, and of the average electron density is shown in Fig. 2 in solid lines.

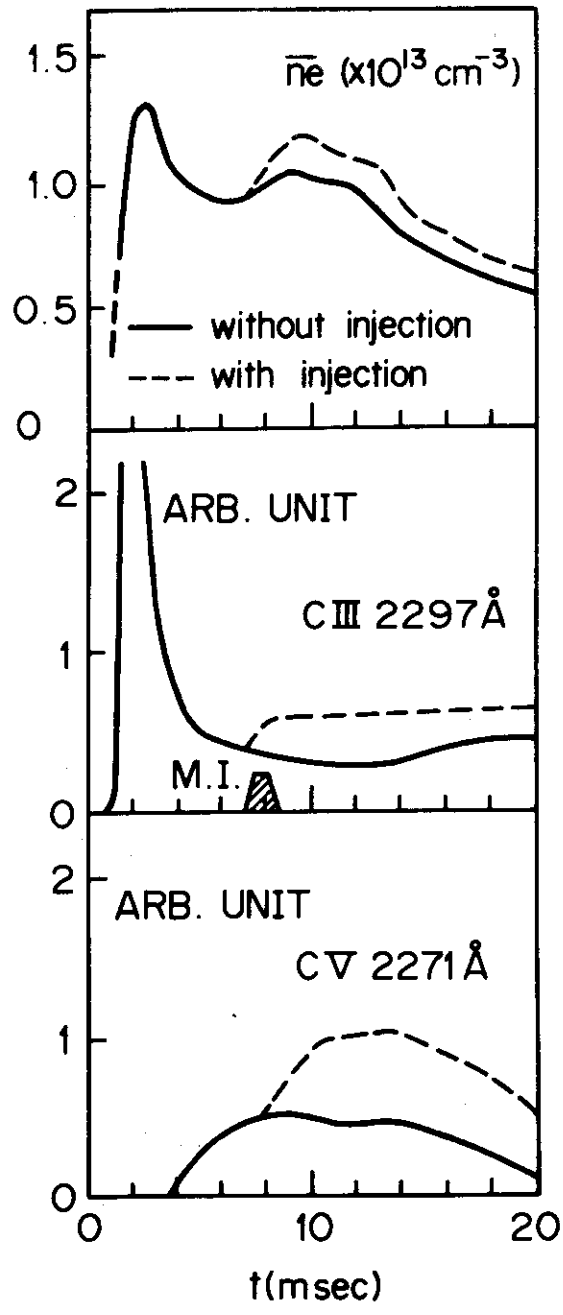

Fig.2 Time behaviour of average electron density $\bar{n}_e$ and line-integrated photon emissions of CIII 2297 Å and CV 2271 Å with and without methane injection (M.I.).

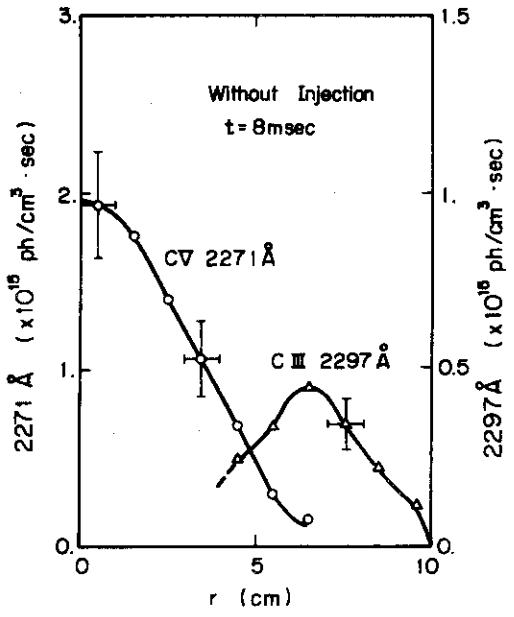

Fig.3 Abel-inverted volume emissions of CIII 2297 Å and CV 2271 Å in the stationary state.

Figure 3 shows Abel-inverted plasma volume emissions of CIII 2297 Å and CV 2271 Å lines at 8 ms. Radial profiles of these photon emissions and the electron density are almost stationary within 10 % from 7 ms to 12 ms in the course of the discharge.

In this stationary state, the peak densities of CV and CIII are deduced from the photon emissivities with the additional knowledge of the radial profiles of electron temperature and density. By using modified coronal models for beryllium-like and helium-like ions given in Ref. [3], the peak densities of CIII and CV are calculated to be 3×10^{10} cm^{-3} (including ^3P metastable state) and 4×10^{11} cm^{-3}, respectively, with an uncertainty, we estimate, of a factor of 2. Using a grazing-incidence VUV monochromator, we observe the line integral of photon signals in the midplace across the minor cross-section. With this measurement, the CVI 34 Å line emissivity is too weak to detect so that the CVI population is estimated to be lower by, at least, a factor of 2 than the CV population. Thus, in the present discharge, a major part of the carbon ions are in the CV state in the central region of the plasma, and the total number of carbon ions in the plasma is almost constant during the period concerned.

Calculation of the ionization times for the j-th state of carbon atoms, $\tau_j = 1/(n_e I_j)$, where n_e is the electron density and I_j is the

electron impact ionization rate coefficient for carbon atoms of the j-th state [4], shows that it takes much less than 0.1 ms to ionize CIV, and above 1 ms to ionize CV in the central region of the plasma. Using radiative recombination rate coefficients [5], in the coronal equilibrium for the electron temperature of 200 eV, the ratio of the CVI population to the CV population is calculated to be 120. From the aforementioned facts, we see that experimental observations in the steady state yield results very different from those of the coronal equilibrium state. This indicates that CV ions are confined within a few milliseconds.

From the photon emissivity of CIII, we estimate the neutral carbon flux into the plasma. The same relation as was discussed by Gervids and Krupin and in Ref. [6] is applied here. For an ion of the j-th state, if confinement and recombination times are long enough compared with the ionization time, the neutral-carbon-atom influx Γ is related to the ionization strength of the j-th-state carbon ions of density n_j by

$$\int \Gamma ds = \int n_j n_e I_j dv$$

where the integrations are carried out over the plasma surface on the left-hand side and over the volume on the right-hand side of the equation. When we apply this relation to CIII and use the modified coronal model mentioned previously, the neutral-carbon-atom source in the discharge is directly related to the photon emissivity of the CIII 2297 Å line and is calculated to be 2×10^{19} s^{-1}. When we take 3 % contamination of the electrons of total number of 1×10^{18} in the discharge, the steady state of the total number of carbon atoms accounts for the fact that the effective confinement time of carbon ions is 1.5 ms. This coincides with the proton confinement time and suggests perfect re-cycling of the carbon atoms at the plasma edge.

3.2.3 Discharge with Methane Injection

A total of 1.5×10^{17} molecules of methane gas are injected at 7 ms into the discharge with a pulse duration of 1.5 ms, which is measured in front of the gas outlet without discharge.

In Fig. 2, the time evolutions of the line integral across the

minor diameter of the photon signals of the CV 2271 Å and CIII 2297 Å lines and the electron density are shown by the dotted lines. These can be compared to discharges without injection as is also shown in Fig. 2. The changes in plasma resistivity, electron temperature, pyroelectric detector signal and thermocouple probe signal which measure the heat flow in the outer edge region are small.

As noted previously, in DIVA plasma, the dominant radiative cooling and Z_{eff} value are caused by metallic impurities of supposedly 1 % contamination (maximum) so that an increase in photon emission from carbon atoms by a factor of two with the injection does not appreciably affect the global thermal balance.

Using the ionization cross-section by electron impact given in Ref. [7], the penetration length of methane molecules of room temperature into the outer edge region of the plasma with $n_e = 1 \times 10^{12}$ cm^{-3} and an electron temperature of 30 eV is estimated to be less than 1 cm. Thus, the injected methane molecules are suddenly ionized after the injection and then the ions move along the field lines.

In Figs. 4 and 5 the time evolutions of the radial profiles in the 2297 Å and 2271 Å photon emission densities are shown. The photon emis-

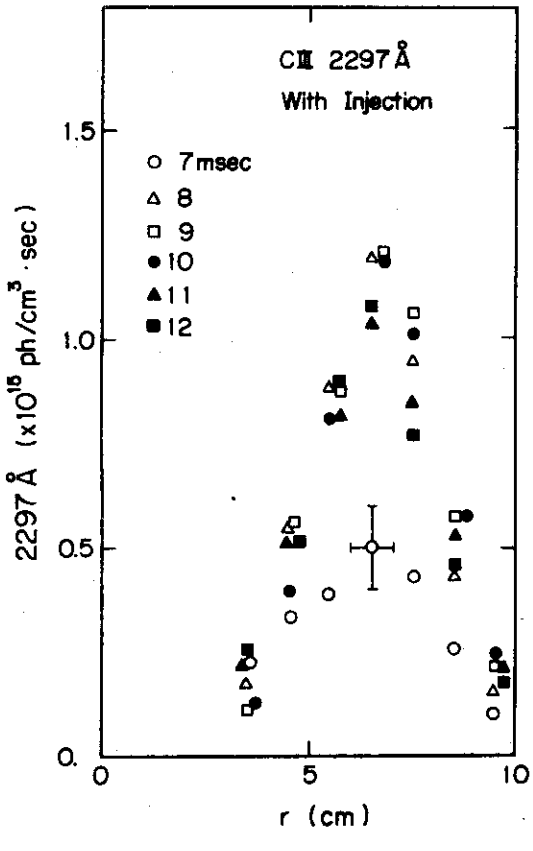

Fig.4 Time behaviour of Abel-inverted volume emission of 2297 Å in the discharge with methane injection.

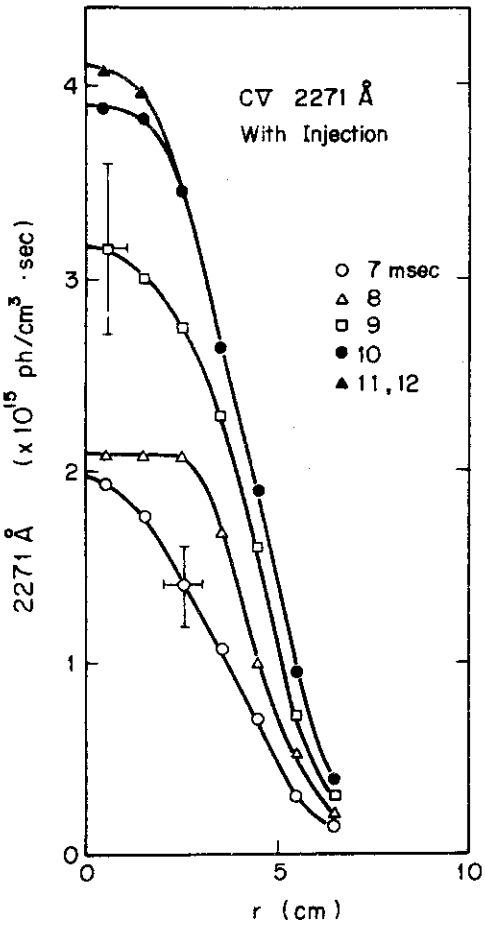

Fig.5 Time behaviour of Abel-inverted volume emission of 2271 Å in the discharge with methane injection.

sion density of 2297 Å rises rapidly just after the beginning of the injection, and then, within 1 ms, the intensity is doubled and stays in a steady state.

The emissivity of 2271 Å rises rather gradually. The penetration of the injected carbon ions into the central region is accomplished at 10 ms. By t = 10 ms, the CV line emission has doubled and is then in a steady state.

In the course of the penetration of the carbon ions, the 2271 Å line emission in the peripheral region is very weak. We expect, however, that there is an abundant amount of CV ions also in this region, but it does not radiate since the excitation energy for the 2271 Å line (304 eV) is much higher than the electron temperature in this region.

The increase of the CV line emission with the injection shows that additional 3 % (3×10^{16}) carbon are introduced into the discharge, which is only 20 % of the injected carbon atoms, i.e. 80 % of the injected carbon are shielded by the outer-edge plasma.

With the injection, the line-integrated electron density increased about 15 % above the non-injection discharge. Also the ion saturation current to a Langmuire probe in the outer-edge region increased about 10 % with the injection. Although there is no exact way from the n_e data to determine what, carbon or hydrogen, causes the density rise, the increase in electron density (1.5×10^{17}) roughly corresponds to the amount of stripped electrons from successfully introduced molecules ($2 \times 4 \times 3 \times 10^{16} = 2.4 \times 10^{17}$, 4 for hydrogen and 4 for carbon in helium-like state). A possible interpretation for this is that a large fraction of the injected particles is trapped on the surface of the gas outlet, which is made of stainless steel, while they strongly interact with the surface during the injection phase. As a fact which may support this interpretation, after the termination of the discharge, we observe the increase in pressure in the vacuum chamber by re-emission which is much larger than that in the non-injected discharge.

In the following section, we shall study these experimental results by comparing them with calculations obtained from a computer code.

3.3 Computer Calculation

3.3.1 Computer Model

Seeing that the impurity ions are in the Pfirsch-Schlüter regime, and neglecting terms associated with temperature gradients, we can give the cross-field ion flux Γ_α of species α (averaged over a magnetic surface) due to the friction with ions of species β by the following [8]:

$$Z_\alpha \Gamma_\alpha = - \sum_\beta \frac{m_{\alpha\beta} n_\alpha}{\tau_{\alpha\beta}} \frac{(1+2q^2)T}{e^2 B_o^{\,2}} \times \left(\frac{1}{Z_\alpha n_\alpha} \frac{\partial n_\alpha}{\partial r} - \frac{1}{Z_\beta n_\beta} \frac{\partial n_\beta}{\partial r} \right)$$

where the collision time has the form

$$\tau_{\alpha\beta} = \frac{3\sqrt{m_{\alpha\beta}}\, T^{3/2}}{4\sqrt{2\pi} Z_\alpha^{\,2} Z_\beta^{\,2} n_\beta e^4 \ell n \Lambda}$$

$$m_{\alpha\beta} = \frac{m_\alpha m_\beta}{m_\alpha + m_\beta}$$

n, m, Z are the density, mass and charge number of each species, and T, q, B_0 are the temperature of protons, safety factor and toroidal magnetic field. The different ion species are assumed to have temperatures equal to the proton temperature.

Besides the classical diffusion flux described above we also take account of some anomalous transport processes, which may affect the impurity transport in DIVA, i.e. we try to simulate the impurity transport by introducing, in addition to the classical flux, an anomalous diffusion flux, which may phenomenologically describe possible anomalous processes, i.e. turbulent diffusion due to micro-instabilities or MHD fluctuation, convection along broken field lines, etc.

As a clue for the magnitude of the anomalous diffusion to be employed in the calculation, we note the proton confinement property. Since, for protons, the diffusion caused by collisions with light impurity ions of a few percent contamination is quite insignificant compared with that due to anomalous processes, it seems to be quite plausible to assume an anomalous diffusion coefficient of impurity ions of the order of the diffusion coefficient inferred from proton confinement in the experiment.

Thus, in the present calculation, we assume that the anomalous diffusion coefficient of the impurity ions is the same as that of the protons.

Thus the continuity equations for ions can be written as

$$\frac{\partial n_\alpha}{\partial t} = -\frac{1}{r}\frac{\partial}{\partial r}(r\Gamma_\alpha) + S_\alpha$$

For the protons, we have:

$$\Gamma_p = -(D_a + \Sigma \frac{n_k Z_k^2}{n_p} D_c)\frac{\partial n_p}{\partial r} + D_c \Sigma Z_k \frac{\partial n_k}{\partial r}$$

$$S_p = I_p n_e n_H$$

where the summation is taken over all ionized states of carbon impurities, and, for impurity ions, we obtain:

$$\Gamma_j = -[D_a + D_c \left(1 + \sqrt{\frac{m_i}{2m_p}} \Sigma \frac{Z_k^2 n_k}{n_p}\right)] \frac{\partial n_j}{\partial r}$$

$$+ D_c \frac{Z_j n_j}{n_p} \left(\sqrt{\frac{m_i}{2m_p}} \Sigma Z_k \frac{\partial n_k}{\partial r} + \frac{\partial n_p}{\partial r} \right)$$

$$S_j = n_e \left[I_{j-1} n_{j-1} - (I_j + R_{j-1}) n_j + R_j n_{j+1} \right]$$

For charge-limit ions, we have, in particular, (CV in the present calculation):

$$S_j = n_e \left(I_{j-1} n_{j-1} - R_{j-1} n_j \right)$$

Here

$$n_e = n_p + \Sigma Z_k n_k$$

$$D_c = 0.5 \left(1 + 2q^2\right) \nu_p \rho_p^2$$

$$\nu_p = \frac{4\sqrt{2\pi}\, e^4 n_p \ell n \Lambda}{3\sqrt{m_p}\, T^{3/2}} \quad , \qquad \rho_p^2 = \frac{2 m_p T}{e^2 B_0^2}$$

Here, I_p, I_j are the electron impact ionization rate coefficients of the hydrogen and carbon atoms [4], respectively. R_j is the radiative recombination rate coefficient [5].

The hydrogen density n_H in the plasma is calculated by Dnestrovskii's formula [9], but with a correction for geometric effects (cylindrical plasma).

The influx of hydrogen atoms is usually determined by the re-cycling condition at the wall. We include an additional hydrogen flux during the period of methane gas injection. In the calculation, fast neutrals up to the second generation are considered. The density distribution and the influx of impurity atoms are also calculated in a similar way.

The boundary conditions for the diffusion equations are given in the following way:

$$\frac{\partial n_p}{\partial r} = \frac{\partial n_j}{\partial r} = 0 \quad \text{at } r = 0$$

$$n_p = 2 \times 10^{11} \text{ cm}^{-3}, \quad n_j = 0 \quad \text{at } r = r_w$$

where r_w is the wall radius.

As the initial condition for the impurity ions, we take the coronal equilibrium state for the electron temperature of 2 eV.

The coupled conservation equations are integrated by the fully implicit Crank-Nicholson method [10].

3.3.2 Computational Results

In the present calculation, the electron and ion temperatures are given and stationary. The electron temperature is taken as the experimental result. The ion temperature is taken to be parabolic with a maximum temperature of 70 eV. The plasma current distribution is determined by the Spitzer conductivity, on the assumption of a constant Z_{eff} value. The total plasma current is 14 kA, and in this case the q-value is 1.3 on the axis.

As noted previously, in the present experiment, the separatrix magnetic surface is located at a distance of about 1.5 cm from the shell surface. The applicability of Pfirsch-Schlüter theory in this scrape-off layer, where the magnetic field is diverted to the burial chamber, is questionable. Nevertheless, in the present calculation, we simply apply the theory in the whole region of minor radius.

As we have mentioned before, we use the anomalous diffusion coefficient from the experimental observation of proton confinement. From the intensity profile of the H_α line emission and the proton density profile, we can locally estimate the anomalous diffusion coefficient by using the ratio of ionization rate to H_α emission. Taking into account the contamination by 1 % of oxygen up to helium-like state, 3 % of carbon up to helium-like state and at maximum 1 % of gold assuming $Z \sim 10$, we estimate that n_p/n_e is 0.7 ~ 0.8. Since the proton density profile (assuming 0.7 ~ 0.8 of the electron density) is approximately parabolic near the axis, and with the absolute H_α line emission, we

find an anomalous diffusion coefficient of 0.4 $m^2 \cdot s^{-1}$ with an uncertainty of a factor of 2 in the central region of the plasma. On the other hand, measurement shows that the diffusion process in the outer-edge region within 2 cm from the shell surface approximately corresponds to the Bohm value. These values of the diffusion coefficient roughly fit Mercier's semi-empirical expression [11]:

$$D_a = C\ (1 + 1.6q^2)\nu_{ei}\rho_e^{\ 2}$$

if C ~ 300. ν_{ei}, ρ_e are the electron-ion collision frequency and the electron gyro-radius in the toroidal magnetic field. In the calculation, we use this expression as the anomalous diffusion coefficient.

3.3.2.1 The Case of No Injection

To study the dominant transport mechanisms for the impurity ions, we make computations for the following three different cases: (a) neoclassical transport, (b) neoclassical + anomalous transport, and (c) anomalous transport.

Assuming 3 % contamination in total number of particles with carbon impurity, we calculate the steady state of the CV density profile and of the CIII 2271 Å and CV 2271 Å photon emission profiles, which are shown in Fig. 6 with proton density profile (case (b)) and in Fig. 7, respectively.

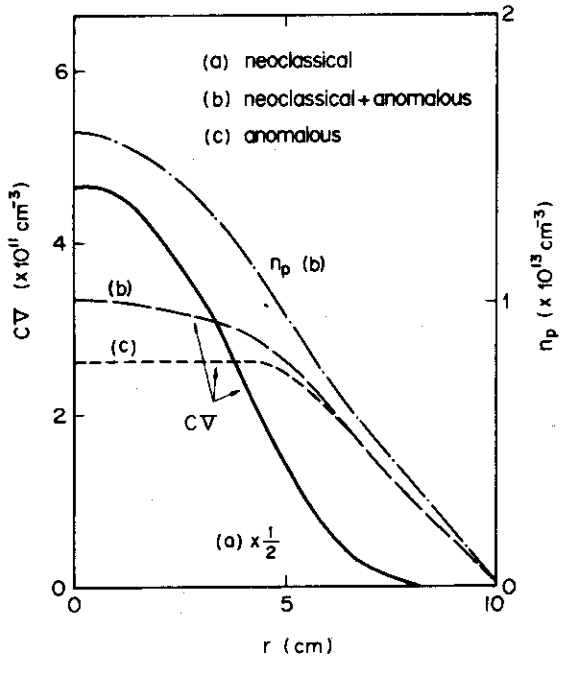

Fig.6 Radial profiles of calculated density of CV and protons in steady state: (a) neoclassical, (b) neoclassical+anomalous, (c) anomalous.

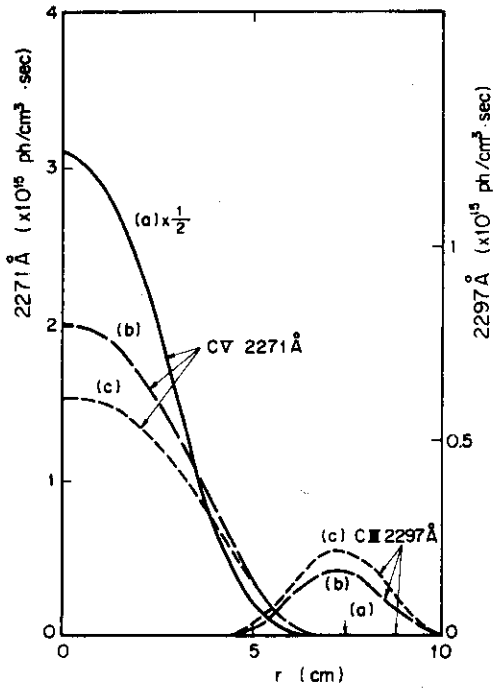

Fig.7 Radial profiles of calculated volume emission of CIII 2297 Å and CV 2271 Å.

As noted previously, since the radial diffusion of protons is dominantly governed by anomalous diffusion, the computational results in the three cases yield almost the same proton density profile, and the proton confinement times are almost the same, i.e. between 1.4-1.6 ms. In these calculations, we took the incoming energy of hydrogen particles as 5 eV and that of the carbon particles as 2 eV, and perfect re-cycling conditions were assumed.

(a) Neoclassical diffusion: When we assume that only the neoclassical theory of impurity diffusion is valid along the whole minor radius, the strong inward force due to friction with protons will sometimes cause imward impurity ion flux from the wall. This physical difficulty can be removed by introducing anomalous diffusion only in the outer-edge region between about 1 cm from the wall. With this assumption, we can study the behaviour of impurity diffusion in the case of neoclassical theory in almost the whole minor-radius region.

As is shown in Fig. 7, in this case, because of the good confinement properties of impurity ions, carbon ions are strongly accumulated in the central region of the plasma, mainly in the CV state. The confinement time of the impurity ions is 28 ms. The impurity ion loss flux and the amount of re-cycling neutral carbon atoms in the edge

region are small compared with cases (b) and (c). The peak value of the CIII 2297 Å photon emission in the minor radius is 9×10^{12} photons$\cdot cm^{-3} \cdot s^{-1}$, although the experimental value is larger by a factor of 50.

(b) Neoclassical + anomalous diffusion: Since, with the present plasma parameters, D_a/D_c is approximately 10, anomalous processes dominate the diffusion of impurity ions. In this case, the impurity confinement time is 1.1 ms, so that it is necessary to consider perfect re-cycling conditions for carbon atoms at the wall surface to obtain a stationary state over a period of several milliseconds. Our assumption of 3 % contamination in the total number of carbon atoms yields good agreement in the CV 2271 Å line emission with the experimental observations in the central region. The peak intensity of the 2297 Å photon emission in the peripheral region is 1.7×10^{14} photons$\cdot cm^{-3} \cdot s^{-1}$, which is within a factor two or three in agreement with the experiment as is shown in Fig. 7.

In Fig. 8, the computed radial density profiles and radial particle fluxes of the individual ionization states are shown. The result shows that carbon atoms are ionized and lost from the plasma mainly in the peripheral region of $r \gtrsim 5$ cm. The result also shows that helium-like

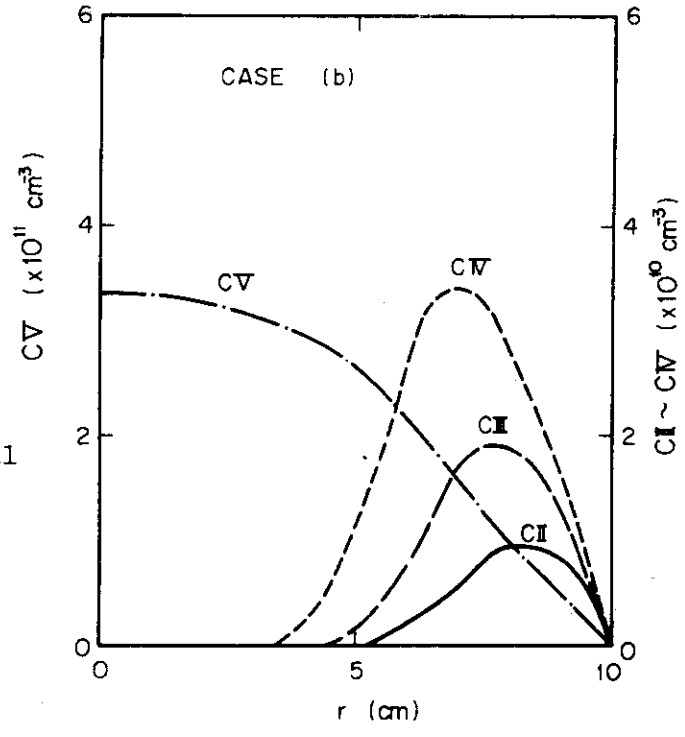

Fig.8(1) Calculated radial density profiles of individual ionized states in the steady state for case (b).

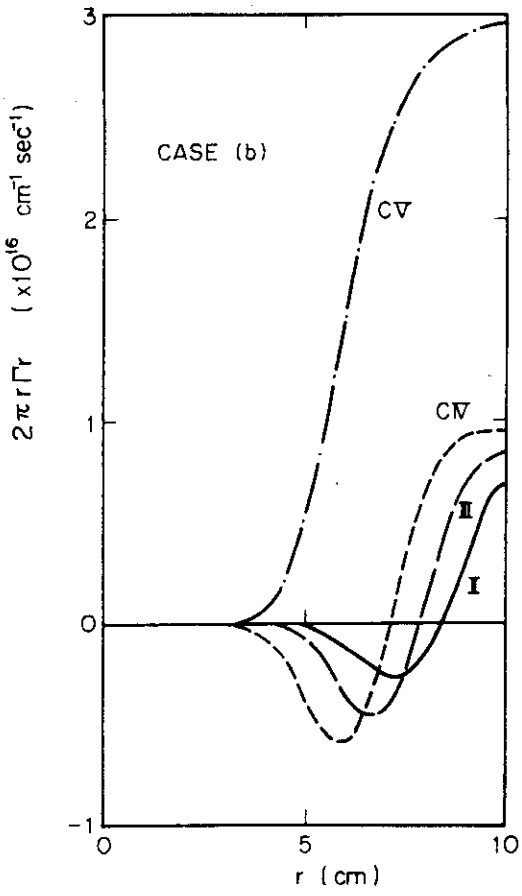

Fig.8(2) Calculated radial particle diffusion fluxes in the steady state for case (b).

CV ions spread to the edge of the plasma since the recombination time of the ions is much longer than the particle confinement time. Although measurement is difficult since helium-like ions have too large an excitation energy to be detected optically in the cold-edge region, the calculation indicates that carbon ions are lost dominantly in the helium-like state.

(c) Anomalous diffusion: In this case, the result is similar to Case (b) as is shown in Figs. 6 and 7, since the anomalous diffusion coefficient is an order of magnitude larger than the classical one. The density distribution of the carbon ions is rather flattened compared with Case (b), i.e. the photon emissivity of the 2271 Å line is decreased and that of 2297 Å line is slightly increased. The confinement time of the impurity ions is 0.8 ms, and the re-cycling flux is increased.

On the basis of what we have been discussing up to now, we see that the experimental observations in the discharge without injection are well described by considering anomalous process and perfect re-cycling.

3.3.2.2 The Case with Injection

In the methane gas injection calculation, we add the injected neutral-particle flux to the recycling flux as noted previously. We take a triangular gas pulse of 1.5 ms duration, which approximately fits the measurement.

In the present calculation, the same amount as is successfully introduced into the discharge in the experiment is taken as the injected number of carbon particles. The hydrogen particle flux is taken to be four times the carbon neutral-particle flux.

The energy of the injected hydrogen particles is forced to be taken as the same value as the re-cycling neutral particles, since our code includes only one energy spectrum for the cold-neutral-particle flux into the plasma. However, since the increase in proton and electron density with the injection is small and the re-cycling process is fast, this assumption will not change the impurity behaviour appreciably. For the influx of neutral impurity particles, our code includes two energy spectra and we can take the room temperature for the injected neutral carbon particles. Since the injected neutral impurities are ionized mostly in the outer-edge region and the re-cycling process is very fast, the computed result is not changed appreciably with injection energy below 2 eV.

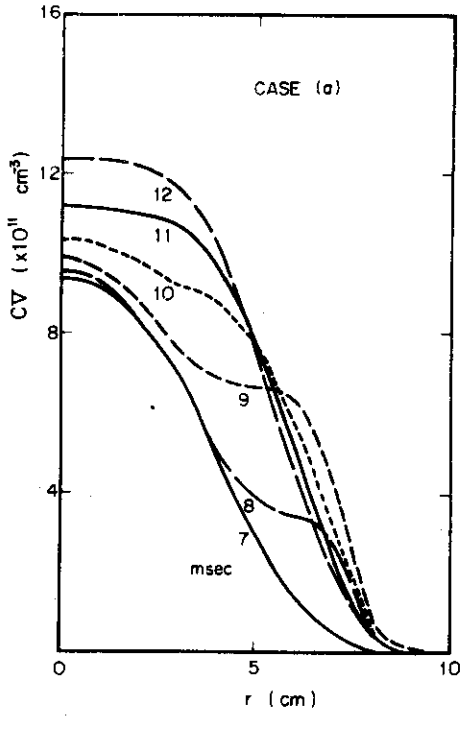

Fig.9(1) Calculated re-arrangement of CV density profiles after methane injection. The accumulation still continues at 12 ms.

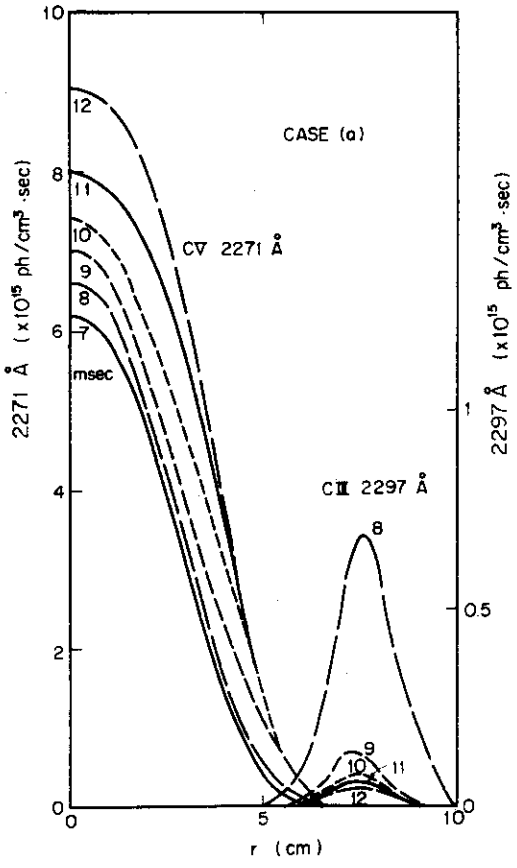

Fig.9(2) Calculated evolutions of volume emission of CIII 2297 Å and CV 2271 Å after methane injection.

With the above noted procedure, three diffusion model cases as previously examined are carried out:

(a) Neoclassical diffusion: With the gas injection, the injected neutral carbon atoms penetrate about 1 cm into the plasma before being ionized. The ionization process continues as the ions are lost or transported towards the central region of the plasma. In Fig. 9 (1), the calculated evolution of the density profile of CV is shown. It shows that the ions present in the peripheral region at 8 or 9 ms are collected towards the central region rather gradually, and this inward diffusion still continues at 12 ms.

A slight increase that can be found at the centre at 8 ms does not show the penetration of the injected impurities, but the still prevailing rearrangement of the radial profile near the central region. It takes a much longer time to reach the exact equilibrium state for the neoclassical diffusion case than for the anomalous case, especially in the central region.

A large discrepancy with the experimental results is found in the time development of the CIII line emissivity. As is shown in Fig. 9 (2),

with the injection, the photon signal rises rapidly and then declines soon after the period of finishing the injection. This is due to the strong inward diffusion of the carbon ions. In the injection phase, the CIII line emissivity grows up to 7×10^{14} photons$\cdot$cm$^{-3}\cdot$s^{-1} at 8 ms, and then decreases to 5×10^{13} photons$\cdot$cm$^{-3}\cdot$s^{-1} at 12 ms. In 2271 Å emission, we also find a discrepancy, i.e. strong increase in the central region is still observed at 12 ms, although in the experiment the penetration is accomplished before this period. Thus, all the computed results are much different from the experimental observations.

(b) Neoclassical + anomalous diffusion: In this case, the diffusion velocity of the carbon ions of the j-th state is predicted to be (only dominant terms are shown):

$$V_j = - D_a \frac{1}{n_j} \frac{\partial n_j}{\partial r} + D_c \frac{Z_i}{n_p} \frac{\partial n_p}{\partial r}$$

Thus, the self-spreading term by anomalous diffusion is dominant, so that more rapid penetration into the central region than in Case (a) is expected. Figure 10 (1) shows the calculated time development of CV density distribution after the injection. At 2 ms after the beginning

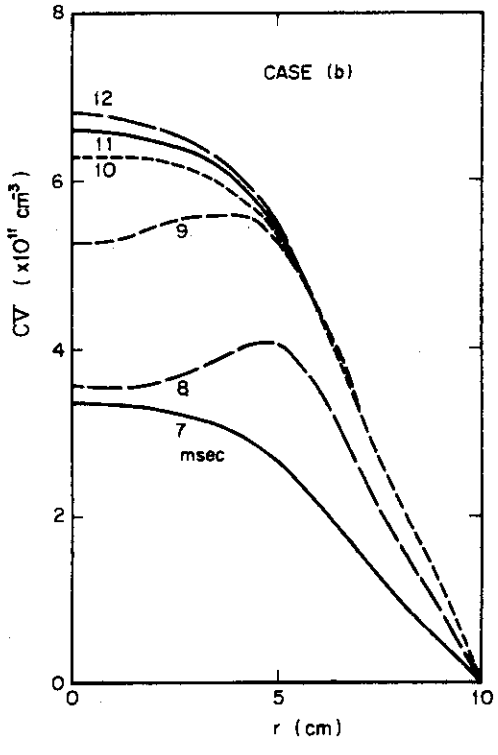

Fig.10(1) Calculated re-arrangement of CV density profiles after methane injection. The arrangement is almost accomplished at 10 ms.

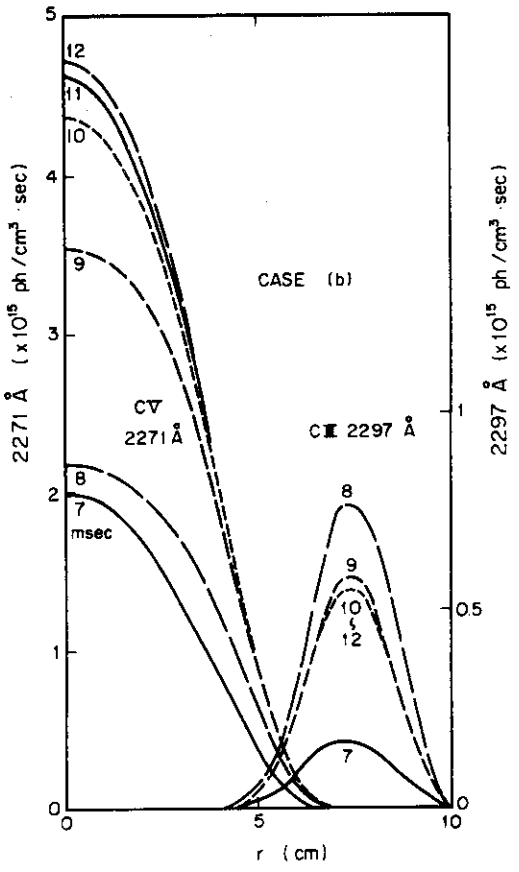

Fig.10(2) Calculated evolutions of volume emission of CIII 2297 Å and CV 2271 Å after the methane injection.

of the injection, a large portion of the injected carbon atoms spreads towards the central region, and, at 10 ms, a new equilibrium state is almost established. In Fig. 10 (2), the time development of the radial photon emission profiles is shown. Good agreement with the experimental observations is found. The 2297 Å line emission suddenly rises with the injection and then stays in steady state at 9 ms. A little overshoot in the emissivity within the injection period (at 8 ms) is probably due to the difference from the experiment in more detailed gas injection process or recycling process.

(c) Anomalous diffusion: Figure 11 shows the computed photon intensity profile with the injection. Similarly to the previous study of the steady-state case, the calculation shows almost the same results as in Case (b). As has been noted in the steady-state case, in the course of the penetration, a tendency of flattening in the profile of carbon ions and intense re-cycling are found.

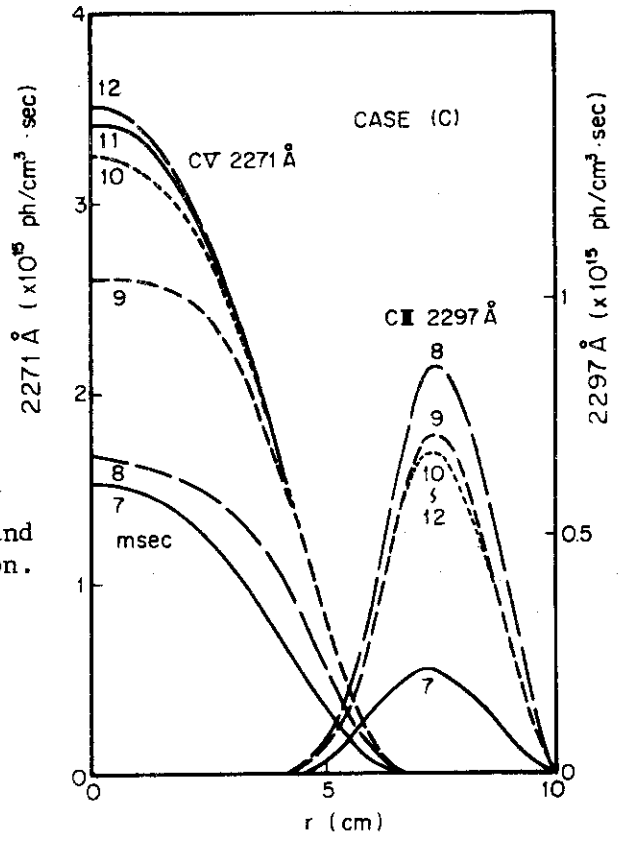

Fig.11 Calculated evolutions of volume emission of CIII 2297 Å and CV 2271 Å after methane injection.

3.4 Discussion

In studying discharges with and without injection, we see that it is necessary to add an anomalous diffusion to the neoclassical one in order to explain the impurity behaviour. Besides the already noted possible anomalous processes that cause a strong spreading effect, we must take into account the spreading effect due to collisions with metal impurities as is expected from neoclassical impurity transport theory.

As noted previously, in the present discharge, a maximum contamination of 1 % by metal impurities is estimated, although its exact amount and radial distribution are not known. Including metal impurities of charge Z_{Mj}, density N_{Mj}, and mass m_M ($m_p/m_M \ll 1$), the radial flux of carbon ions of the j-th state is given by

$$\Gamma_j = -[D_a + D_c \left(1 + \sqrt{\frac{m_c}{2m_p}} \Sigma \frac{n_k Z_k^2}{n_p} + \sqrt{\frac{m_c}{m_p}} f_M \langle Z_M^2 \rangle\right)] \frac{\partial n_j}{\partial r}$$

$$+ D_c \frac{Z_j n_j}{n_p} \left(\frac{\partial n_p}{\partial r} + \sqrt{\frac{m_c}{2m_p}} \Sigma Z_k \frac{\partial n_k}{\partial r} + \sqrt{\frac{m_c}{m_p}} \Sigma Z_{Nk} \frac{\partial N_{Mk}}{\partial r} \right)$$

where

$$< Z_M^2 > = \frac{\Sigma N_{Mj} Z_{Hj}^2}{\Sigma N_{Mj}} , \qquad f_M = \Sigma N_{Mj} / n_p$$

and m_c is the mass of the carbon atom.

Thus, neoclassical theory predicts an additional spreading diffusion and also predicts inward or outword diffusion of carbon ions, its sign being given by the gradient term of the metal impurity density.

If we take f_M and $< Z_M^2 >$ so that $f_M < Z_M^2 > \sim 1$ and assume that the density gradient of the metal impurity is of the order of that of the protons, the spreading term is considered to be rather important. In this case, the spreading effect due to collisions with metal ions is larger by a factor of $\sqrt{m_c/m_p}$ than that with the protons. In the present plasma, the parameter D_a/D_c is approximately 10, so that $0.1\sqrt{(m_c/m_p)}$ (~ 0.35) of the spreading strength by the anomalous diffusion which we have considered is expected to be due to collisions with metal impurities.

If only neoclassical diffusion including speading diffusion due to collisions with metal impurities were considered, the results would change by roughly a factor of 3, i.e. impurity confinement time and radial penetration time of the injected impurity should be increased by a factor of three. It cannot be allowed within the accuracy of the present experiment: confinement time within a factor of two, radial penetration time within 30 %. Thus, the spreading effect due to collisions with metal impurities is not sufficient for an explanation, and anomalous diffusion must be considered.

3.5 Conclusion

We have injected a pulse of methane gas into the DIVA tokamak and measured the transient radial diffusion of injected carbon ions across the whole minor radius. The major part of the injected impurity was shielded by the outer-edge plasma, i.e. only 20 % of the injected carbon were introduced into the discharge. 3 ms after the injection, the radial penetration was accomplished, the accumulation doubled and the

new steady state was sustained over the period of proton confinement time. The transient radial diffusion process of injected carbon was compared with calculations by using a transient code which includes diffusion, ionization, recombination and re-cycling processes. The behaviour of the carbon impurity along the whole minor radius is well described by assuming perfect re-cycling at the gold-plated shell surface and by using neoclassical diffusion superposed by anomalous proton diffusion. It is shown that the radial transport of impurity ions is strongly influenced by anomalous process. The calculated result indicates that carbon ions are dominantly lost in the He-like state.

REFERENCES

[1] JOHNSON, L.C., HINNOV, E., J. Quant. Spectr. Radiat. Transfer 13 (1973) 333.

[2] MAEDA, H., et al., in Plasma Wall Interaction (Proc. Symp. 1976) Pergamon Press (1977) 537.

[3] GABRIEL, A.H., JORDAN, C., "Case Studies in Atomic Collision Physics II, Chapter 4", North-Holland (1972).

[4] LOTZ, W., Z. Physki. 216 (1968) 241.

[5] VON GOELER, S., et al., Nuclear Fusion 15 (1975) 301.

[6] TFR Group, Fontenay-Aux-Roses Report EUR-CEA-EC-777 (1975).

[7] RAPP, D., GOLDEN, P.E., J. Chem. Phys. 43 (1965) 1464.

[8] TUDA, T., TANAKA, M., Japan Atomic Energy Research Institute Report JAERI-M 5376 (1973).
RUTHERFORD, H.P., Phys. Fluids 17 (1974) 1782.

[9] DNESTROVSKII, Yu.N., KOSTOMAROV, D.P., PAVLOVA, N.L., Atomnaya Energiya, 32 (1972) 301.

[10] HOGAN, J.T., Oak Ridge National Laboratory Report, ORNL-TM-5153 (1975).

[11] MERCIER, C., Fontenay-aux-Roses Report, EUR-CEA-FC-812 (1976).

4. IMPURITY SHIELDING AND SWEEPING-OUT BY THE DIVERTOR

4.1 Introduction

In this chapter the following two fundamental divertor actions on the impurity are investigated: shielding of the impurity influx, and sweeping-out the impurity ions diffusing from the main plasma into the burial chamber. For this purpose we have injected a pulse of methane gas and a short burst of aluminum into DIVA plasma at the farthest point from the divertor. Radial diffusion process across the scrape-off layer, and the parallel excursion along the scrape-off field lines into the burial chamber of the injected impurity ions, are investigated with visible and vacuum ultraviolet spectroscopies.

In Section 4.2, the experimental arrangement is presented. In Section 4.3, comparison of the accumulation of the injected impurity in discharges with and without divertor are presented. In Section 4.4, observation of the parallel excursion of the injected impurity ions along the scrape-off field lines is presented. In Section 4.5, the experimental results are discussed. The conclusion is presented in Section 4.6.

4.2 Experimental Set-Up and Discharge Conditions

In the present experiment, the toroidal field is fixed at 20 kG, and no titanium is flashed in the burial chamber.

Figure 1 shows the positions of CH_4 and aluminium injections and the arrangement of the three monochromators. The monochromator system 1 (M.1) consists of 1) a 3-m grazing-incidence vacuum monochromator calibrated by means of the atomic branching ratio method, and 2) a visible and UV monochromator calibrated by means of a standard tungsten ribbon lamp and a standard NBS-UV hydrogen discharge lamp. In a section placed at 45° from the gas inlet in the toroidal direction, this system allows a shot-to-shot vertical scan with a space resolution of 1 cm (VUV) and 1.6 cm (visible and UV).

The monochromator 2 (M.2) is a non-calibrated 1-m Czerny-Terner-type vacuum monochromator, which is placed 135° from the gas inlet. By scanning an aluminium mirror horizontally, the line emission from

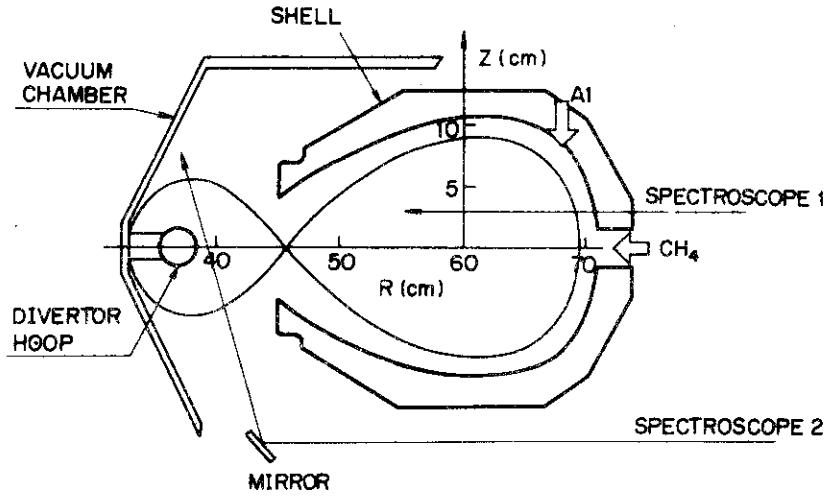

Fig.1 Cross-sectional view of DIVA tokamak and experimental arrangement showing the position of methane and aluminium injections and sight paths of three monochromators. A pulse of methane is injected with a fast-acting gas valve. A short burst of aluminium is produced by means of high-power laser irradiation on an aluminized glass glide. In diverted discharges, 30 % of the particle flux and 70-80 % of the heat flux diffusing from the main plasma are guided into the burial chamber. In non-diverted discharges, no particle and heat flux into the burial chamber is observed.

plasma in the burial chamber and in the inner half of the main plasma is measured with a space resolution of 2 cm.

For an easy comparison of the amounts of injected impurities accumulated, discharges with identical electron temperatures and densities are desirable. For the same plasma current, the same toroidal field and the same average electron density, the electron temperature profiles differ widely in discharges with and without divertor, because the divertor increases the maximum electron temperature and broadens the radial temperature profile [1]. For this reason, discharges with and without divertor, into which the impurities are injected, are set up under the following conditions: for diverted discharges, the plasma current I_p = 30 kA, and the ratio of the divertor hoop to the plasma current I_D/I_p = 1.56; for non-diverted discharges we have I_p = 40 kA and I_D/I_p = 0.46.

With the help of a 2-mm and a 5-channel 4-mm microwave interferometer, the line-integrated electron density profile is measured. The electron temperature profile is measured by means of Thomson scattering and the saft-X-ray energy spectrum. Figure 2 shows the time develop-

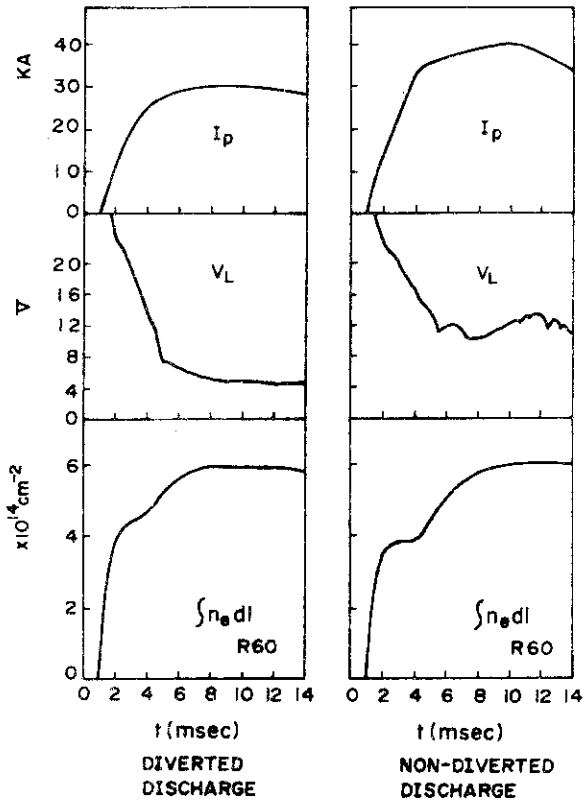

Fig.2 Time development of plasma current I_p, plasma loop voltage V_L, and line-integrated electron density $\int n_e d\ell$ at R = 60 cm for discharges with and without divertor.

ment of I_p, the plasma loop voltage V_L and the line-integrated electron density at R = 60 cm in discharges with and without divertor. Figure 3 shows the radial electron temperature profiles and line-integrated electron density profiles along the major radius for both discharges at the current plateau when the impurities are injected. The peak ion temperatures in both discharges are 200-240 eV.

In diverted discharges, the separatrix magnetic surface is located at about 1.5 cm from the shell surface [2], and 30 % of the particle flux and 70-80 % of the heat flux diffusing from the main plasma are guided into the burial chamber. The scrape-off plasma parameters in the burial chamber are: the peak density in the vertical profile measured by a Langmuir probe is 4×10^{12} cm^{-3}, the peak electron temperature measured by a Faraday cup [3] is 60-70 eV, the ion temperature obtained by Doppler broadening is 80 eV (CV), 40 eV (CIV), and, measured by a Faraday cup, 60 eV. In non-diverted discharges, no

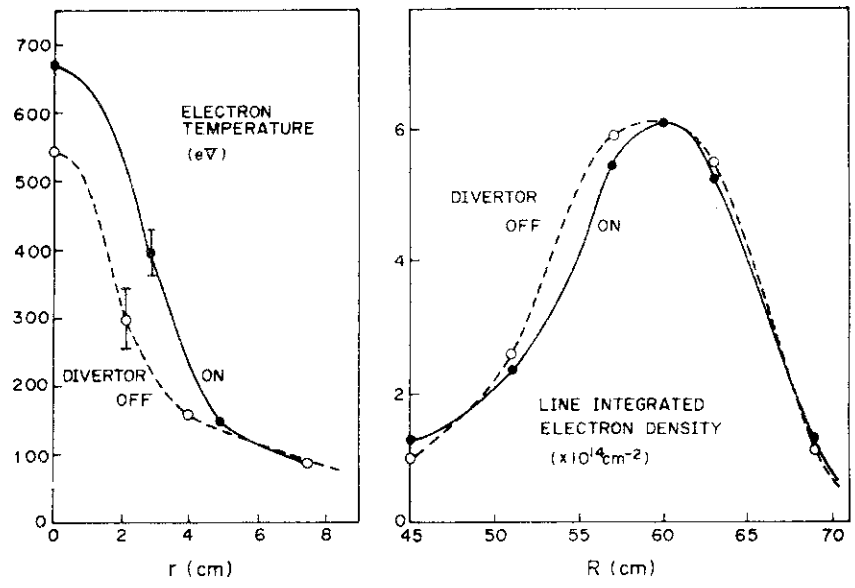

Fig.3 Electron temperature profiles along minor radius, and line-integrated electron density profiles along major radius in discharges with (solid lines) and without (dotted lines) divertor at the current plateau.

particle and heat fluxes into the burial chamber are observed.

The particle confinement time obtained from the ion saturation current to the shells and the burial chamber wall is 2 ms for both discharges.

Figures 4 shows the radial profiles of the line radiations from the intrinsic carbon ions at the current plateau. Solid lines and dotted lines indicate discharges with and without the divertor, respectively. These Abel-inverted volume emissions of CVI 33.7 Å, CV 2270.9 Å, CIII 2296.9 Å are obtained by scanning the M.1 vertically and neglecting the non-circular effect.

Figure 4 shows that, in diverted discharges, the intensity of lines from CIII is reduced by 30 % and that from CV and CVI by a factor of 2 compared to the non-diverted discharges. The line intensities from the CIII ions, which are "burnt" much more rapidly than the time required for their cross-field diffusion, represent the influx of carbon atoms at the outer plasma edge. Therefore, it appears that the impurity influx at the plasma edge is 30 % smaller, and the accumulation of higher ionized impurities in the main plasma is reduced to half of its value by the divertor action. This situation is similar

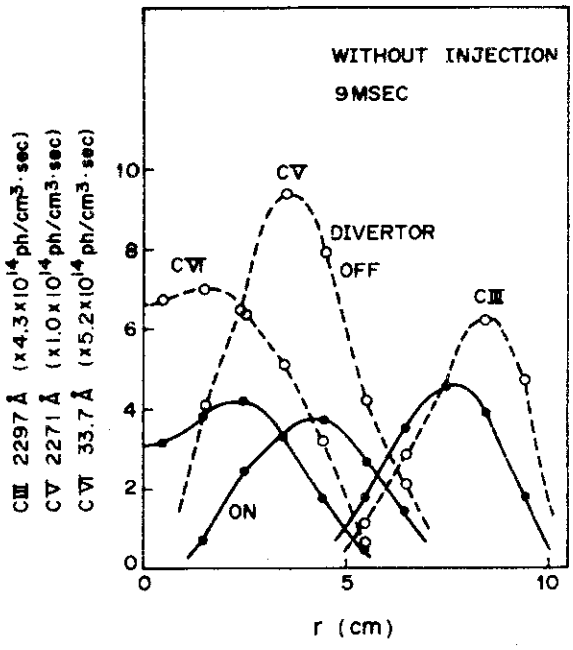

Fig.4 Comparison of line emissivities from ionization states of intrinsic carbon ions for discharges with and without divertor. In diverted discharges, line intensities from oxygen (OV 630 Å, OVI 1032 Å, OVII 21.6 Å) and metal impurities (pseudo-continuum) are also reduced by a factor 2 to 3 with respect to non-diverted discharges.

to one where oxygen and metal impurities are present in the discharge, i.e. in a diverted discharge; line intensities from oxygen (OV 630 Å, OVI 1032 Å, OVII 21.6 Å) and metal impurities (pseudo-continuum emission in the range from 45 Å to 250 Å [4]) are reduced by factor of 2 to 3 with respect to the non-diverted discharge.

Impurities are injected at 5 to 6 ms into the discharge in the following manner: by using a magnetically fast-acting gas valve, 6.3×10^{17} methane molecules are injected, with a pulse duration of 1.5 ms, through the gas inlet placed at the point farthest from the divertor.

A short burst of neutral aluminium atoms with a velocity of 5×10^5 $cm \cdot s^{-1}$ is produced by irradiating a 0.2-μm-thick aluminized glass slide with a 2.6-mm-diameter focused high-power laser spot size. The glass slide is located 6 cm from the outer plasma edge. The velocity of the neutral atoms is deduced from that of the aluminium plasma [5] measured with two Langmuir probes placed in front of the glass slide. Estimated $4 \pm 2 \times 10^{16}$ atoms, probably including some fraction in the form of clusters [6], are directed obliquely to the outer-edge magnetic surface

through a shell gap. The reproducibility of the aluminium injection, deduced from the increase of line emission from the injected aluminium ions in the plasma, lies within 10 %.

The injected impurity atoms penetrate into the plasma before they are ionized. The ionization process continues as the ions move rapidly along the field lines and, less rapidly, move across them. The transport of the injected carbon ions towards the central region of the main plasma is observed by M.1 and M.2, and that into the burial chamber is observed by M.2.

4.3 Accumulation of the Injected Impurities in Discharges with and without Divertor

4.3.1 Methane Injection

With methane injection into the diverted discharge, the increase in plasma resistivity and the total radiation loss measured by a pyroelectric detector [4] are small and less than 15 %. The electron density increases by 15 % and the electron temperature of the main plasma column decreases by 10 %. Since the changes in the plasma parameters are slight, the increase in impurity accumulation with injection is proportional to that of the line intensity. This situation does not change in non-diverted discharges with a methane injection of the same amount.

Figure 5 shows the time development of the increase in line intensities from CIII, CV, CVI for both discharges with methane injections of the same amount. Solid lines refer to discharges with and dotted ones to discharges without the divertor.

Figure 5a shows the injection phase, 1 ms after the gas valve is opened. Almost the same increase in the CIII line emission in both discharges indicates the same amount of additional carbon influx into the plasma edge. This is consistent with the same amount of injected carbon atoms. Figure 5b represents the situation at 2 ms. It shows the radial penetration phase of the injected impurity towards the central region of the plasma. An increase in the CV line emission for both discharges with and without divertor indicates that the impurity influx into the main plasma column is reduced to half to its value by

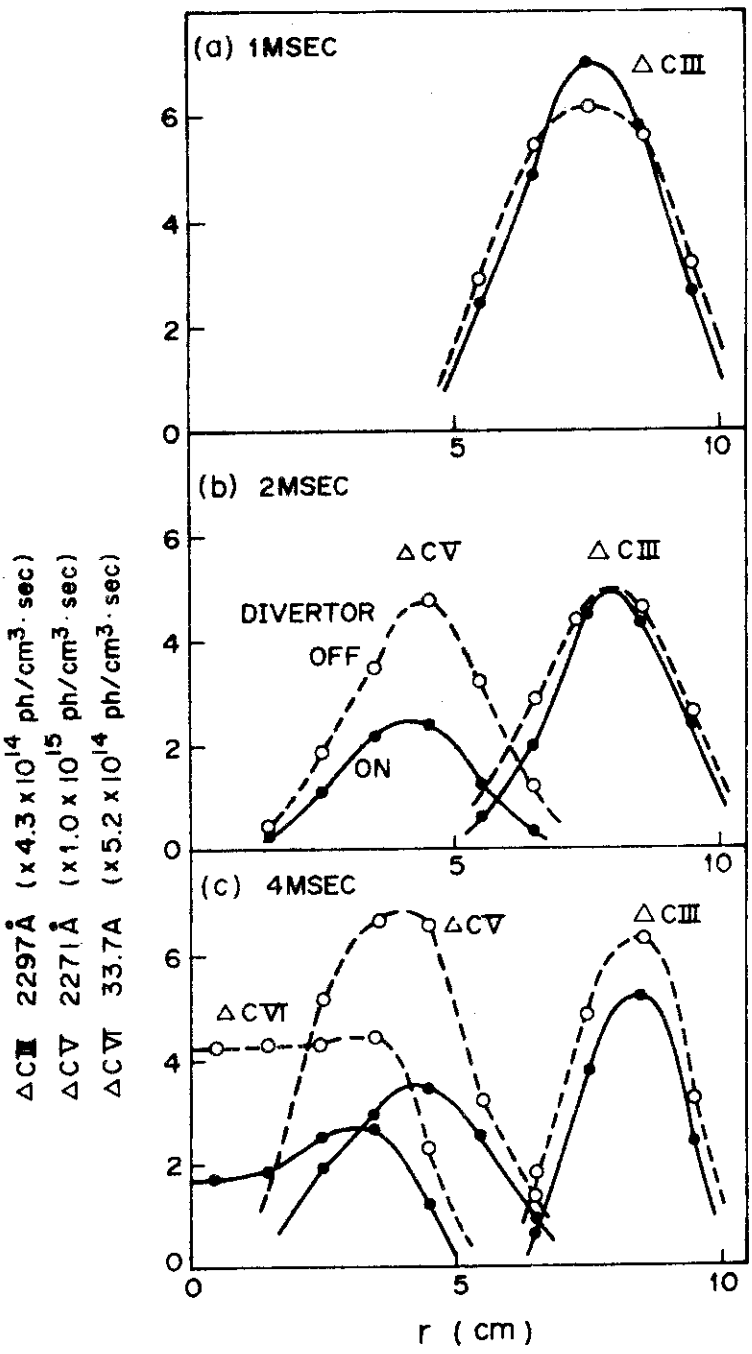

Fig.5 Time development of increase in CIII 2297 Å, CV 2271 Å, and CVI 33.7 Å after start of methane injection: a) during injection phase, b) during radial penetration phase, c) after penetration has been accomplished. Accumulation of the injected carbon ions in the main plasma is reduced to half of its value by the divertor.

the divertor action.

Figure 5c refers to 4 ms when the radial penetration is accomplished. The CVI and CV line emissions are reduced to half of their values in the diverted discharge.

These observations make it clear that the radial impurity influx towards the plasma centre is reduced during the ionization process from CIII to CV by the divertor action. This is apparently due to the magnetic channelling of the scrape-off plasma into the burial chamber and suggests that half of the inward carbon flux is guided into the burial chamber at an ionization state around CIV.

At 4 ms in Fig. 5, the peak densities of the increased carbon ions along the minor radius are: CIII ~ 9×10^{10} cm^{-3}, CV ~ 2×10^{11} cm^{-3}, which are calculated by using the modified coronal model for Be- and He-like ions [7], and CVI ~ 1.7×10^{11} cm^{-3}, which is calculated by using the coronal model and employing the excitation rate coefficient given in Ref. [8]. The ionization time τ_I of CVI in the central region is ~0.3 ms [9]. Therefore, the injected carbon ions are dominantly in the fully stripped state CVII at this time. On the assumption that the increase in n_e with methane injection is due to stripping of ten electrons from each of the injected methane molecules, increase of 15 % in the electron density, for a total number of 3.5×10^{18}, indicates that the total number of accumulated carbon ions is 5.3×10^{16}. By using the CVI density obtained by spectroscopic measurements and the CVII density deduced from the increase in n_e, a rough estimate of the confinement time τ of the CVII ions in the central region can be obtained:

$$\tau = \tau_I \cdot \mathrm{CVII/CVI} \sim 3 \text{ ms}$$

As a result of the injection of 6.3×10^{17} carbon atoms, 8 to 9 % of the injected carbon atoms are accumulated in the plasma. This also indicates that, for non-diverted discharges, approximately 15-20 % of the injected carbon accumulates in the plasma. It appears that a shielding effect against the injected impurities is present even in non-diverted discharges. A possible interpretation of this phenomenon is that a large fraction of the injected particles is trapped near the stainless-steel gas outlet, whereas they interact strongly with the

surface at the outer edge of the plasma during the injection phase. The rest of the carbon atoms spreads along the field lines, diffuses across them and is re-cycled at the gold-plated shell surface. During this process at the outer edge, half of the ions are lost into the burial chamber in diverted discharges.

4.3.2 Aluminium Injection

Since there is no intrinsic content of aluminium ions in the DIVA discharges, the aluminium injection with sufficient line intensity from the accumulated aluminium ions can be performed with no detectable change - above ~ 2 % - in plasma resistivity and electron density.

Figure 6a shows the time evolution of the line integral (across the minor diameter) of photon signals of AlXI 550 Å with an aluminium injection of the same amount for discharges with and without divertor. Figure 6b shows the radial profiles of the corresponding volume emission 3 ms after injection. Solid lines indicate a discharge with and dotted ones a discharge without the divertor.

In both discharges, the signal rises after 600-700 μs from laser irradiation, reaches its peak value at 3 ms and then decays with a 3-5 ms time constant. Since AlXI 550 Å ($\Delta n = 0$ transition) is insensitive to the electron temperature above 20 eV, the signal is proportional to $n_e N_{AlXI}$, where N_{AlXI} is the AlXI density. Therefore, the increase in intensity in Fig. 6a indicates radial penetration of the injected aluminium ions towards the plasma centre, and the decay process reflects ionization up to the AlXII state or diffusive loss towards the wall. In contrast to the case of carbon injection, the signal indicates no continued re-cycling of injected aluminium at the wall. As a result, for diverted discharges, the accumulation of injected aluminium is reduced by a factor of 3 to 4 compared to non-diverted discharges.

The amount of maximum accumulation along the minor radius deduced from the line intensity and the excitation rate coefficient given in Ref. [8] is 2.3×10^9 cm^{-3} for diverted discharges. The ionization time τ_I of AlXI and AlXII in the central region of the plasma is 0.2 ms and 17 ms, respectively, so that the dominant state is expected to be AlXII (He-like state).

Since the line emissivity from the He-like state of the aluminium

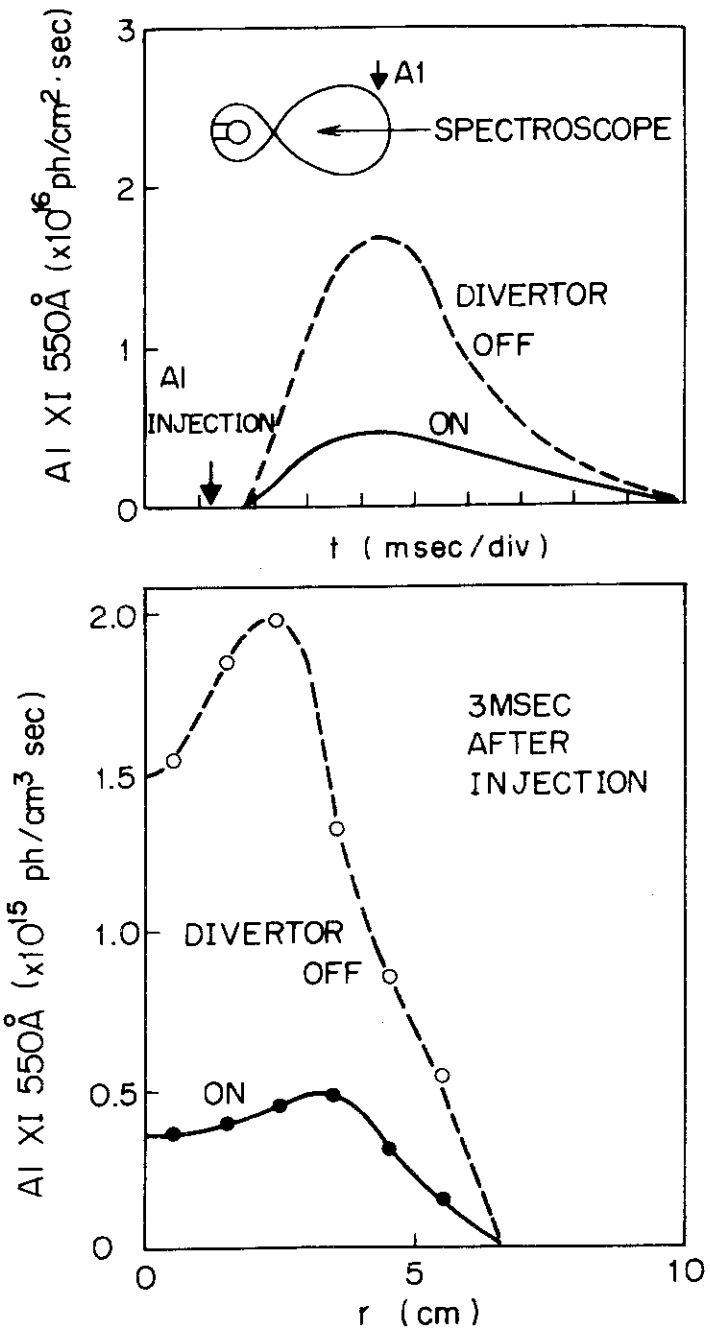

Fig.6 a) Time development of the line integrated emissivity of alXI 550 Å with aluminium injection; b) Abel-inverted volume emission of AlXI 550 Å 3 ms after injection. Accumulation of injected aluminium ions in the central plasma region is reduced by a factor of 3 to 4 by the divertor.

ion is too weak to be detected, the AlXII density is deduced by employing a much higher aluminium contamination, with a detectable change in n_e ($\Delta n_e/n_e$ ~ 7 %) and by assuming that $\Delta n_e = 11\ N_{AlXII}$. With this, and with the spectroscopic measurement of the AlXI density, we obtain that $N_{AlXII}/N_{AlXI} = 22$ in the central region. By using this ratio, we estimate that roughly 2×10^{15} aluminium ions accumulate in the diverted discharge. The confinement time τ of AlXII ions in the central region is $\tau = \tau_I N_{AlXII}/N_{AlXI}$ ~ 4 to 5 ms. Thus, for the injection of $4(\pm 2) \times 10^{16}$ aluminium atoms, with an uncertainty of a factor of 2 to 3, 5 % and 15-20 % of the injected aluminium atoms accumulate in the discharge with and without divertor, respectively.

These results are very similar to those for the case of carbon injection. Possible reasons for the small fraction of penetrating aluminium atoms, compared with methane, might be oblique injection, absence of re-cycling at the wall, or a difference in plasma perturbation due to injection.

4.4 Observation of Parallel Flow of Injected Impurities along the Scrape-Off Field Lines

By scanning the aluminium mirror horizontally in the diverted discharge with methane injection, an increase in the line emissions from the injected carbon ions in the burial chamber and in the main chamber is observed. Figure 7 shows the line-integrated photon emissivity along the two paths indicated in the figure. The solid lines indicate the line emissivities from the intrinsic carbon content and the dotted lines those from the content of injected carbon atoms. In the main plasma, a sudden increase in the CII-CIV line intensities indicates the spreading of the injected impurity ions at the outer edge of the main plasma. As was discussed in Section 4.3, the increase of the CV line intensity mainly indicates cross-field diffusion of the injected carbons towards the hot main plasma.

The appearance of an increase in line emission in the burial chamber is rather interesting. The increase of the CII line emission is very slight. The time behaviour of the increase in the CIII 2297 Å line emission is consistent with the waveform of the methane gas pulse of 1.5 ms duration. The largest increase can be found in the CIV line

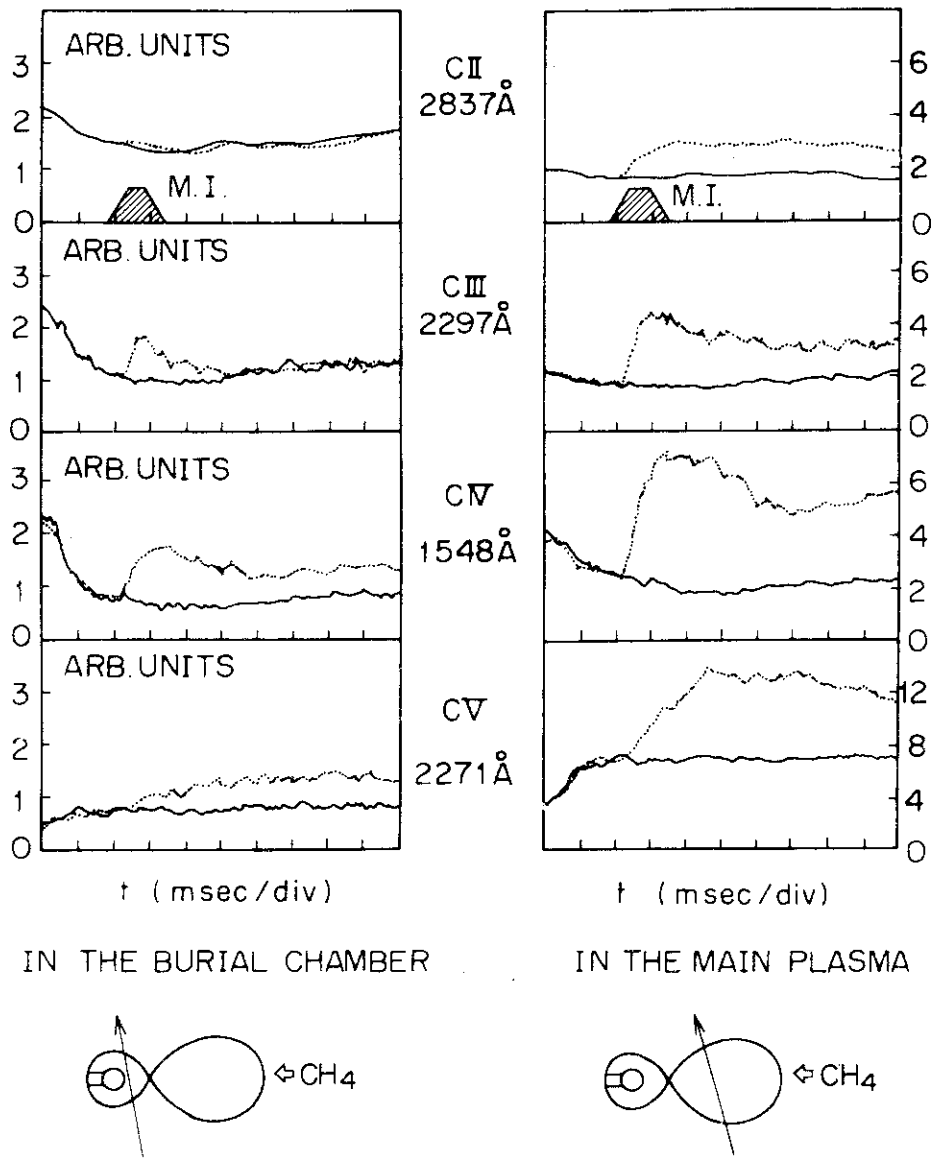

Fig.7 Time development of the increase of line intensity from ionization states of carbon ions in burial chamber and main plasma with the methane injection (M.I.) for diverted discharge.
———: without injection, ...: with injection.

emission. The increase of the CV line emission is not so steep as that in the main plasma.

Figure 8 shows the delay time of the flow front of the injected carbons (in CIII state) at the divertor throat (R = 46 cm). It shows that it takes 300 ± 100 μs to appear in the burial chamber.

These observations in the burial chamber demonstrate the following facts:

1) The fact that there is no increase in the CII line emission in the burial chamber indicates that the observed increase in CIII emission is not due to an ionization of the increased neutral carbon atoms in the burial chamber caused by something other than injected CH_4; that is to say, the injected carbons are ionized successively during their poloidal excursion along the scrape-off layer. Part of them reaches the burial chamber in the CIII state.

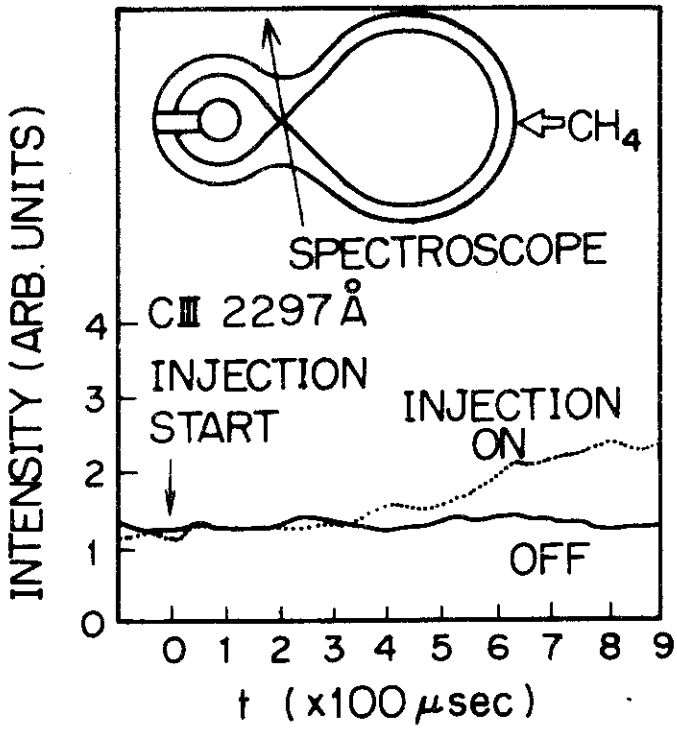

Fig.8 Increase in CIII 2297 Å line emission in the burial chamber with methane injection. The time delay in the increase with respect to the start of the injection represents the time needed for poloidal excursion of injected carbon ions along scrape-off field lines.

2) Although we have not carried out an absolute measurement of the various carbon ionization states in this experiment, the signal suggests that the injected carbon atoms appear in the burial chamber dominantly around the CIV state.

3) The increase in CV line emission in the burial chamber does not, primarily, reflect the direct flow of the injected carbons into the burial chamber along the scrape-off field lines, but the guidance of the diffusive loss flux of highly ionized ions from the main plasma through the scrape-off field lines into the burial chamber.

Now, it seems that the appearance of an injected impurity flow in the CIII-CIV states in the burial chamber corresponds to the vertical observations presented in Section 4.3, i.e. half of the injected impurity influx disappeared during the successive ionization process from CIII to CV.

In addition to this shielding effect brought about by the divertor, we should note the following:

As a result of methane injection, the carbon content of the main plasma is nearly doubled. The loss flux of the carbon ions to the shell surface is also doubled. This is shown in Fig. 7. In this figure, the CII and CIII line emissivities from the main plasma edge, which represent the re-cycling flux at the gold-plated shell surface, increase by a factor of two. This can be recognized from the confinement properties of the carbon ions ($\tau \sim 3$ ms) discussed in Section 4.3. Similarly to this impurity loss flux to the shell surface across the field lines, the increase of the CV line intensity in the burial chamber represents the impurity loss flux in a highly ionized state into the burial chamber through the scrape-off field lines, i.e. a part of the highly ionized impurity outflux from the main plasma is swept out into the burial chamber.

4.5 Discussion

In this section, we focus our interest on the transport of injected carbon ions along the scrape-off field lines into the burial chamber.

The electron impact ionization times of the ionization states of carbon atoms [9] in a scrape-off plasma of an electron density of

$\bar{n}_e \sim 2 \times 10^{12}$ cm^{-3} and an electron temperature of ~60-70 eV are: 4, 20, 100 and 400 μs for CI, CII, CIII, CIV, respectively. The fact that the observed ionization states of the injected carbon atoms in the burial chamber are around the CIV state is consistent with the successive ionization process inferred from these ionization times in the scrape-off plasma during the 300 ± 100 μs of the poloidal excursion time.

The injected carbon atoms are rapidly ionized (~20-30 μs) up to the CIII state at the plasma edge before they can carry out any substantial poloidal excursion. In this ionization state, by collisional heat exchange between the ions ($Z_{eff} \sim 3$), the injected carbon ions are heated up to the bulk ion temperature (~40 eV) with a time constant of 60 μs.

The thermalized CIII or CIV ions undergo many collisions with the bulk ions before they reach the burial chamber at a thermal velocity of v_t; $\pi qR/v_t\tau \sim 8$-15, where τ is the impurity-ion collision time and q (~5) is the safety factor. Therefore, the diffusion process along the scrape-off field lines is dominated by collisional effects. The diffusion time needed for the poloidal excursion is $(\pi Rq)^2/\tau v_t^2 \sim 4$-8 ms. This is longer than was observed experimentally. This seems to attest to the existence of strong directional forces towards the burial chamber. Since the collisional momentum transfer time in the scrape-off plasma is only 60 μs, the injected carbon ions should be accelerated by the bulk scrape-off plasma flow.

The flow velocity of the bulk plasma along the scrape-off field lines in the burial chamber measured by a one-directional probe [3] is 0.2-0.5 C_s, where C_s is the velocity of sound. With this flow velocity, the transit time is $\pi Rq/0.3\ C_s \sim 190$ μs. The observed transit time of the injected carbons is well explained by this velocity. In addition to this collisional process, the transport process of the impurity ions should be affected by the space potential along the scrape-off field lines. Impurity transport including the above-mentioned directional forces and atomic processes in the scrape-off layer is under investigation by a numerical method; the results will be published elsewhere.

4.6 Conclusions

We have injected a pulse of methane gas and a short burst of aluminium into DIVA discharges with and without divertor. The results are as follows:

1) For methane and aluminium injection of the same amount, the accumulation of the injected impurity ions in the main plasma is reduced by a factor of 2 to 4 by the effect of the divertor.

2) In the methane injection for the diverted discharge, the radial impurity flux towards the main plasma centre is reduced during the successive ionization process from CIII to CV. This corresponds to the fact that the ionization states of the injected carbon ion flow into the burial chamber are around CIV. This represents the impurity shielding effect of the divertor.

3) The impurities shielded in the scrape-off layer are rapidly guided into the burial chamber. The time needed for the poloidal excursion of the injected impurities in the scrape-off layer is equal to that of the scrape-off plasma.

4) The impurity ion flux of highly ionized states into the burial chamber increases with the increase of the impurity content of the main plasma. This exhibits the sweeping effect of the divertor, i.e. a part of the impurity ions diffusing from the main plasma is swept out into the burial chamber through the scrape-off layer.

REFERENCES

[1] DIVA GROUP, Divertor Experiment in DIVA, to be published in Nuclear Fusion.

[2] YAMAMOTO, S., SENGOKU, S., KIMURA, H., et al., Nucl. Fusion 18 (1978) 205.

[3] KIMURA, H., NAGAMI, M., YAMAMOTO, S., et al., Japan Atomic Energy Research Institute Report JAERI-M 6971.

[4] SHIHO, M., ODAJIMA, K., SUGIE, T., et al., Japan Atomic Energy Research Institute Report JAERI-M 7432 (1977).

[5] YAMAUCHI, T., OKUDA, T., ISHIKAWA, N., Electr. Eng. Jpn. 95 (1975) 15.

[6] MARMAR, E.S., CECCHI, J.L., COHEN, S.A., Rev. Sci. Instrum. 46 (1975) 1149.

[7] GABRIEL, A.H., JORDAN, C., "Case Studies in Atomic Collision Physics II, Chapter 4" North-Holland (1972).

[8] MEWE, R., Astron. and Astrophys. 20 (1972) 215.

[9] LOTZ, W., Zeitschrift für Physik 216 (1968) 241.

5. PRODUCTION AND CONFINEMENT PROPERTIES OF METAL IMPURITY

5.1 Introduction

As already noted in Chapter 1, divertor reduces the plasma-wall interaction by guiding the diffusing plasma from the main confinement region into the remote burial chamber. Since the sputtering due to the highly ionized ions accelerated by the potential drop between the wall and the plasma is the dominant process in the mechanisms of the metal impurity release [1], the important aspects of divertor operation controlling the plasma-wall interaction are: 1) reducing the impurity flux onto the first wall by guiding the diffusing highly ionized impurity ions from the main plasma into the remote burial chamber, 2) reducing the electron temperature of the scrape-off plasma, which contacts the first wall, due to the large electron heat conduction along the scrape-off field lines, because the potential difference between the plasma and the material surface is determined by the electron temperature.

In this situation, on the other hand, the material surface which contacts a high temperature scrape-off plasma is replaced by a neutralizer plate in the burial chamber, and in this case the impurity efflux from the neutralizer plate becomes the problem. Therefore it is important to investigate the effect of the impurity backflow from the neutralizer plate into the main plasma. If the impurity backflow becomes serious and/or the reduction of metal impurity production at the first wall with divertor operation is not sufficient, then a farther control of plasma wall interaction in the burial chamber and main chamber has to be necessary. One of the methods of additional control of plasma-wall interaction is cooling the scrape-off plasma with light-impurity or cold fuel injection.

In this chapter these methods controlling the impurity origin are experimentally investigated, and then the penetration and confinement property of metal impurity ions in the plasma is investigated.

Section 2 presents the outline of metal impurity in the DIVA plasma. Section 3 presents the observation of impurity flux onto the main chamber wall in discharges with and without divertor, and the impurity backflow from the burial chamber to the main plasma. Section 4 presents the suppression of metal impurity production at the main chamber wall by cooling the divertor scrape-off with light-impurity injection. Section 5 presents the confinement

property of metal impurity ions in the plasma. Section 6 presents the discussions on the experimental observation of the radial transport of metal impurity ions using an impurity transport code. Conclusions are presented in Section 7.

The experimental set-up is almost the same as was described in the previous chapter. In the present experiment, another monochromator and aluminum injection system are added. Figure 1 shows the experimental arrangement.

The monochromator M3, is a 1 m visible and UV monochromator. By scanning a mirror horizontally, line emission from the divertor throat (R = 45 cm, R is the major radius) to the outer edge in the major radius (R = 71 cm) can be observed with a space resolution of 1 cm. For studying the impurity backflow problem, aluminum injections both into the outer edge of the main plasma and the scrape-off plasma in the burial chamber are employed. The aluminum is released from small arc tips and injected into the plasma along the two chords indicated in the figure.

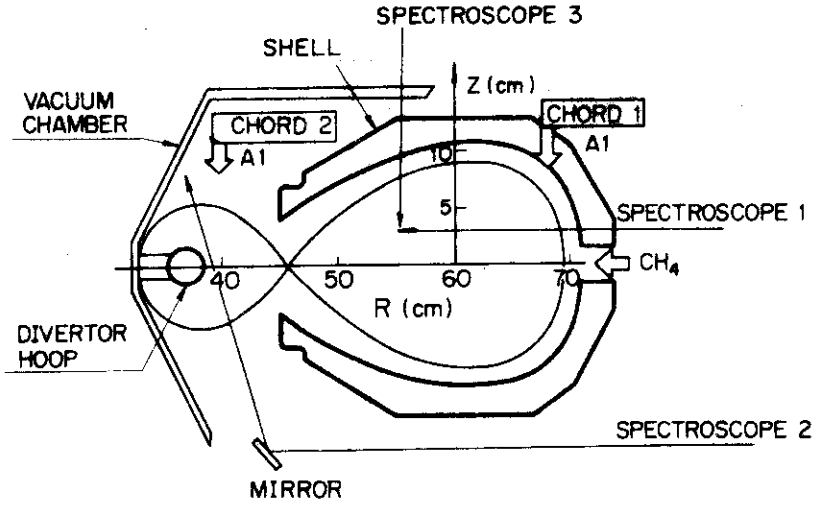

Fig. 1 Experimental arrangement. In the present experiment, the monochromator M-3 and aluminum injection into the scrape-off plasma in the burial chamber are added to the experimental arrangement in the previous chapter.

5.2 Outline of the Metal Impurity in the DIVA Plasma

The radiation spectrum emitted from the DIVA plasma has crowded many lines between 40 Å to 200 Å in 40 kA discharges. The origin of this complex radiation spectrum has been believed to be gold [2], which is the surface material of the first wall and guard limiters, because when the movable shells which are ion-plated with gold is inserted into the scrape-off plasma, this many lines and AuII 1800 Å radiation increase. This is also confirmed from the fact that the emission of many lines (pseudo-continuum emission) increases when a small amount of gold is injected into the plasma by using a ruby-laser blow-off technique [3].

Figure 2 shows the VUV-spectrum at the current plateau of 40 kA discharges with (solid line) and without (dotted line) divertor. A microphotometer trace of the spectrograph in a wavelength region of 10 to 350 Å is shown in ref. [4]. In nondiverted discharge the radiation intensity increases by more than a factor of 3 to 4 especially around 100, 140 and 180 Å. The

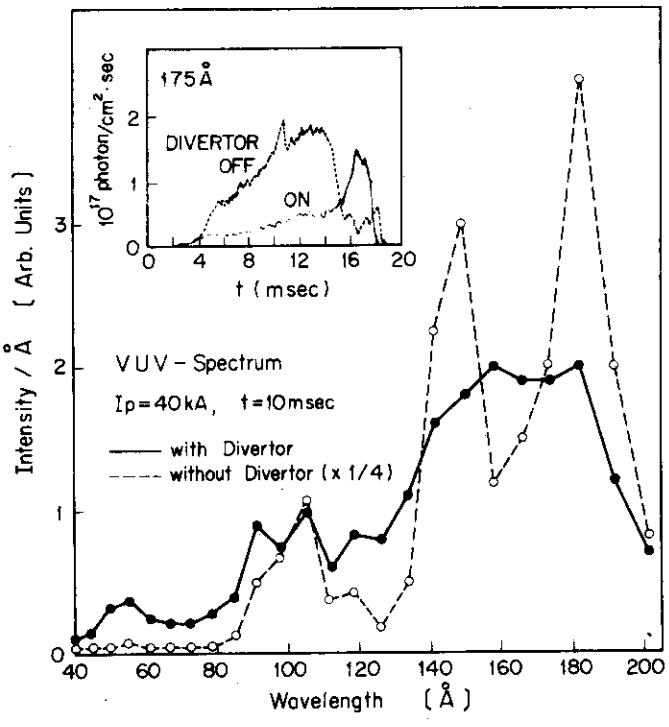

Fig. 2 The wavelength distribution of radiance of the many lines (pseudo-continuum emission) emitted from gold ions in discharges with (solid line) and without (dotted line) divertor.

photon emissivity can be obtained from the absolute sensitivity calibration of the grazing-incidence monochromator presented in ref. [5]. Using this calibration, the radiation power due to the many lines between 40 to 200 Å results in 27 kW in diverted discharge [6].

The amount of gold ions accumulated in the discharge is difficult to estimate because the lack of atomic data on gold ions. However, using the total radiation power emitted from gold ions in coronal equilibrium state calculated with average-ion model [7], and the total radiation power obtained by summing the photon emissivity in the spectral range between 40 to 200 Å, we can estimate roughly that the contamination level of gold ions are 0.05% and 0.15-0.2% of the electron density in discharges with and without divertor respectively.

5.3 Observations of Impurity Flux onto the Main Chamber Wall and Impurity Backflow from the Burial Chamber to the Main Plasma

It is pointed out in ref. [1] that in the plasma condition of DIVA, where the potential difference between the plasma and the vacuum chamber wall is 100-300 V ($\sim 3 \cdot T_e$, where T_e is the electron temperature of the outer edge plasma), sputtering by light-impurity or gold ions is the most possible candidate causing metal impurity release at the first wall. Divertor has the impurity sweeping action that reduces the impurity ion flux diffusing from the main plasma onto the main chamber wall, thereby is capable of reducing the metal impurity production at the wall caused by ion-sputtering. The impurity ion-flow into the burial chamber due to this impurity sweeping action is already observed in the previous chapter. In the present experiment, we investigate the impurity flux onto the main chamber wall by observing the recycling of impurity ions in the plasma outer edge.

Before describing the impurity flux onto the wall (shell surface), the effect of guard limiters must be noted. In the diverted discharge, three guard limiters which are made of gold are inserted at 5 mm from the surface of the shell to prevent the surface from the serious damage caused by such as high energy electrons. We examine the effect of these guard limiters on the plasma contamination by gold. When these guard limiters are extracted from the surface of the shells, no changes larger than 10 % in the pseudo-continuum emission and the plasma loop voltage are observed. This result can be recognized from the following facts: At typical diverted discharge

employed in this work where plasma current 30 kA and I_D/I_P = 1.56, the ion saturation current falling onto these limiters is only 5 % of the total loss flux onto the shell surface, burial chamber wall and guard limiters. Furthermore the electrical potential measured with respect to the burial chamber are almost the same for three limiters and the shells; between -20 to -30 V. This exhibits that the ion current density and accelerating electric field is the same for limiters and shells, therefore it seems clear that gold impurity is mainly released from the surface of the shell.

From the above noted facts and from the uniformity of ion-saturation current falling onto the four sector pieces of shell which are placed in toroidal direction within 20 %, we can assume that the plasma-wall interaction caused by ions hitting the wall surface is uniform in toroidal direction.

For gaseous impurities, the location in the poloidal plane where the highly ionized ions are lost on the chamber wall can be judged by observing the line intensity distribution from lower ionized state ions such as OII or CII in the plasma outer edge, because they make perfect recycling at the gold plated shell surface as was observed in chapter 3, and are proportional to the recycling flux in the plasma outer edge, and also because their excursion in the poloidal plane is small: In the outer edge region of DIVA plasma, where $T_e \sim 70$ kV and $n_e \sim 5\times10^{12}$ cm^{-3}, the mean ionization free path along the field lines with a thermal velocity of 40 eV is 60 cm. This corresponds to a poloidal excursion of 10 degree in a magnetic surface of $q \sim 5$. Unfortunately, the loss flux of gold ions is difficult to observe, because the observation of AuI line emission itself includes the impurity

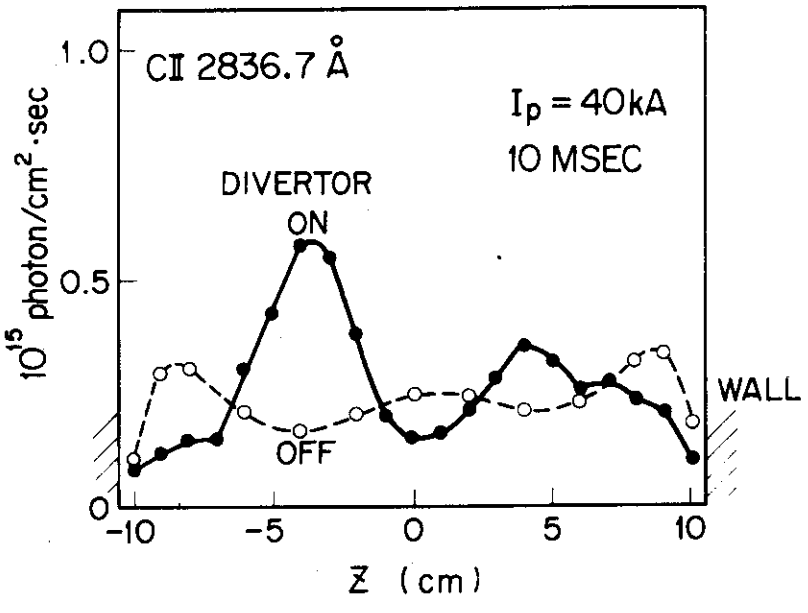

Fig.3(a)

Fig.3(b)

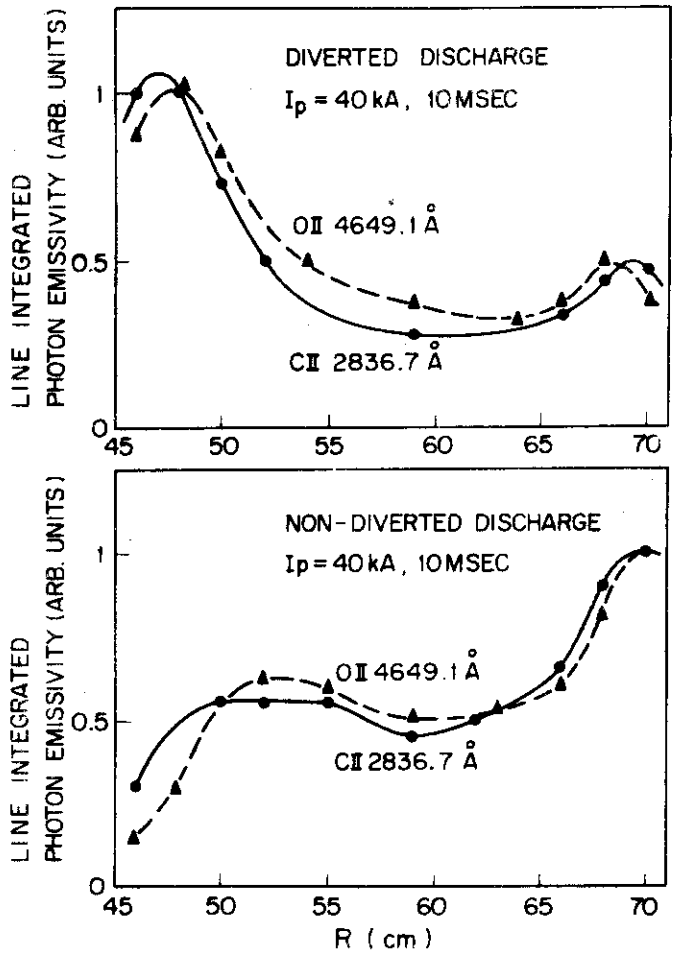

Fig. 3 Vertical (a) and horizontal (b) distributions of CII and OII line emissivities in discharges with and without divertor. Impurity recycling occurs in the plasma edge region near the wall in non-diverted discharge. With operating the divertor, the impurity recycling is reduced near the first wall, and is located on the divertor side.

production caused by all of the possible ions. Therefore in the following we will discuss the divertor action controlling the impurity flux onto the first wall only for gaseous impurities.

Figure 3(a) shows the line integrated vertical profile of CII 2836.7 Å line emission in discharges with (solid lines) and without divertor (dotted lines) at the current plateau. It indicates that, in non-diverted discharge, impurity recycling occurs in the plasma outer edge region near the wall, as is observed in ordinary tokamaks. On the other hand, in diverted discharge, the impurity recycling is reduced near the wall, and is located at $Z \sim \pm 4$ cm. This situation is more clarified by the observation of horizontal distribution of the line emission. Figure 3(b) shows the line integrated horizontal

profile of CII 2836.7 Å and OII 4649.1 Å line emissions. The figure indicates that the loss processes of oxygen and carbon in the outer edge region are the same, and they are lost to the divertor side when the divertor is operated. It becomes clear that the position of the maximum intensity of vertical profile of CII line emission in diverted discharge corresponds to that of the divertor throat. It apparently shows that the impurity ions diffusing from the main plasma is guided towards the burial chamber with the divertor operation. On the other hand, the impurity ions are directly lost to the surface of the wall in non-diverted discharge. As a result, in the diverted discharge, impurity loss flux onto the main chamber wall is reduced, and the impurity loss flux is located on the divertor side. These phenomena can be well recognized from the presence of a strong flow of impurity ions towards the burial chamber in the scrape-off layer, which is presented in the previous chapter.

Thus although the reduction of impurity flux onto the first wall is small due to the small width of scrape-off layer in DIVA, divertor exhibits the action reducing the plasma-wall interaction at the main chamber wall. The second problem we investigate is the impurity backflow already noted in Section 1. In order to investigate the effect of the impurity backflow from the neutralizer plate, aluminum injection is performed along chord 1 and 2 (Fig. 1). Figure 4 shows the experimental result: solid lines with injection, dotted line without injection. Injection along chord 2 has no effect on the main plasma and, according to spectroscopic measurements of AlXI, there is no observable accumulation in the main plasma. However, injection along chord 1 has significant effects and results in large disruptions and the breakdown of plasma confinement. These experimental results show that the impurity ions in the burial chamber hardly flow back to the main chamber along the scrape-off field lines. The amount of accumulation of aluminum in the main plasma in the case of injection in the burial chamber is only 1/15 of the case of injection in the edge of the main plasma. Since 5 % of the aluminum injected into the main plasma edge accumulates in the diverted discharge, which is presented in the previous chapter, this experimental result shows that roughly 0.3 % of the aluminum ions injected into the scrape-off plasma in the burial chamber accumulate in the main plasma due to the impurity backflow.

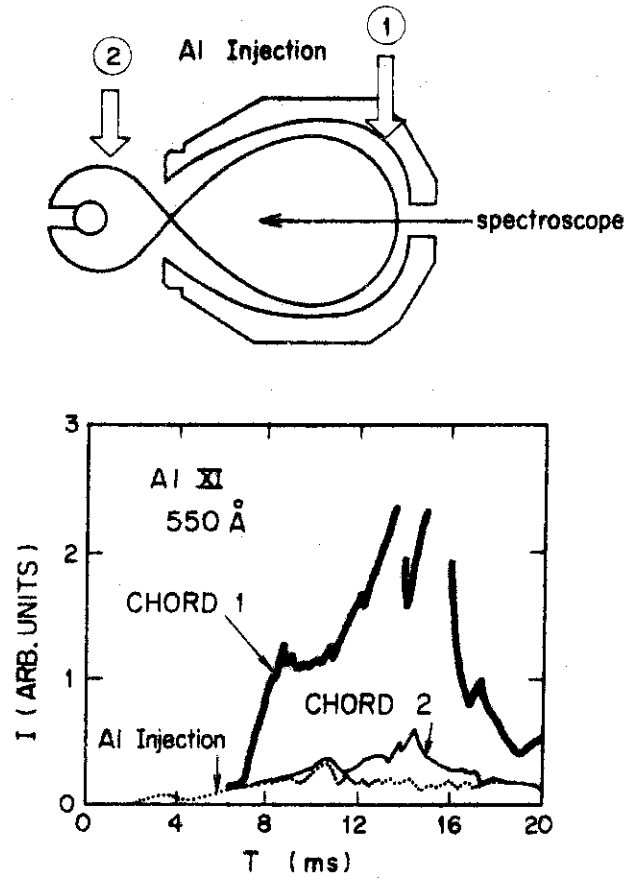

Fig. 4 Demonstration of the backflow of the aluminum ions from the burial chamber into the main plasma; solid lines indicate with the injections along chords 1 and 2, and dotted line indicates the background level of the AlXI 550 Å line emission.

5.4 Suppression of Metal Impurity Production by Cooling the Scrape-Off Plasma with Light-Impurity Injection

According to the property of ion-sputtering yield, it is important to reduce the electron temperature of the scrape-off plasma which contacts the material surface, since the potential difference between the plasma and the material surface is determined by the electron temperature. Therefore, cooling of the outer edge plasma with additional gaseous impurity or cold fuel injection is supposed to suppress the production of metal impurity.

We investigate this cooling effect by employing a methane gas feeding of 1.5 msec duration for 30 kA diverted discharge of relatively low $\bar{n}_e$. Figure 5 shows the time development of plasma current I_p, plasma loop voltage V_L, line-averaged electron density $\bar{n}_e$ and the line integrated radiation power

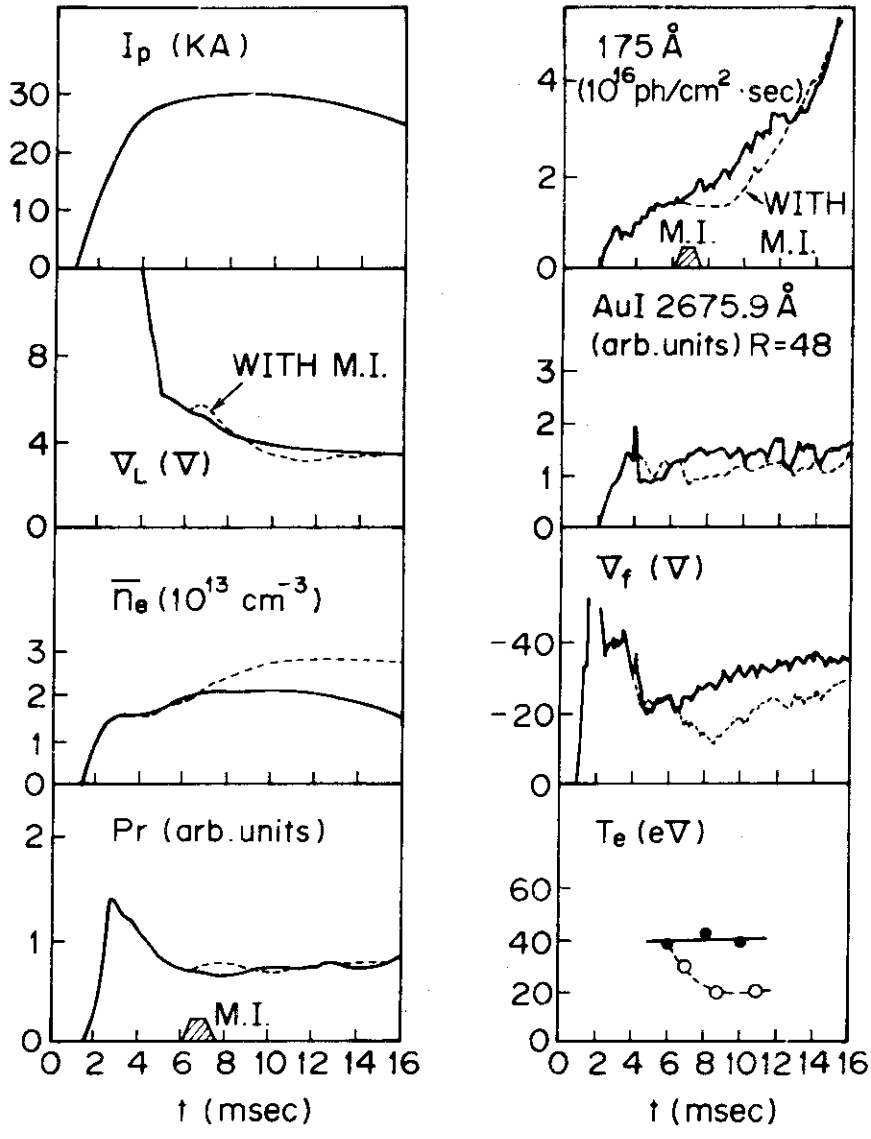

Fig. 5 Suppression of metal impurity production by cooling the scrape-off plasma with light-impurity injection. Time evolutions of plasma current I_p, plasma loop voltage V_L, line-averaged electron density $\bar{n}_e$, the total radiation power P_r, the line integral (across the minor diameter) of photon signals of 175 Å (bandwidth 1 Å), AuI 2675.9 Å line emission near the divertor throat (R = 48 cm), the floating potential of the shell with respect to the vacuum chamber V_f, and the electron temperature of the scrape-off plasma at 5 mm from the shell surface at the divertor throat with (solid line) and without (dotted lines) methane injection (M.I.). The cooling of the scrape-off plasma effectively suppresses the gold impurity production at the first wall by reducing the ion-sputtering yield, thereby reduces the accumulation of gold ions in the discharge.

P_r in discharges with and without methane gas feeding. With the gas feeding the electron density increases 40 %. The changes in plasma resistivity and radiation loss are small and less than 20 %. Figure 5 also shows the changes with the gas feeding in the line integral (across the minor diameter) of photon signal of 175 Å (bandwidth 1 Å), AuI 2675.9 Å line emission near the divertor throat (R = 48 cm), floating potential of the shell with respect to the vacuum chamber and the electron temperature of the scrape-off plasma at 5 mm from the first wall at the divertor throat measured with a Langmuir probe. Figure 6 shows the horizontal profile of vertically integrated line emission of AuI 2675.9 Å. It shows the horizontal distribution of the intensity of gold generation at the wall surface. The solid line indicates the gold generation in the discharge without methane injection, and the dotted line indicates that at 2 msec after starting the methane injection. With the gas feeding, the impurity generation at the whole surface of the first wall is suppressed. Also at this time the outer edge of the scrape-off plasma is cooled down by a factor of 2, thereby the reduction of potential difference between the plasma and the first wall occurs. This appears that

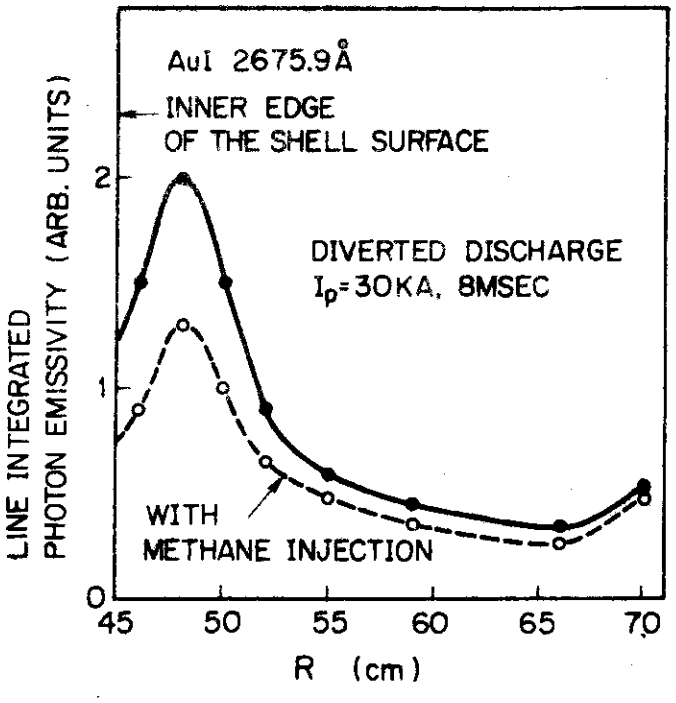

Fig. 6 Horizontal profiles of line integrated photon emissivity of AuI 2675.9 Å in diverted discharge. It shows the horizontal distribution of gold impurity production at the first wall. Cooling of the scrape-off plasma with methane injection reduces the impurity production over the whole surface of the shell.

the observed reduction of impurity generation with the gas feeding is attributed to the reduction of ion-sputtering yield by reducing the potential difference (sheath potential) between the plasma and the first wall. As previously noted, since the ion currents onto the four sector pieces of shell are almost the same within 20 % in toroidal direction, the change in the AuI line emission at the observed position proportionally corresponds to that of the total gold influx into the plasma.

With the gas feeding the radiation from the gold ions in the plasma center is reduced by 30 %. It is expected that this reduction is attributed to the reduction of impurity influx (generation). There can be, however, other aspects to explain this result, i.e. the reduction of the metal impurity contamination by cold gas injection may be due to the enhanced shielding action and/or pumping-out due to the neoclassical impurity transport process, which is caused by the change in the radial density profile of protons or light-impurities.

In order to clarify this problem, accumulations are compared in discharges with and without gas feeding for a same amount of aluminum injection. Figure 7 shows the experimental result. The observation of the AlXI 550 Å line emission from the plasma center results in a less than 10 % reduction

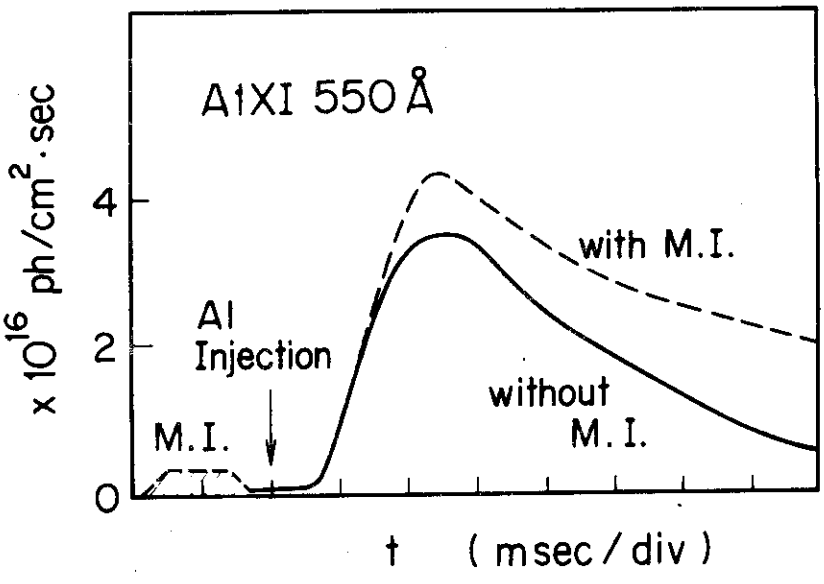

Fig. 7 Accumulations of injected aluminum ions with and without methane injection. This simulation experiment makes it clear that the reduction of gold accumulation with the methane injection is not due to a change in the transport of gold ions, but the reduction of gold influx from the wall.

of the aluminum accumulation with gas feeding. Judging from these simulation experiments, impurity transport does not change essentially. It is concluded that the observed reduction of the metal impurity ions in the plasma is mainly attributed to the reduction of impurity influx by cooling the scrape-off plasma.

5.5 Confinement Property of Metal Impurity Ions in the Discharge

After the metal impurity, which is released from the wall, penetrates into the main plasma, the transport across the minor radius becomes the problem. In this section, the confinement property of metal impurity ions in the discharge is investigated by observing the diffusion process of pulsively injected metal impurity ions.

For the first experimental evidence, gold is released from the shell surface by pulsively biasing the shell negatively with respect to the plasma. With the negative bias, as is expected from the ion-sputtering yield property, gold is easily released due to the sputtering by the ions accelerated in the applied electric field at the surface of the shell. The experiment is performed in the following discharge conditions; line-averaged electron density 1×10^{13} cm^{-3}, toroidal field 10 kG and plasma current 14 kA. Typical plasma parameters of this discharge are: peak electron temperature 200-250 eV, peak ion temperature 70 eV, energy confinement time 0.7 msec, and particle confinement time 1 msec.

In this discharge, which is conditioned so that the plasma contamination by the light-impurity is suppressed to small, the radiation power measured with the pyro-electric detector is strictly proportional to the total radiation power emitted from the gold ions in the whole wavelength range between 120 to 250 Å. Moreover, both of the measured radiation power, calibrated by using the radiation from highly resistive discharges and by means of the atomic branching ratio method respectively, coincide within a factor of 2 [8].

The gold is released at the current plateau of the discharge. Figure 8 shows the time developments of the ion current onto the shell, radiation intensity at 180 Å in the pseudo-continuum emission, and the total radiation power measured with the pyro-electric detector, which are observed along the major chord of the minor radius. After the gold injection the radiation in the whole wavelength range between 120-250 Å increases and then declines. The

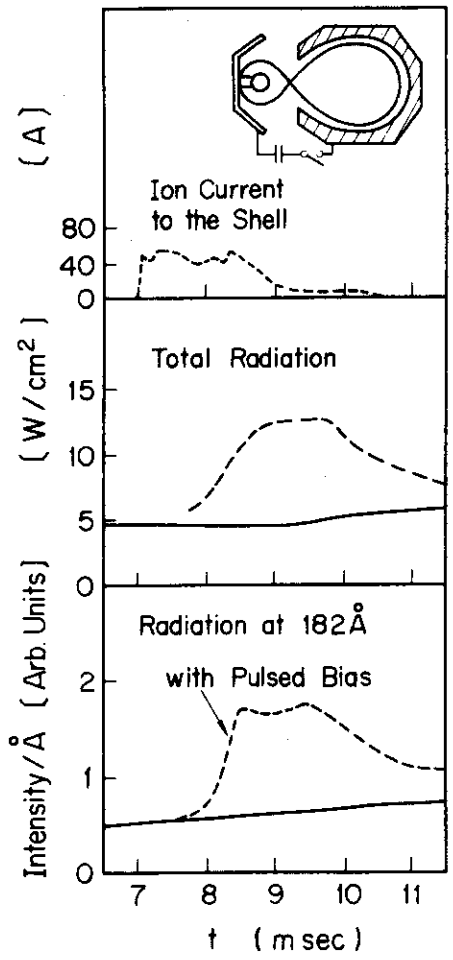

Fig. 8 Time development of the accumulation of gold ions with pulsed gold injection by biasing the shell negatively with respect to the scrape-off plasma; ion current to the shell, line-integrated total radiation power measured with pyro-electric detecter, and the radiation of many lines at 182 Å emitted from gold ions.

dotted line in Fig. 9 shows the increase of the pseudo-continuum emission 2 msec after starting the injection. The time development in the radial penetration of the radiation is measured by scanning the pyro-electric detector vertically with a space resolution of 2 cm, which is shown in Fig. 10. Since the intensity of the radiation emitted from various ionization states of gold ions is almost independent on the electron temperature in the present discharge (110-250 eV) [7], the radiation power can be assumed to be proportional to $n_e \cdot N_{Au}$, where N_{Au} is the density of gold ions. Therefore the experimental observation indicates that the gold ions released from the first wall diffuse inward up to the plasma center within 1-2 msec, and then diffuse out to the wall. After the outward diffusion of the impurity ions, the accumulation level comes back to the intrinsic level of the non-injected discharge. These behavior indicates a finite confinement property of the metal impurity ions of the order of that of protons in the low density discharge. No strong peaking and long confinement time of the gold ions in the plasma center, which are expected from neoclassical theory

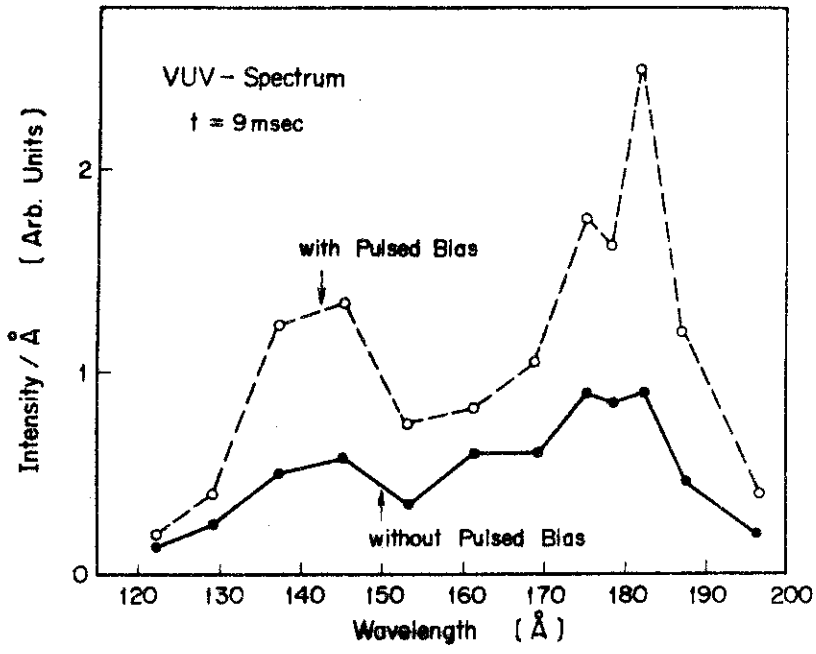

Fig. 9 VUV-spectrum with and without pulsed bias of the shell.

especially for high-Z ions, are observed. These experimental results will be compared with the transport model presented in Chapter 3 in the next section.

Another experimental evidence of the confinement property of metal impurity ions can be found in aluminum injection experiment presented in the previous section. In the methane injection followed by aluminum injection, which is presented in Fig. 7, comparison of the life time of AlXI ions can be made in discharges with and without additional methane injection. In the figure, the time needed for reaching the peak intensity in the line emission shows the radial diffusion time of the injected aluminum ions up to the region near the maximum population (r=3 to 4 cm) of AlXI state in minor radius. The decay time constant of the AlXI line emissivity in both discharges are 5.7 msec and 2.9 msec with and without the methane injection respectively. Because the reduction of the electron temperature with methane injection is small ($\sim$10 %) in the central region of the plasma, the difference in the decay time constant is not due to an increment of population density of AlXI state caused by the change in the electron temperature, but the reduction of cross diffusion velocity through the region of the electron temperature corresponding to the maximum population of AlXI ions.

Since the particle confinement time is proportional to $\bar{n}_e$, as was

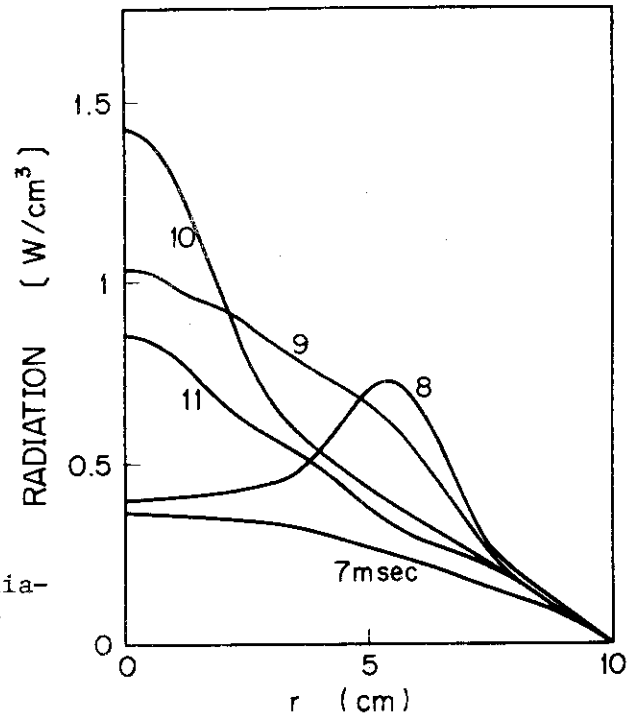

Fig. 10 Radial diffusion of radiation power density after the release of gold from the shell surface.

presented in Chapter 2, it seems that the reduction of anomalous diffusion coefficient with the increase of the electron density results in the decrease of radial diffusion velocity and the increase of the life time of AlXI ions. In other words, it is concluded that with the increase of energy and particle confinement time with increasing the electron density, the lifetime of metal impurity ions in the plasma increases, because the outward diffusion due to anomalous process is weakened and the inward diffusion due to collisional process is strengthened. As a result, in this situation, more severe control of metal impurity flux than that of today will be needed in a future tokamak device operating with long energy confinement time.

5.6 Discussion

In this section we compare the experimentaly observed radial transport of metal impurity ions with the results of an impurity transport code. For a transport model of light impurity ions, we have employed a neoclassical diffusion superposed by an anomalous diffusion for protons, which has described well the radial transport of intrinsic and injected carbon ions. Namely, the radial flux of impurity ions Γ is given as:

$$\Gamma = - D_a \frac{\partial N}{\partial r} + \Gamma_{NC}$$

where, D_a is an anomalous diffusion coefficient, N is the density of impurity ions, and Γ_{NC} is the radial flux due to the neoclassical theory.

In the present calculation, we apply this scheme also for the metal impurity ions. The neoclassical cross-field ion flux $\Gamma_{NC,\alpha\beta}$ of species α due to the friction with ions of species β is given as

$$\Gamma_{NC,\alpha\beta} = - C_c \sqrt{\frac{m_{\alpha\beta}}{m_p}} \left[n_\beta Z_\beta^2 \frac{\partial n_\alpha}{\partial r} - Z_\alpha Z_\beta n_\alpha \frac{\partial n_\beta}{\partial r} \right] .$$

By summing up these ion fluxes for all the ionization states of respective ion species, the diffusion equations for the proton density n_p, light impurity density (oxygen) N_L and heavy impurity density N_H are given as

$$\frac{\partial n_j}{\partial t} = - \frac{1}{r} \frac{\partial}{\partial r} r\Gamma_j + S_j \quad ,$$

$$\Gamma_p = - D_a \frac{\partial n_p}{\partial r} - C_c \left(N_L < Z_L^2 > + N_H < Z_H^2 >\right) \frac{\partial n_p}{\partial r}$$

$$+ C_c \{< Z_L > \frac{\partial N_L}{\partial r} + N_L \frac{\partial <Z_L>}{\partial r} + < Z_H > \frac{\partial N_H}{\partial r} + N_H \frac{\partial <Z_H>}{\partial r}\} n_p \quad ,$$

$$\Gamma_L = - D_a \frac{\partial N_L}{\partial r} - C_c \left(n_p \frac{\partial N_L}{\partial r} - < Z_L > N_L \frac{\partial n_p}{\partial r}\right)$$

$$- \sqrt{A_L/2}\, C_c \{(< Z_L^2 > - < Z_L >^2) N_L \frac{\partial N_L}{\partial r} - N_L^2 < Z_L > \frac{\partial <Z_L>}{\partial r}\}$$

$$- \sqrt{A_L}\, C_c \{N_H < Z_H^2 > \frac{\partial N_L}{\partial r} - N_L N_H < Z_L > \frac{\partial <Z_H>}{\partial r} - N_L < Z_L >< Z_H > \frac{\partial N_H}{\partial r}\} \quad ,$$

$$\Gamma_H = -D_a \frac{\partial N_H}{\partial r} - C_c \left(n_p \frac{\partial N_H}{\partial r} - \langle Z_H \rangle N_H \frac{\partial n_p}{\partial r}\right)$$

$$- \sqrt{A_H/2}\, C_c \left\{\left(\langle Z_H^2 \rangle - \langle Z_H \rangle^2\right) N_H \frac{\partial N_H}{\partial r} - N_H^2 \langle Z_H \rangle \frac{\partial \langle Z_H \rangle}{\partial r}\right\}$$

$$- \sqrt{A_L}\, C_c \left\{N_L \langle Z_L^2 \rangle \frac{\partial N_H}{\partial r} - N_H N_L \langle Z_H \rangle \frac{\partial \langle Z_L \rangle}{\partial r} - N_H \langle Z_H \rangle \langle Z_L \rangle \frac{\partial N_L}{\partial r}\right\}$$

where $N = \sum_z N_Z$, $\langle Z \rangle = \sum_z Z N_Z/N$, $\langle Z^2 \rangle = \sum_z Z^2 N_Z/N$. The electron density is given by $n_e = n_p + \langle Z_L \rangle N_L + \langle Z_H \rangle N_H$.

Here N_Z is the density of ions in the ionization state Z, and $A_L = m_L/m_p$, $A_H = m_H/m_p$, where m_j being the mass of ions j. For the neoclassical impurity flux, we take the simple expression presented in ref.[9]

$$C_c = 0.5(1 + 2q^2) \frac{4\sqrt{2\pi}\, e^4 \ell n\lambda}{3\sqrt{m_p}\, T^{3/2}} \cdot \frac{2m_p T}{e^2 B^2} \quad ,$$

where q is the safety factor, B the toroidal magnetic field, and T the common temperature of all ions. S_p is the particle source of protons, which is obtained by solving the transport equations presented by Dnestrovskii. In the calculation, fast particles up to the fifth generation are treated. S_L and S_H are the particle sources of the respective impurity species, which are obtained from simple transport equations for the penetrating neutral particles with a constant velocity while ionized by plasma electrons. The neutral particle fluxes at the plasma edge are determined from the recycling conditions (reflection coefficient R) and the additionally injecting flux. For the protons and light element we take R = 1, and for the heavy element R = 0. For the anomalous diffusion coefficient, we take the same expression as is used in Chapter 3.

To determine the neoclassical flux density, it is necessary to know the quantities $\langle Z \rangle$ and $\langle Z^2 \rangle$. For oxygen, gold, and aluminum, we use those calculated for the coronal equiliblium state presented in ref.[7]. In the simulations, the electron temperature, ion temperature, and the current density profiles are held constant in time. The temperature

profiles are given by the experimental results, and the current density profile is taken to be proportional to $T_e(r)^{3/2}$.

5.6.1 Radial Diffusion of Pulsively Injected Gold Ions in Low Density Discharge

We first calculate the radial transport of gold ions pulsively released from the shell surface. Plasma parameters such as electron temperature, ion temperature, and line-averaged electron density are taken to be the same as the experiment presented in Section 5. For a typical case, a pulsed gold flux of 5×10^{18} sec^{-1}, 1.5 msec duration is added to a constant influx of 1×10^{18} sec^{-1}. For the coefficient C of the anomalous diffusion coefficient, we take 300.

With this value, the calculated particle confinement time of protons during the gold injection is 1.2 msec. Figure 11 shows the computational result. The injected gold ions diffuse up to the plasma center within 1-2 msec. After the termination of the injection, the gold ions present near the wall is rapidly lost to the wall, thereby the gold ions accumulate in the plasma center. Then, the accumulation of gold ions returns to the intrinsic level of non-injection discharge with a decay time constant of 1.2 msec. Comparing this result with the experimental

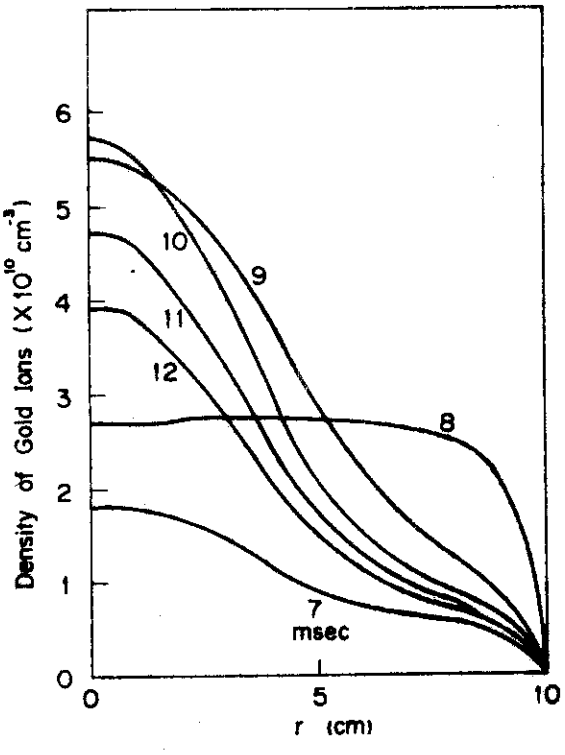

Fig. 11 Calculated radial diffusion of pulsively injected gold ions. The present impurity transport model describes well the experimental observation presented in Fig.10.

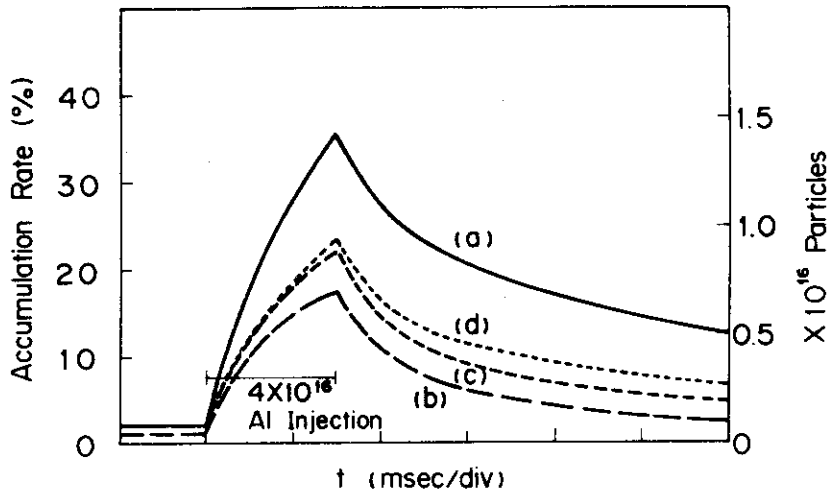

Fig. 12 Time development of the amount of trapped aluminum ions in the discharge for a neutral aluminum injection of 4×10^{16} particles; (b) anomalous diffusion coefficient used in case (a) is doubled, (c) mean Z is reduced to half of that for coronal equilibrium state, (d) mean Z is reduced to half of that for coronal equilibrium state only in the region of 1.7 cm width from the wall.

observation (Fig.10), this transport model well describes also the radial transport of metal impurity ions.

5.6.2 Amount of Impurity Accumulation in the Plasma for a Neutral Impurity Influx from the Wall

The second problem that we consider is: for a flux of neutral metal impurity from the wall, what is the amount of metal impurity ions that accumulate in the main part of the plasma? The experimental observation of aluminum injection, which was presented in Chapter 4, shows that only 20 % of the neutral impurity flux penetrates into the main plasma. We examine this problem by employing the present impurity transport model. The plasma parameters such as electron and ion temperatures, and electron density are taken to be the same as the experiment presented in Chapter 4. We take the energy of incoming neutral aluminum of 5 eV. For the coefficient C of the anomalous diffusion coefficient, we take 200 to obtain the proton confinement time of 2.4 msec, which fits the experimental result.

4×10^{16} aluminum neutral atoms is injected with 1.5 msec duration adding to a constant influx of 10^{18} sec^{-1} after a steady state is accomplished. Figure 12 shows the time development of total aluminum

ions trapped in the discharge. Case (a) in the figure shows the computational result. The penetration process of the injected aluminum ions into the plasma center is similar to that is presented in the calculation of gold injection (Fig.11). In this case, at the time just after the termination of the injection, the trapping rate of the injected aluminum is 35 %. The rest of the injected impurity ions is lost towards the wall due to anomalous diffusion process which spreads the radial profile of aluminum ions. This effect is clarified by the similar calculation with the increased anomalous diffusion coefficient. The case (b) presents the impurity accumulation when C = 400. In this case, the outward flux towards the wall due to the anomalous diffusion is increased, thereby the accumulation is reduced to 18 %. The confinement time of the accumulated aluminum ions in the case (a) are 1.8 msec and 3.2 msec at 0.5 msec and 3.5 msec after the termination of the injection respectively. The former is mainly due to the rapid loss of the aluminum ions present near the wall. The later shows the good confinement property of impurity ions present in the plasma center. This is due to the collisional inward force strengthened because of high Z value of metal ions. This effect is confirmed by the fact that the accumulation is reduced to 22 % when the effective charge of the aluminum ions are reduced to half of that in case (a). The result is shown in the figure as case (c). Similar result is obtained in the comparison of the accumulation of gold and aluminum ions. Figure 13 shows the time development of the accumulation of gold and aluminum ions for a same constant neutral-impurity influx of 1×10^{18} sec^{-1} (incoming energy of 5 eV). Gold needs a longer time for reaching a steady state than that of aluminum, and results in a larger accumulation because of its higher mean Z value.

Taking into account that the collisional inward force increases with the increase of the mean Z of the ions, and that the charge state of the aluminum ions in the experiment is rather lower than that of the coronal equilibrium state especially in the outer edge region, it can be said that the present impurity transport model well describes the trapping rate of below 20 % observed in the experiment (case (d) shows the trapping rate when the mean Z is reduced to half of that for coronal equilibrium state only in the region of 1.7 cm width from the wall).

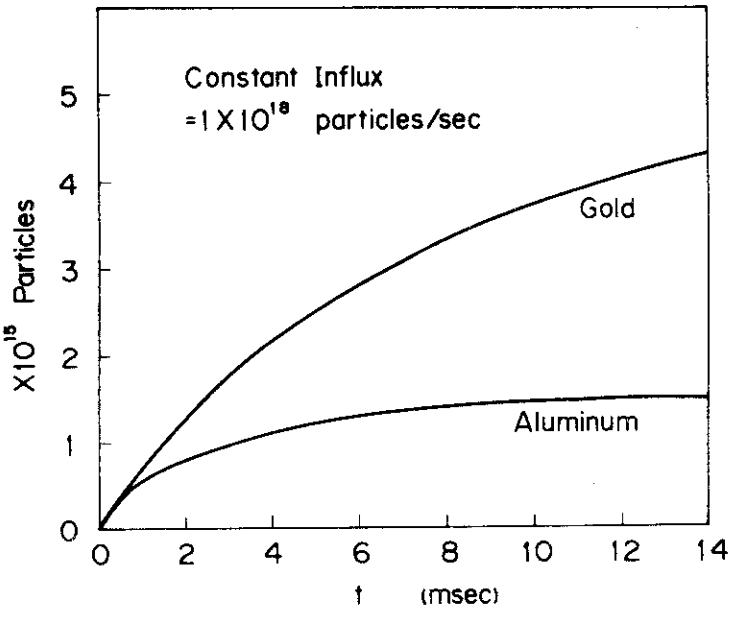

Fig. 13 Time development of the accumulation of gold and aluminum ions for a same constant neutral-impurity influx of 1×10^{18} sec^{-1}.

5.7 Conclusions

Divertor action controlling the plasma-wall interaction caused by diffusing impurity ions, control of the scrape-off plasma with light-impurity injection, and the confinement property of metal ions in the plasma are investigated. The results are summarized as follows:

(1) Divertor reduces the impurity ion flux onto the main vacuum chamber by guiding the impurity ions diffusing from the main plasma into the burial chamber, thereby reduces the plasma-wall interaction caused by diffusing impurity ions at the main vacuum chamber. The impurities produced in the burial chamber hardly flow back to the main plasma through the scrape-off layer. Roughly only 0.3 % of the impurity flux into the scrape-off plasma in the burial chamber penetrates into the main plasma due to the impurity backflow.

(2) A slight cooling of the scrape-off plasma by light-impurity injection effectively suppresses the metal impurity production at the chamber wall by reducing the ion-sputtering yield, thereby reduces the accumulation of the metal impurity ions in the main plasma.

(3) The transport of metal impurity ions is influenced by anomalous diffusion for protons. Due to this process, which spreads the radial

density profile of impurity ions, the accumulation of the impurity ions in the plasma center is only below 20 % of the neutral influx in the outer edge even in non-diverted discharge.

(4) With the increase of energy and particle confinement time with increasing the electron density, the lifetime of metal impurity ions in the plasma increases, because the outward diffusion due to anomalous process is weakened and the inward diffusion due to collisional process is strengthened. As a result, more severe control of metal impurity influx from the wall than that of today will be needed in a future tokamak device operating with long energy confinement time.

REFERENCES

[1] OHASA, K., MAEDA, H., YAMAMOTO, S., NAGAMI, M., OHTSUKA, H., et al., Nuclear Fusion 18 6 (1978) 872.
SHIMOMURA, Y., Nucl. Fusion 17 (1977) 626.

[2] MAEDA, H., OHTSUKA, H., SHIMOMURA, Y., et al., in Plasma Wall Interaction (Proc. Int. Symp. 1976), Pergamon Press (1977) 537.

[3] YAMAUCHI, T., NAGAMI, M., SENGOKU, S., KUMAGAI, K., Metal-Impurity Injection into DIVA Plasma with a Q-Switched Laser Beam, JAERI-M 7809.

[4] KASAI, S., FUNAHASHI, A., NAGAMI, M., SUGIE, T., YAMAUCHI, T., Spectroscopic Measurements of Impurities on the Upgraded DIVA Tokamak Plasma, to be published in J. Phys. Soc. Japan.

[5] KASAI, S., FUNAHASHI, A., KONOSHIMA, S., NAGAMI, M., SUGIE, T., MORI, K., Japan J. Appl. Phys. 17 (1978) 1625.

[6] KASAI, S., FUNAHASHI, A., NAGAMI, M., SUGIE, T., Radiation Due to Closely-Crowded Many Lines from High-Z Impurities on the Upgraded DIVA Tokamak Plasma, to be published in Nucl. Fusion.

[7] POST, D.E., JENSEN, R.V., TARTER, C.B., GRASBERGER, W.H., LOKKE, W.A., Steady State Radiative Cooling Rates for Low-Density High-Temperature Plasmas, Princeton Plasma Physics Lab., Report PPPL-1352.

[8] SHIHO, M., ODAJIMA, K., SUGIE, T., MAEDA, H., KASAI, S., et al., Spectroscopic and Bolometric Measurements of Radiation Loss in DIVA, JAERI-M 7397.

[9] TUDA, T., TANAKA, M., J. Phys. Soc. Japan 38 (1975) 1228.

6. SUMMARY

Detailed conclusions derived from this work were presented at the end of each chapter in the text. This summary includes an abbreviated collection of those results and brief discussions on the impurity control in future large devices.

(1) The divertor shields the impurity flux entering into the main plasma, and guides the shielded impurity ions into the remote burial chamber, thereby reduces the impurity flux into the main plasma by a factor of 2 to 4. The poloidal excursion time of the shielded impurity ions in the scrape-off layer is roughly equal to that of the scrape-off plasma. Divertor reduces the impurity ion-flux onto the main vacuum chamber by guiding the impurity ions diffusing from the main plasma into the burial chamber, thereby reduces the plasma-wall interaction caused by diffusing impurity ions at the main vacuum chamber. The impurity ions produced in the burial chamber may flow back to the main plasma through the scrape-off layer. Roughly only 0.3 % of the impurity flux into the scrape-off plasma in the burial chamber, however, penetrates into the main plasma due to the impurity backflow. Cooling of the divertor scrape-off with light-impurity injection further reduces the production of metal impurity at the first wall by reducing the potential difference between the plasma and the wall, thereby reduces the accumulation of the metal impurity in the plasma.

(2) Radial transport of impurity ions is not described only by neoclassical theory, but is strongly influenced by anomalous process. Radial diffusion of impurity ions across the whole minor radius is well described by a neoclassical diffusion superposed by the anomalous diffusion for protons. Due to this anomalous process, which spreads the radial density profile of impurity ions, the accumulation of impurity ions in the main part of the plasma is only below 20 % of the neutral impurity influx from the wall even in non-diverted discharge. With the increase of energy and particle confinement time with increasing the electron density, the lifetime of metal impurity ions in the plasma increases, because the outward diffusion due to anomalous process is weakened and the inward diffusion due to the collisional process is strengthened. As a result, more severe control

of metal impurity influx from the wall than that of today will be needed in a future tokamak device operating with long energy confinement time.

(3) In this work, the effectiveness of the divertor controlling the impurities is investigated in relatively small tokamak. Further experimental investigation is necessary in a large device in order to clarify the possibility of complete impurity control by employing a divertor in a reactor operating with a large auxiliary heating. In addition to this divertor approach, non-divertor approach has to be investigated, because of the engineering complexity of employing magnetic divertors into a reactor. Radiation cooling by low-Z impurity is one of the simple non-divertor impurity-control schemes, as was observed in this work. This method, however, relies on using low-Z limiter and wall, or by injecting suitable impurity gases in a controlled fashion. Furthermore, the basic difficulty with this approach is how to cool the plasma edge without cooling the plasma core. Therefore, experimental investigation on the following problems is necessary in a large device: 1) whether the radial transport and recycling of impurity ions permit the desirable radiation cooling, and 2) whether the production of low-Z impurity used as the first wall and limiter materials can be suppressed below tolerable amount.

ACKNOWLEDGEMENTS

The auther expresses his sincere gratitude to Professor Atsuo Iiyoshi of Kyoto University who first introduced him to the thermonuclear field and whose continuing encouragement and advice have been invaluable. He also wishes to express his appreciation to Professors Koji Uo and Ryohei Itatani of Kyoto University for the advice and constructive criticism during the preparation of this manuscript.

The auther wishes to express his appreciation to Dr. Shigeru Mori, Head of Fusion Research and Development Center in JAERI, for his continuing encouragement during the course of this research. He also wishes to express his appreciation to Dr. Yukio Obata, Head of Division of Thermonuclear Fusion Research, for his continuing encouragement and advice.

He would like to thank Dr. Masaji Yoshikawa for the instruction of the importance of impurity problems in tokamaks and the invaluable advice from the early stage of the DIVA program. He also wishes to express his appreciation to Drs. Yuji Tanaka and Masatoshi Tanaka for the continuing encouragement and useful suggestions of this work.

He would like to express his especial thank to Drs. Yasuo Shimomura and Hikosuke Maeda for the excellent guidance in the cource of this work. He also wishes to thank Drs. Hideo Ohtsuka, Shin Yamamoto, Kazuo Odajima, Seio Sengoku, Kazumi Ohasa and Haruyuki Kimura for their co-works and valuable discussions.

He would like to thank Dr. Akimasa Funahashi for the complete preparation and arrangement of various diagnostics in the course of the experiments, and the members of diagnostic group, especially Drs. Satoshi Kasai, Makoto Shiho and Tatsuo Sugie for instructions on spectroscopy and co-works in this research, and Dr. Toshihiko Yamauchi for the arrangement and co-work in the metal impurity injection experiment using high-power laser light.

It is a pleasure to thank Mr. Katsuto Anno and the other members of operation group of DIVA for the excellent assistance in the experiment.

APPENDIX

RADIATIVE COOLING CAPABILITIES OF CARBON, OXYGEN, AND NEON IN THE OUTER EDGE OF A TOKAMAK PLASMA

A.1 Introduction

Low-Z impurities, which can be fully stripped in the plasma center and present in partially stripped states in a peripheral region of the tokamak plasma, cool the periphral region of the discharge with the intense line radiation. Excessive cooling with high contamination level of the low-Z impurity causes the current channel to shrink, thereby leads the discharge to poor energy-confinement states or disruptive ends. On the contrary, in a controlled and then moderate contamination level, this radiative cooling yields a favorable situation, because as observed in many experiments, the cooling down of the outer edge plasma suppresses significantly the production of metal impurity, which cause large radiation loss power even in a central region of the discharge of several keV. Therefore, in future large tokamaks, where plasma-wall interaction becomes much more serious, this situation may become one of the most promising methods controlling the contamination level of metal impurities.

The radiative cooling capability due to a low-Z impurity in the outer edge of tokamak plasma was recently evaluated by Breton et al.[1], using a rather simple impurity diffusion model. Assuming constant inward and outward diffusion velocities, they calculate the radiation power by oxygen impurity in TFR tokamak. This transport model, however, is a rather crude one: the incoming impurities diffuse inward up to the center and then diffuse outward to the surface of the discharge. As a result this causes the large radiation power that cannot explain the whole energy balance of the discharge[2].

In this Appendix, with the most probable diffusion model describing the recycling impurities, which was presented in Chapter 3, the radial density distributions of individual ionization levels are calculated and the resultant radiation loss power is evaluated in DIVA-sized tokamak. As for the low-Z impurities, carbon, oxygen and neon are investigated.

A.2 Calculation of Radiation Loss

Number of efforts have been made to evaluate the radiation power emitted from various impurities in coronal equilibrium state. For example, in Ref.[1], the authors calculated the ionization equilibrium of an element that is determined by the equations of steady state coronal equilibrium. The radiation loss was then calculated by adding the emission due to bremsstrahlung, radiative and dielectronic recombination and line radiation.

The present interest is the radiative cooling in the outer edge region of tokamak plasma where the electron temperature is below few hundreds of eV. In this region, the most important radiation mechanism is line radiation due to partially stripped ions. As is presented for oxygen in Ref.[1], the other mechanisms, i.e. radiative and dielectronic recombinations and bremsstrahlung, are one or two order lower than the line radiation power. Therefore we calculate the radiation power only of line radiation.

If n_z is the density of the ion of charge Z (cm^{-3}), the power density P_r (Watts/cm^3) by line radiation of the ion is

$$P_r = 1.6 \times 10^{-19} \, n_e n_z \sum_j E_{exj} \, S_j \quad .$$

n_e is the electron density in cm^{-3} and the summation in j is for all transitions of the ion Z. It is assumed that the lines are emitted by radiative deexcitation of the upper levels of transitions excited from the ground state. E_{ex} is the excitation energy in eV and S_j is the excitation rate coefficient. We use for S_j the following expression given by Mewe [3]

$$S_j = 1.58 \times 10^{-5} \frac{f_i \bar{g}}{\sqrt{T_e} \, E_{exj}} \exp(- E_{ex}/T_e) \quad ,$$

where T_e is the electron temperature in eV, S_j the absorption oscillation strength and $\bar{g}$ the average effective Gaunt factor. For the ionization rate coefficients of an impurity ion, we use the expression proposed by Lotz [4]. The radiative and dielectronic recombination rate coefficients are calculated by using the expression given in Ref.[5] and [6].

We first calculate coronal equilibrium states, and using the results

of fractional abundances, calculate radiation losses as a function of the electron temperature. As for the line radiation power, the transitions in the calculation are similar to those by Breton et al.[1], which are shown in the table. E_{ex} and f are taken from the NBS table.

In Fig.1, the ratios, $P/n_e \cdot n_z$, are shown for carbon, oxygen and neon as a function of the electron temperature. Also the same relation given by Tarter [7] for oxygen is shown in the same figure. In these curves, maxima in the lower side of the electron temperature correspond to regions in which transitions among levels having the same principal quantum number are strongly excited. The minima in the curves occur when closed shell configurations are predominant (helium-like state), so that the ion cannot be excited at that temperature. On the higher side of electron temperature, there are small maxima due to excitation of 1s-np transitions. As is shown in Ref.[1], at higher temperatures, the contribution by dielectronic recombination and bremsstrahlung is no negligible. The corresponding deviations from the results of Tarter is found in the present calculation at high temperature. However, on the lower side of temperature, Tarter's result and ours are in agreement.

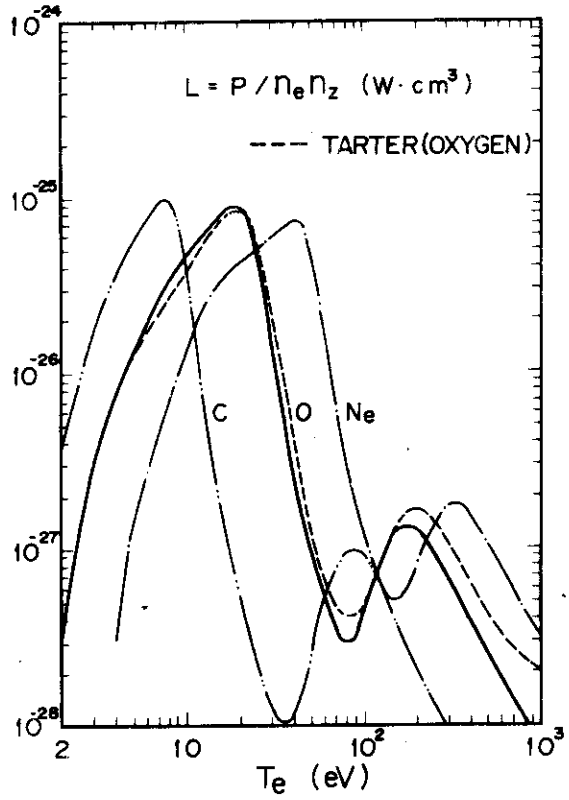

Fig.1 Line radiation power from carbon, oxygen and neon at coronal equilibrium as a function of the electron temperature T_e.

TABLE

The Transitions Included in the Calculations

Iso. el. seq.	Transitions Configurations	Terms	Iso. el. seq.	Transitions Configurations	Terms
H	1s -2s	$^2S-^2S$	Be	$2s^2$ -2s2p	$^1S-^1P$
	1s -2p	$^2S-^2P$		$2s^2$ -2s3s	$^1S-^1S$
	1s -3s	$^2S-^2S$		$2s^2$ -2s3p	$^1S-^1P$
	1s -3p	$^2S-^2P$		$2s^2$ -2s3d	$^1S-^1D$
	1s -3d	$^2S-^2D$		$2s^2$ -2s2p	$^1S-^3P$
	1s -4s	$^2S-^2S$		$2s^2$ -2s3s	$^1S-^3S$
	1s -4p	$^2S-^2P$		$2s^2$ -2s3p	$^1S-^3P$
	1s -4d	$^2S-^2D$		$2s^2$ -2s3d	$^1S-^3S$
He	$1s^2$-1s2s	$^1S-^1S$	B	$2s^22p$-$2s2p^2$	$^2P-^2P$
	$1s^2$-1s2p	$^1S-^1P$			$^2P-^2S$
	$1s^2$-1s3s	$^1S-^1S$			$^2P-^2D$
	$1s^2$-1s3p	$^1S-^1P$			
	$1s^2$-1s3d	$^1S-^1D$			
	$1s^2$-1s2s	$^1S-^3S$	C	$2s^22p^2$-$2s2p^3$	$^3P-^3P$
	$1s^2$-1s2p	$^1S-^3P$			$^3P-^3S$
	$1s^2$-1s3s	$^1S-^3S$			$^3P-^3D$
	$1s^2$-1s3p	$^1S-^3P$			
	$1s^2$-1s3d	$^1S-^3D$			
			N	$2s^22p^3$-$2s2p^4$	$^4S-^4P$
Li	2s -2p	$^2S-^2P$			
	2s -3s	$^2S-^2S$	O	$2s^22p^4$-$2s2p^5$	$^3P-^3P$
	2s -3p	$^2S-^2P$			
	2s -3d	$^2S-^2D$			
			F	$2s^22p^5$-$2s2p^6$	$^2P-^2S$

A.3 Radiative Cooling in the Outer Edge due to Recycling Impurities

A.3.1 Calculation of the Radial Density Distribution of Impurity Ions

To study the radiative cooling in the outer edge of a tokamak plasma, we treat the case of DIVA discharge in the toroidal field 20 kG, the plasma current 40 kA, and the average electron density $3\sim4 \times 10^{13}$ cm^{-3}.

To evaluate the radial distributions of radiation power, calculation of the radial density distributions of individual ionization levels is necessary. We calculate them with a radial transport model that have yielded good fit to the experimentally observed transient radial diffusion of pulsively injected carbon ions presented in Chapter 3. That is, the transport of impurity ion is described by neoclassical diffusion superposed by anomalous diffusion for protons.

Figure 2 shows the model plasma for radial profiles of electron and ion temperatures. In the present calculations, the electron and ion temperatures are constant with time and the radial density distributions of protons and total impurity ions are initially parabolic. The initial ionization population is determined as a coronal equilibrium state of the electron temperature of 30 eV. Energies of the incoming neutral hydrogen and impurity atom are taken as 10 eV.

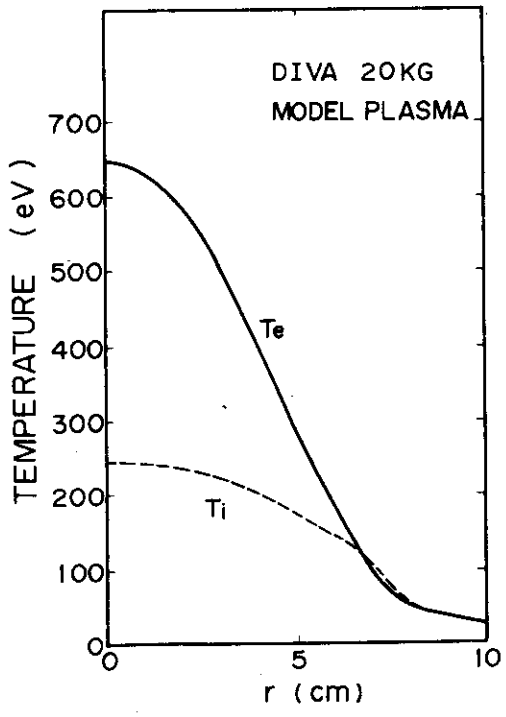

Fig.2 Electron and ion temperature profile, T_e, T_i, used in the calculation.

For the anomalous diffusion coefficient D_a, we apply the same expression as is used in Chapter 3. We take 200 for C in that expression, and in the region where q < 1, the value is multiplied by a factor of 5 to simulate the enhanced diffusion due to the sawtooth oscillation.

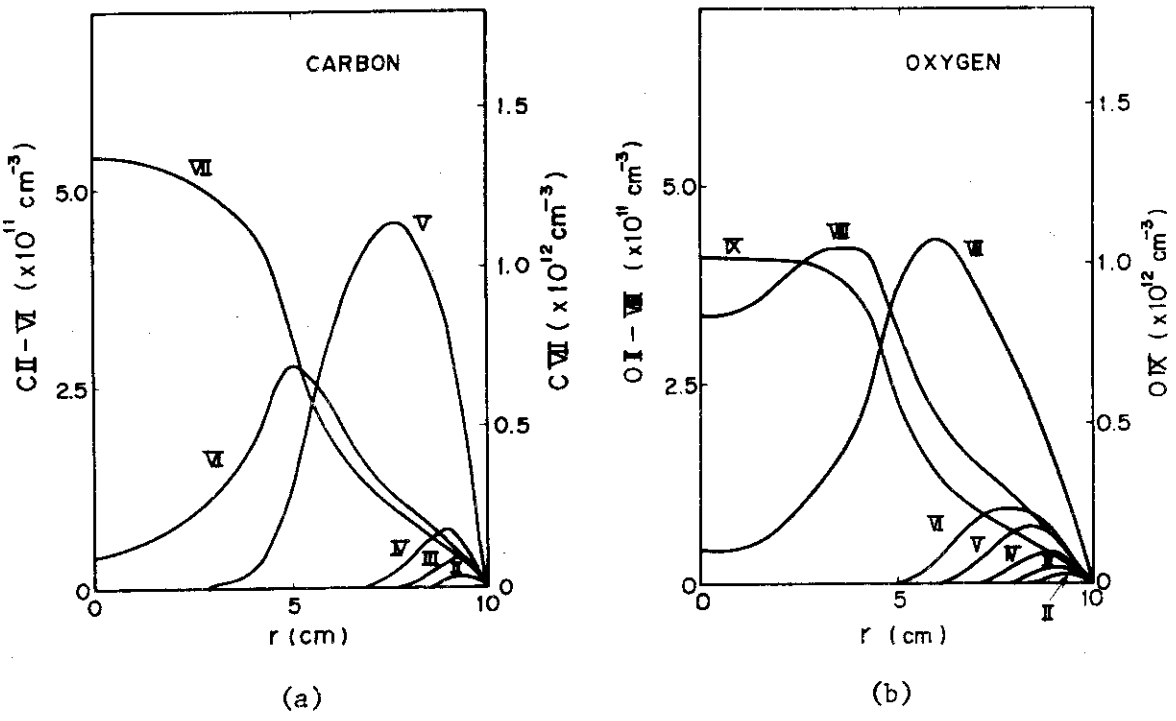

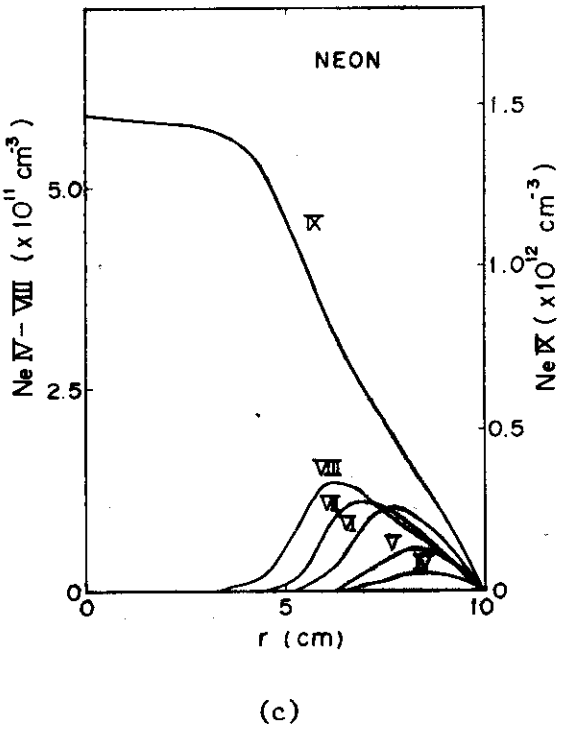

Fig.3 Computed results of the radial density distribution of individual ionization levels; (a) carbon, (b) oxygen, (c) neon. For neon, our treatment is limited up to the He-like state, and the ionization levels below N_eIV are omitted in the figure.

Figure 3 shows calculated radial density distributions of individual ionization levels, which are almost in steady state. In the three respective species, we assume a contamination 3 % the total number of protons. Calculated results for the three species show that the particle confinement time of protons and impurity ions are 1.6-1.8 msec and 1.9-3.9 msec respectively. As indicated in the figure, carbon and oxygen are dominantly in fully ionized state in the central region of the discharge, and in partially ionized states below lithium-like state in the outer edge region.

The calculation code used takes into account up to the ninth ionization level, so that for neon, the treatment is up to helium-like state, NeIX. The results show that the self-spreading anomalous diffusion gives relatively broad radial density profiles, compared with those by Breton et al.

A.3.2 Radiative Cooling

Figure 4 shows calculated radial distributions of radiation power. The intense radiation is caused by partially stripped ions below lithium-like state present in the outer edge although the population and the electron density are rather small. Therefore, width of the intense radiation is determined by ionization energy of lithium-like state for a given radial electron temperature profile. The ionization energy of the lithium-like state is 239 eV for neon, 138 eV for oxygen, and 64 eV for

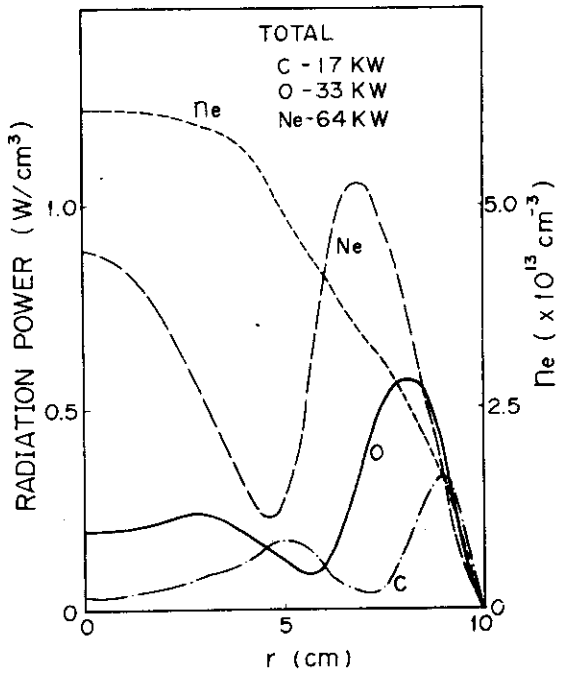

Fig.4 Typical electron density profile, n_e and radial power distributions radiated as line radiation for three low-Z species.

carbon, so that for a given electron temperature profile, neon has the largest width. Since the total radiation power is attributed mainly to that from the outer edge region, the results show that neon emits the largest power: 64 kW for neon, 33 kW for oxygen and 17 kW for carbon.

In Fig. 5 for oxygen, the width of intense radiative cooling is shown for three different electron temperature profiles, narrow (a) to broad (c). The results show that the existence of lithium-like state is limited in the region of electron temperatures below about 150 eV.

Besides the results of width of the intense radiative cooling, it should be noted that, in the present transport model, the narrow radial profile of electron temperature gives poor confinement of the impurity ions ((a) 2.3 msec, (b) 3.2 msec, (c) 4.1 msec) and causes more intense recycling.

Enhancement of the incoming flux of neutral impurity atoms due to the poor confinement of impurity ions results in increase of the partially stripped ions below lithium-like state leading to rize of the radiation power. On the other hand, good confinement provides the opposite situation, i.e. reduction of the radiation power in the outer edge region.

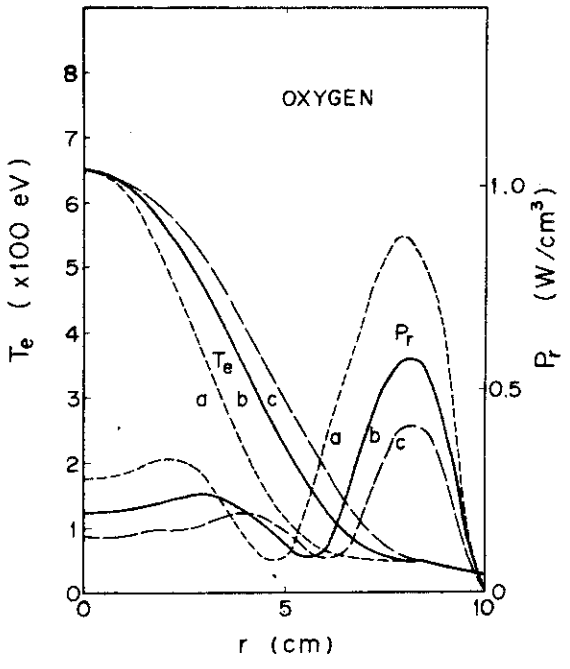

Fig.5 Radial power distributions for different electron temperature profiles for oxygen.

A.3.3 Comparison in Impurity Radiation between Coronal and Non-Coronal Calculations

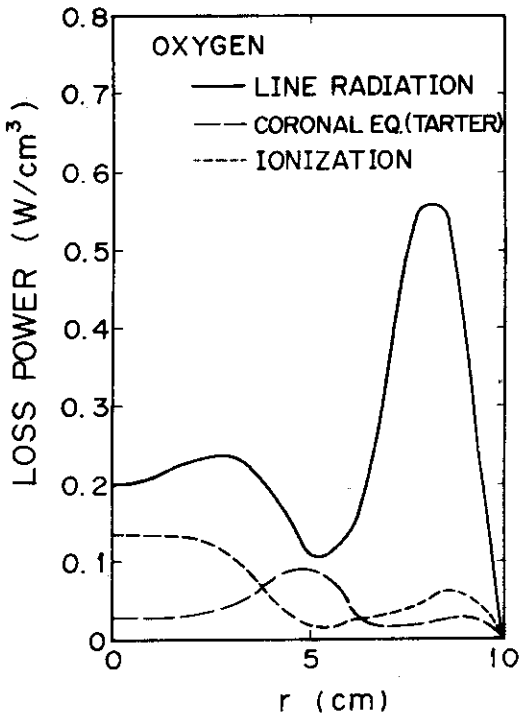

Fig.6 Radial distributions of radiation power from recycling impurities and from impurities of coronal equilibrium(Tarter) for oxygen. Ionization loss is also shown.

Figure 6 shows the comparison of the present computational result and the coronal calculation given by Tarter in the radial profile of the radiation power. The latter is calculated by using the radial distribution of total ionization levels and of electron temperature. Due to the strong recycling in the peripheral region, the impurity ions are in lower ionized levels than coronal equilibrium state, so that the computed result yields a radiation power in a factor of 20 larger in maximum than predicted for the coronal equilibrium state.

To evaluate the actual cooling effect by low-Z impurity, the ionization loss must also be considered. Incoming neutral impurities are suddenly ionized in the outer edge region, and successive ionizations continue while the ions diffuse inward or outward in the discharge. Furthermore the stripped electrons are thermalized up to local electron temperature. Thus the local power loss, P_i, due to the ionization of impurity ions is expressed as

$$P_i = 1.6 \times 10^{-19}\, n_e \sum_z n_z S_{ion} \left[E_{ion} + \frac{3}{2} T_e\right] \quad (W/cm^3) \quad ,$$

where S_{ion} and E_{ion} are the ionization rate coefficient and the ionization potential in eV respectively. In Fig. 6, the calculated radial

distribution of ionization loss for oxygen is shown. The total power is 5.7 kW, which is 17 % of the line radiation power.

A.4 Conclusion

Radiative cooling capabilities of three species of low-Z impurity, i.e. C, O and Ne have been shown in DIVA-sized tokamak. With the most probable diffusion model (neoclassical diffusion superposed by anomalous diffusion for protons) of recycling impurities in a tokamak plasma, the radial density distributions of individual ionization levels were calculated and using the results, the line radiation loss power was evaluated.

Impurities recycling from and to the wall deviate from the local coronal equilibrium state, thereby yield a radiation power which is larger by a factor of about 20 than estimated from the coronal equilibrium state in the outer edge of the discharge. Width of this intensive cooling layer is governed by the ionization energy of lithium-like state of the impurity, so that neon gives the largest layer with the highest radiation intensity.

REFERENCES

[1] BRETON, C., DE MICHELIS, C., and MATTIOLI, M., EUR-CEA-FC-822 (1976).

[2] TFR GROUP, EUR-CEA-FC-892 (1977).

[3] MEWE, R., Astron. and Astrophys. 20 (1972) 215.

[4] LOTZ, W., Zeitschrift für Physik 216 (1968) 241.

[5] VON GOELER, S., STODIEK, W., EUBANK, H., FISHMAN, H., GREBENSHCHIKOV, S., and HINNOV, E., Nucl. Fusion 15 (1975) 301.

[6] BURGESS, A., Astrophys. J., 141 (1965) 1588.

[7] TARTER, C.B., UCRL-78119 (1976).

PUBLICATION LIST CONCERNING THIS THESIS

CHAPTER 1,2;

NAGAMI, M., SHIMOMURA, Y., MAEDA, H., OHTSUKA, H., SHIHO, M., SUGIE, T., YAMAMOTO, S., ODAJIMA, K., SENGOKU, S., KIMURA, H., Formation of a Light-Impurity-Free Plasma in DIVA, Nucl. Fusion 18 4 (1978) 529.

CHAPTER 3

NAGAMI, M., MAEDA, H., SHIHO, M., SUGIE, T., SHIMOMURA, Y., YAMAMOTO, S., ODAJIMA, K., UEDA, N., SENGOKU, S., KIMURA, H., YOKOMIZO, H., Pulsed Methane Injection Experiment on DIVA, Nucl. Fusion 18 9 (1978) 1217.

CHAPTER 4

NAGAMI, M., SHIMOMURA, Y., MAEDA, H., KASAI, S., YAMAUCHI, T., SENGOKU, S., SUGIE, T., YAMAMOTO, S., ODAJIMA, K., KIMURA, H., OHASA, K., Impurity Shielding and Sweeping-Out by an Axisymmetric Divertor in DIVA, Nucl. Fusion 18 10 (1978) 1347.

CHAPTER 5

NAGAMI, M., MAEDA, H., KASAI, S., YAMAUCHI, T., SENGOKU, S., SUGIE, T., KIMURA, H., OHASA, K., ODAJIMA, K., YAMAMOTO, S., SHIMOMURA, Y., Divertor Experiment for Impurity Control in DIVA, contributed paper of 3rd International Conference on Plasma Surface Interactions in Controlled Fusion Devices, Culham (1978) Paper 27; J. Nucl. Mat. 76 & 77 (1978) 521.

APPENDIX

NAGAMI, M., Radiative Cooling in the Outer Edge of a Tokamak Plasma by Low-Z Impurities, JAERI-M 7432 (1977).